Isolation and Analysis of Circulating Tumor Cells in Genitourinary Cancers

by

Molly Kozminsky

A dissertation submitted in partial fulfillment
of the requirements for the degree of
Doctor of Philosophy
(Chemical Engineering)
in the University of Michigan
2017

Doctoral Committee:

Associate Professor Sunitha Nagrath, Chair
Professor Mark L. Day
Professor Nicholas A. Kotov
Professor Joerg Lahann
Dr. Todd M. Morgan

Molly Kozminsky

mollykoz@umich.edu

ORCID iD: 0000-0001-7040-1641

Dedication

To Mark, Denise, and Eli Kozminsky. It's been a journey.

Acknowledgements

The process of getting my PhD has been enabled by the unparalleled support of a great many people and resources.

I would first like thank my advisor, Professor Sunitha Nagrath, for her guidance and mentorship. She encouraged me to develop as a researcher and writer and welcomed me to the world interdisciplinary research. She taught me the importance of perseverance and positivity, and her dedication to cancer research is contagious to everyone around her. It has been wonderful to work with her during this first phase of my career, and I look forward to our relationship in the years to come.

I would like to thank my committee members - Professor Mark L. Day, Professor Nicholas A. Kotov, Professor Joerg Lahann, and Dr. Todd M. Morgan - for their support, suggestions, and collaboration over the past five years. They have been instrumental in helping me tie together the strands of this interdisciplinary work.

I am grateful for the opportunity to have collaborated with several labs across my multiple projects. In the lab of Dr. Todd Morgan, I would like to acknowledge Dr. Jae-Seung Chung and Dr. Yugang Wang for maintaining the prostate cancer patient database with Amy Gursky, Clinical coordinator. I would also like to thank Dr. Ajjai Alva and Dr. David Smith for furnishing patient samples. I am grateful also to Dr. James Henderson (CSCAR) for his patience and advice with regards to R programming and statistical analysis. From the lab of Dr. Max Wicha, I would like to thank Shamileh Fouladdel and Dr. Ebrahim Azizi for their help with RT-qPCR.

From the lab of Professor Mark Day, I am grateful for support, collaboration, and friendship I experienced in my work with Kathleen C. Day, Luke Broses, Dr. Guadalupe Lorenzatti Hiles, and Dr. Monica Liebert. Their hard work and commitment to cancer research inspire anyone lucky enough to work with them. I would also like to acknowledge Dr. Phillip L. Palmbos and his lab for their help on the bladder CTC project.

I would like to acknowledge Professor Jinsang Kim and Dr. Apoorv Shanker for their work on the CTC release chip project as well as Dr. Nallasivam Palanisamy for his help with proof-of-principle downstream analysis.

I would also like to thank my funding sources, the National Science Foundation Graduate Research Fellowship Program (NSF GRFP) and the Rackham Conference Travel Grant, for the opportunities they have afforded me. I would additionally like to acknowledge the many core facilities at the University of Michigan that enabled my work: Vector, Flow Cytometry, Pathology, (MC)2, and ULAM. I would like to express my gratitude to the Lurie Nanofabrication Facility and its wonderful staff.

I am eternally grateful to the patients who generously donated blood samples to my research. I appreciate the valuable opportunity I had in conducting this research.

I would like to thank the past and present member of the Nagrath Lab for their support. I'd like to express my gratitude to Professor Hyeun Joong Yoon for training, guidance, and mentorship. Thank you also to the other members of the GO Team: Yang (Angela) Wang, Tae Hyun (Kevin) Kim, and Heather Fairbairn. Our work also relies on the dedication of our undergraduate students. Thank you in particular to Head Duckling Christopher Dunlay, An Shi, Lauren Deneszczuk, Qu Jin, Sindhu Sreedhar, and Richard Cheung.

I would like to thank a number of student groups at the University of Michigan for the communities they have built as well as everything they have taught me: ChEGS, RELATE, MiSciWriters, and the Engineering Teaching Consultants.

The third floor of NCRC is a very special place. I have appreciated the friendship and encouragement from Lianette Rivera, Joe Nguyen, Lukasz Ochyl, Dr. Zhuo (Jen) Zhang, Mina Zeinali, Dr. Vasudha Murlidhar, Ting-Wen Lo, Sarah Owen, Dr. Sasha Cai Lesher-Perez, Professor Brendan Leung, and Dr. Patrick Grogan.

At every point in my life I have made close friends who have provided unfailing support. Thank you to my B-entry family for supporting me long distance, even though we don't all live together anymore (and I chose to live in the Midwest): Mary, Prannay, George, Jeff, Kirsten, Jamal, Emily, Andy, and Elise. Thank you to Tim and Lilo for being my Michigan family, joining me in my science and baking endeavors, and supporting me emotionally. I am grateful to Joe Bazzill for making this whole process more fun than it had any business being. I am forever indebted to my best friend and on-call biologist Laura for everything.

Finally, I would like to thank my parents, Mark and Denise, and my younger brother, Eli, for 27 years of love and encouragement and for guiding me and supporting me from day 0.

Table of Contents

Lists of Tables

List of Figures

Abstract

While accessible by a relatively noninvasive blood draw, circulating tumor cells (CTCs) remain difficult to study because of their rarity and their presence amongst the billions of surrounding normal blood cells. Of particular promise and utility to the in-depth study of CTCs are those technologies making use of microfluidics and nanomaterials, such as the graphene oxide (GO) Chip.

The GO Chip has been applied to a 41-patient metastatic castrate resistant prostate cancer (mCRPC) cohort. CTCs were enumerated from whole blood for all patients (range: 3-166 CTCs/mL, median: 20 CTCs/mL). Clusters of CTCs, defined as two or more directly adjacent CTCs, were observed in 26/41 patients, and ranged in size from 2-8 CTCs/cluster. Within the CTC population, the percentage of CTCs present as clusters ranged from 0-54.8%. Additionally, a parallel device was run for 36 patients to ultimately obtain RNA to use in RT-qPCR to assess levels of 96 genes of interest. Enumeration and RNA expression data were compared with clinical outcomes including overall survival, radioclinical progression, and PSA progression. An eight-gene score was determined to be highly prognostic of overall survival (AUC: 0.88), with the genes comprising the score suggesting the importance of a dedifferentiated expression phenotype in poor prognosis.

Follow-up work in prostate cancer investigated the role of HER2 and EGFR in prostate cancer metastasis. Analysis of tissue microarrays showed HER2 expression in prostate cancer and bone metastases. Primary and secondary prostate sphere formation was dependent on high EGFR

expression as determined by FACS, but not on HER2 expression. EGFR was also implicated in survival in transit as shown by the presence of EGFR+ CTCs isolated by the GO Chip in 9/10 mCRPC patients assays, with an average of 35.5% of CTCs showing EGFR expression. Dual inhibition of HER2 and EGFR in mouse xenograft models prevented tumor growth.

HER2 and EGFR as well as ADAM15 and CD31 were studied in bladder cancer CTCs as well. In a preliminary study primarily for optimization, antibodies were chosen for higher sensitivity capture as well as to stain bladder CTCs for the markers of interest. Ultimately, CTCs were isolated from five metastatic bladder cancer patients (range: 5-499 CTCs/mL), and a combination of staining antibodies that showed low background in the healthy control was chosen. EGFR+ and CD31+ CTCs were observed, while HER+ and ADAM15+ CTCs were not, and clusters of CTCs were isolated from some patients.

To address drawbacks in the current technology, two strategies were attempted to enable cell release. A layer-by-layer (LbL) substrate enclosed in a microfluidic chamber featured different disadvantages based on film composition, but a thermosensitive polymer substrate enable release when cooled below its lower critical solution temperature of 12-13°C. The polymer-GO composite showed between 84.9 and 95.2% capture efficiency of EpCAM expressing cell lines and released over 91% of cells captured from whole blood. Using this device, CTCs were captured from 2/3 pancreatic cancer patients and 8/10 breast cancer patients. FISH for HER2 was performed on CTCs isolated from one breast cancer patient.

With high performing technologies to separate them from the noise of other cells in the blood, CTCs can provide information about disease spread in genitourinary cancers. The future incorporation of CTC-related information into clinical decision making has the potential to better inform treatment selection and disease prognosis.

Chapter 1 Introduction

1.1 Metastasis

An intimidating aspect of cancer is its ability to spread, with metastasis causing 90% of cancer-related deaths (2, 5). Metastasis is a multistep process in which tumor cells escape from the primary tumor site, enter the bloodstream, arrest at a secondary site, extravasate, and proliferate to form secondary tumor colonies (**Figure 1-1**) (6, 7). To migrate through the primary tissue and intravasate into the blood, the cell experiences several changes. Increased mobility and the loss of adhesive proteins allow the cell to traverse the extracellular matrix components and the basement membrane in its initial location (2, 8-10). Many of these transformations are characteristic of the epithelial-mesenchymal transition (EMT), a process normally seen in embryogenesis that allows cancer cells to gain the motile phenotype coupled with the loss of distinguishing epithelial markers (11-13). The cell persists through phenotypic refinement, but without interaction with its environment, it would be unable to progress. An aggressive tumor cell is able to fight impediments to intravasation posed by the microenvironment such as hypoxia and an immune response using the tools at hand: stromal cells and their secreted factors are hijacked into both helping the tumor cell enter the blood stream as well as prepare the secondary environment for colonization (2). Similarly, once the tumor cell has left the primary environment and entered the blood, it can aggregate with platelets to avert the immune response and gain protection from the shear stress caused by fluid flow. But arrival at the secondary microenvironment does not guarantee proliferation as the cell may remain dormant or even die (6). Only a small percentage of these

tumor cells will ultimately grow into micrometastases, and of those micrometastases few still will proceed into full blown macrometastatic lesions. This process occurs in parallel to the development

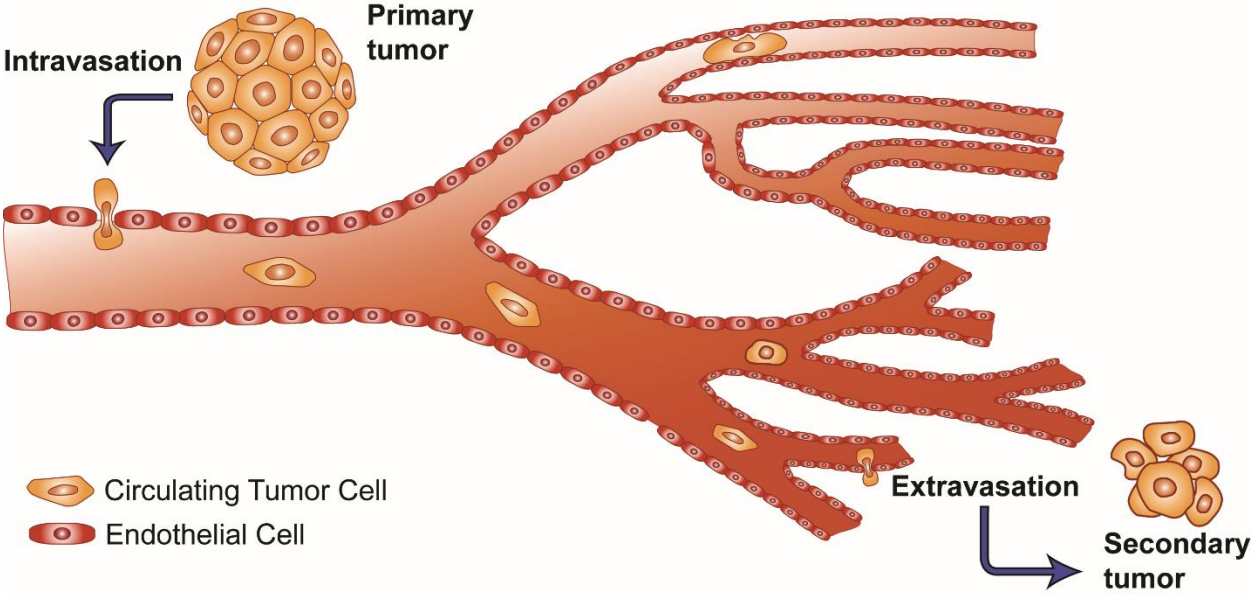

Figure 1-1 Schematic view of the metastatic process showing CTC transit: the CTCs exit the primary tumor, intravasate into the blood stream, circulate, and extravasate into a secondary site where they may ultimately achieve different fates including dormancy and full-blown metastasis.

of the primary tumor, and often before that tumor is initially detected (14). Very few of the initially disseminated cells complete the metastatic process (15), and yet it is these few cells lead that charge of cancer mortality. To be able to isolate and identify these cells is a clear direction of interest in cancer research (16, 17).

1.2 Circulating tumor cells (CTCs)

The ease of drawing blood coupled with the wealth of potential information about metastatic mechanisms make circulating tumor cells (CTCs) a tantalizing target for study, particularly given their clinical relevance. Several studies correlate CTC counts with various clinical time points including overall survival and progression free survival. Most of these studies set discrete cut-offs and have evaluated the associations within cohorts in cancers such as breast (18-20), colorectal (21-23), prostate (24), and melanoma (25). In some cases, these cut-offs have

been shown to better predict overall survival than traditional biomarkers such as the prostate specific antigen (PSA) (24). However, while CTCs have been used in American Society of Clinical Oncology (ASCO) recommendations (26), more widespread use of CTCs as prognostic indicators is hindered by the lack of Stage III clinical data (27). Difficulties in including CTCs as potential biomarkers in clinical trials include the low number of CTCs recovered (hindering downstream analysis), the inconsistent biological and molecular characterization of CTCs, and questions regarding the usefulness of CTC enumeration (28). Other open questions involve the nature of these spreading cells: do they travel as individual cells or as clusters (29). However, to address concerns regarding the use of CTCs, they first must be isolated for study.

1.3 CTC isolation technologies

To facilitate enumeration and isolation, various devices and technologies have been developed to capture CTCs. However, their operating principles are often at odds with heterogeneous and metaphoric nature of the cells of interest. While all technologies are broadly based in the principle of separating based on how CTCs differ from surrounding blood cells, be it in their surface marker expression or their relative size, each technology features advantages and drawbacks. On-going research in CTC isolation technologies seeks to address these downsides.

1.3.1 Commercially available CTC isolation technologies

1.3.1.1 FDA Approved Cell Search CTC Isolation Technology

Although tremendous progress has been made in the field of CTC isolation techniques in the past two decades, there are very few technologies that are commercially available for clinical and research use. One example is the CellSearch™ system (Veridex LLC), which was the first US Food and Drug Administration (FDA) approved system for the detection and enumeration of CTCs in metastatic breast (30), prostate (31), and colon cancer patients (22). Using magnetic beads

coated with antibodies against the epithelial cellular adhesion molecule (EpCAM), CellSearch™ isolated CTCs from the peripheral blood, after which they were fixed with 4% paraformaldehyde (PFA), immunostained with fluorescently labeled anti-cytokeratin (CK, an epithelial intermediate filament), anti-CD45 (a membrane antigen expressed by leucocytes), and DAPI (4',6-diamidino-2-phenylindole, a nuclear stain), and enumerated by automated cell image capture and analysis. Cells designated as CTCs were characterized by low eccentricity, size greater than 5 μm, a visible nucleus, positive staining for CK, and negative staining for CD45. To verify the accuracy, precision, and linearity of the CellSearch™ system, Allard *et al.* evaluated the number of CTCs per 7.5 mL of blood using spiked samples as well as in 145 healthy donors, 199 patients with nonmalignant diseases, and 964 patients with various types of metastatic carcinomas (32). The average recovery of SKBR-3 tumor cells spiked into 7.5 mL of blood was 85%. In blood samples from cancer patients, between 0 to 23,618 CTCs were recovered per 7.5 mL, with 36% of specimens yielding at least 2 CTCs.

CellSearch™ has been widely applied to the study of prostate cancer CTCs, though the numbers of CTCs isolated remains relatively low. In a study of 63 metastatic castrate resistant prostate cancer (mCRPC) patients (33), a median of 16 CTCs were isolated per 7.5 mL blood (range: 0-847 CTCs/7.5 mL) with 65% of patients having greater than 5 CTCs/7.5 mL This study also examined androgen receptor (AR) amplification through fluorescence *in situ* hybridization (FISH) and saw this amplification in five samples, all of which had over 50 CTCs/7.5 mL. Further immunofluorescence analysis detected EGFR in 18 of 20 assayed patients. Another study examined 120 CRPC patients with the CellSearch system, with 112 patients having "evaluable" CTC counts (median: 9 CTCs/7.5 mL), and found that baseline CTC counts were strongly associated with survival from the time of blood draw (34). There have been a number of subsequent

studies investigating the stratification into favorable and unfavorable categories (24); AR and MYC amplification (35); AR, ERG, and PTEN amplification, rearrangement, and loss (36); potential for use as a surrogate biomarker (37); and change in response to treatment (38).

While the CellSearch™ system represented a breakthrough in CTC separation technology both in principles and in clinical applications, it is not without room for improvement. Given the rarity of CTCs, higher recovery and sensitivity would be desirable for most applications. Additionally, increased purity and the isolation of viable cells would allow more downstream analysis that could be informative for the study of cancer biology and for use in personalized medicine. The system itself requires expensive equipment. This technology represents an innovative milestone in CTC research, but it is a platform upon which the body of literature can build.

1.3.1.2 Size Based Filtration Techniques

Based on his observation that tumor cells in the blood were often larger than other blood components such as erythrocytes, leukocytes, and platelets, Seal first used a simple sieve as a filter to separate what are now known as CTCs from the blood in 1964 (39). Isolation by Size of Epithelial Tumor Cells (ISET), a filtration technique commercially available as the Rarecells system®, was an improvement over previous filtration methods as it did not require a preliminary separation through techniques such as immunomagnetic and flow cytometric cell separation (40). Following dilution of the blood sample, the CTCs could be separated from the solution using a Track-Etch polycarbonate membrane with 8 μm diameter cylindrical pores. To characterize ISET, cells from liver, breast, cervical, and prostate cancer cell lines (HepG2, Hep3B, MCF-7, HeLa, and LNCaP) were spiked into 1 mL of peripheral blood. Captured cells could then undergo genetic analyses such as fluorescence *in situ* hybridization (FISH) and the polymerase chain reaction

(PCR). Efficacy of the system was further assessed using samples from primary liver cancer patients, with CTCs found in 23 of the 44 patients and none of the healthy control subjects (41). Cells were classified as CTCs based on size, nucleus to cytoplasm area ratio, and nuclear irregularities. Primer extension pre-amplification (PEP) and PCR were performed on the separated tumor cells as proof of ISET's applicability in cancer study.

Modifications to the filtration process are an area of continuing research, with advances being made in both the materials used and their fabrication (discussed below). This further optimizes a technique that allows viable cell separation for staining and morphological observation as well as an immediate platform for cell culture. However, most filtration methods are still plagued by inconvenient preprocessing steps such as dilutions, flow cytometry, and immunomagnetic separation, which also affect overall throughput. Membrane clogging can result in issues with purity, while variability in CTC size can lead to the loss of these rare cells.

1.3.1.3 Other commercially available systems

The Epic Platform makes use of high throughput imaging based analysis without enrichment from surrounding white blood cells. To prepare samples using the Epic Platform, samples undergo red blood cell lysis and centrifugation, after which the entirety of the resulting supernatant is mounted on a series of slides. These slides may be stained for standard CTC makers, i.e. cytokeratin, CD45, and DAPI. The slides are then fluorescently scanned and analyzed using an algorithm that assesses fluorescence levels and morphology to identify CTCs. This method detected CTCs in 39 out of 46 mCRPC samples during validation (42). Subsequent studies investigated the presence of the AR splice variant AR-V7 in a cohort of 161 patients (43) and AR expression, PTEN deletion, and ERG rearrangement (44). This last study also detected clusters in

7/41 patients. Due to the high contamination by white blood cells and the preparation of the samples as slides, studies performed using this technology are limited to imaging based analysis.

1.3.2 Microfluidic CTC isolation technologies

Microfluidic devices provide innovative solutions to logistical problems, affording the advantages of high sensitivity, low cost, low reagent usage, small size, and several established fabrication techniques (45). Operating on this length scale allows for laminar flow, yielding parallel streamlines with minimal mixing resulting only from diffusion (46). In general, these labs-on-a-chip or micro total analysis systems (μTAS) consist of several elements from the microfluidic tool box including pumps, valves, reservoirs, and mixers, in addition to other thermal and electrical components (47). Devices are often constructed from glass or silicon substrates, however the low expense and plethora of simple fabrication methods have led to the development of a number of polymer-based devices (46). PDMS (polydimethylsiloxane) in particular has emerged as a fundamental material in microfluidics, facilitating inexpensive prototyping (48). Arising from an array of small scale analytical techniques (45), an early biological application of microfluidics was a device that performed PCR, improving upon large-scale methods by decreasing the time of each step (49). Other applications include on-chip molecular separation, protein analysis, immunosensing, and electronics cooling (50). Given the many benefits of microfluidics, including a length scale amenable to cellular analysis, it is unsurprising that microfluidic devices are a staple in CTC isolation and analysis (**Figure 1-2**).

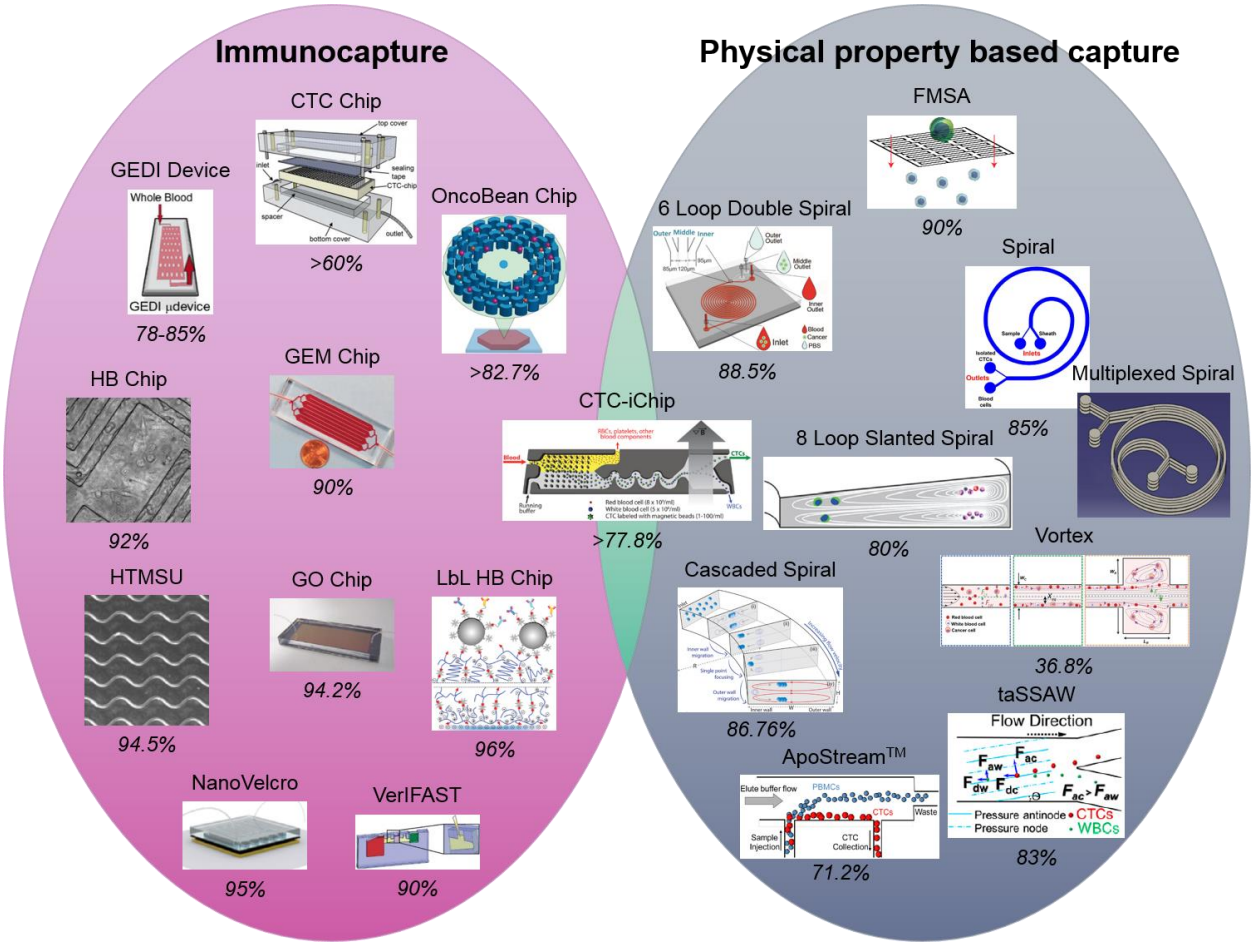

Figure 1-2 Microfluidic CTC isolation technologies. Examples of antigen based (immunocapture) and physical property based separation in microfluidic systems. Percentages denote capture efficiency as determined through cell line optimization. (1, 2)

1.3.2.1 Microscale CTC isolation based on physical properties

CTCs also differ from blood cells in size and deformability, offering molecular marker-independent, high-throughput, and inexpensive options for isolation. CTCs are generally larger and stiffer than WBCs, leading to the early use of commercial filters (51, 52). To solve problems with earlier filters including fixation requirements, non-uniform pore sizes, and low pore density, the separable bilayer (SB) microfilter was microfabricated by etching parylene polymer via reactive ion etching to precisely control pore sizes and density (53). Parylene is ideal for this application because it is mechanically strong while still malleable, with good biocompatibility and low membrane fouling. The bilayer design consisted of a bottom layer with 8 μm pores and a top

layer with 40 μm pores, trapping CTCs between the two layers that could be separated easily, leaving CTCs accessible. A flexible micro spring array (FMSA) was designed as a high-porosity filter (54) capable of processing 7.5 mL whole blood without clogging while still preserving viability. CTCs were detected in 76% of clinical samples from breast, colorectal, and lung cancer patients. Microclusters and multinucleated CTCs were enriched from patients from all three cancers.

An alternative approach to separation exploited unique properties of particles moving in microchannels. Under laminar flow, deterministic lateral displacement (DLD) within an array of microposts has been used to separate particles of different sizes (55). Depending on the geometry of the microarrays, particles above and below a certain size follow different and predetermined migration paths. The CTC-iChip utilized DLD to first separate nucleated cells (CTCs and WBCs) from red blood cells (RBCs) using an array of microposts with 32-μm gaps (56). When flowing through the device, small cells like RBCs remained along their original streamlines, whereas larger cells like CTCs and most WBCs were fully deflected into the coincident running buffer stream by the end of the array.

Other separation approaches exploited inertial forces. Within microchannels, particles of different sizes can migrate across streamlines to focus at different positions due to the shear induced lift force and the wall induced lift force. In vortex technology, cells of various sizes are aligned by size in different streamlines in straight channels by inertial focusing followed by multiple expansion-contraction reservoirs to create laminar microvortices that can trap large cells within reservoirs (57). As cells entered the expanding regions, wall lift forces were diminished and cells mainly experienced lateral lift forces, which are proportional to the cell volume. The larger

lift forces on CTCs pulled them into the vortices while other blood cells experiencing smaller forces passed through the vortex and remained in the main stream.

Curvature in microchannels causes particles to experience an additional lateral Dean drag force because fluids in curved channels develop a secondary lateral flow. The combination of the inertial lift force and the Dean force leads to particle migration which can result in high resolution separation. Single spiral, double spiral, cascaded spiral, and slanted spiral structures have been designed and optimized to maximize separation efficiency for various parameters including channel length, height, width, radius of curvature, and flow rate (58-61). Generally, near the outlet of spiral devices, larger CTCs focus near the inner wall due to the combination of the inertial lift force and the Dean drag force. To this end, Hou *et al.* designed a multiplexed spiral device that detected CTCs in clinical samples from breast and lung cancer patients (62).

CTC enrichment by size offers a fast, inexpensive, and label-free way to harvest CTCs. However, as there is a wide range of CTCs sizes, sized based separation often suffers from low purity and the risk of losing smaller CTCs. Additionally, size based separation often requires preprocessing of blood, like RBCs removal and further, dilution or runs the risk of device clogging. To date, size based technologies have shown proof-of-concept clinical validation but have not been applied in large scale clinical or biological investigation.

Other separation methods based on physical properties include the interplay of dielectrophoresis (DEP) forces and inertial forces in microfluidic devices to lead to different patterns of cell migration to viably separate cells (63). Similarly, acoustophoresis causes particles within the fluid to move toward regions with minimal acoustic radiation forces in distinct migration patterns (64, 65). Although promising, approaches like DEP and acoustophoresis have

the disadvantages of low throughput, low sensitivity and purity, and additional required steps like RBC lysis and may require further clinical validation.

1.3.2.2 Microfluidic immunoaffinity based CTC isolation

The alternative to separation of CTCs based on size is their separation based on cell surface marker expression. Nagrath *et al.* pioneered a silicon-based microfluidic device for the immunocapture of CTCs from cancer patient blood samples (66). This device featured viable cell isolation in addition to lacking sample preprocessing steps. The CTC-chip had an array of 78,000 silicon microposts which were subsequently coated with anti-EpCAM capture antibodies. The optimal flow rate was determined to be 1-2 mL/hr in order to maximize the capture efficiency, which was greater than 60% for the NCI-H1650 cells spiked into whole blood. As the normalized number of CTCs recovered from the blood has been correlated with efficacy of treatment (67), demonstrating an emerging clinical significance of the enumeration of CTCs, CTCs were enumerated in samples from 68 patients with non-small-cell lung (n=55), prostate (n=26), pancreatic (n=15), breast (n=10), and colon (n=10) cancers. Using fluorescent staining, CTCs were identified as those stained cells with DAPI+/CK+/CD45-, and were detected in 115 of 116 (99%) samples. While the number of CTCs in a patient sample did not reflect the size of the primary tumor, it did correspond to the patient's response to treatment. Because of its high yield, sensitivity, specificity, and clinical relevance, this chip represented great strides in the field of CTC isolation. The research team went on to show further clinical applications using the Scorpion Amplification Refractory Mutation System (SARMS) technology to identify the T790M mutation in the epidermal growth factor receptor (EGFR) (68). This mutation is associated with tumor resistance to tyrosine kinase inhibitors, and the data gained from this study could potentially be used to determine the appropriate course of treatment. Using the CTC-chip, CTCs were isolated from non-

small-cell lung cancer patient samples for analysis and compared with results from the primary tumor as well as free plasma DNA. The mutation was found in the CTCs of 11 of 12 patients whose primary tumors featured this mutation and the free plasma DNA of 4 out of these 12 patients. Increased CTC counts were correlated with tumor progression and further EGFR mutations. This demonstrated the utility of an immunocapture micropost device in a noninvasive genotyping procedure.

In addition to the circular posts used by Nagrath *et al.*, microposts on silicon chips have been designed to optimize capture through the manipulation of streamlines using alternative post geometries. Termed geometrically enhanced differential immunocapture (GEDI) (69), octagonal posts were staggered to maximize collisions with cells. The immunocapture aspect was achieved with a monoclonal antibody against the prostate-specific membrane antigen (PSMA), J591, and as such, the device was characterized with the LNCaP prostate cancer cell line. Applications of this device were demonstrated by performing capture with prostate cancer patient samples, as well as proof-of-principle *ex vivo* drug testing using the taxanes docetaxel and paclitaxel (70). The device has been additionally functionalized with antibodies against HER2 to capture cancer cells known to have this membrane receptor upregulated (71). Following the selection of the most optimal anti-HER2 antibody, the device was characterized with high and low HER2-expressing breast cancer cell lines, yielding capture efficiencies of 78% and 26% respectively. Clinical efficacy was verified through the analysis of nine blood samples from five breast cancer patients and two gastric cancer patients with an average of 74 CTCs/mL identified in breast cancer patients and 120 CTCs/mL in gastric cancer patients.

In another example of silicon structures, pillars were deep reactive ion etched into a silicon wafer to form a capture surface which was then anodically bonded to glass wafer patterned with

microfluidic chambers, a capture and recovery chip (CRC) (72). This CRC was functionalized with streptavidin to capture cells pretreated with hybrid nanoparticles (HNPs) consisting of an antibody, a quantum dot, and biotinylated DNA, which bound to the avidin on the surface. Three different HNPs were prepared, each with a different antibody (anti-EpCAM, anti-EGFR, or HER2), quantum dot (Qdot(525 nm), Qdot(565 nm), or Qdot(625 nm)), and DNA sequence, allowing the specific marking and release of different breast cancer cell lines. Respective quantum dot fluorescence ratios were reflective of established cell line expression patterns, and cell spike experiments using whole blood yielded capture efficiencies of 81.3%, 91.2%, and 90.0% for the cell lines MCF-7, SKBR-3, and MDA-MB-231, with identification accuracies of 94.7%, 99.3%, and 83.3% based off said fluorescence patterns. Using restriction enzymes, cells were released into 96-well plates with efficiencies of 78.6%, 93.7%, and 86.0%, where they were able to adhere and proliferate.

In contrast to the silicon based substrate used with the original CTC-chip, glass is an attractive substrate for CTC capture chips due to its transparency for clear imaging, allowing for a wide variety of light microscopy based techniques yielding both bright field and fluorescent images. Shortly after the advent of the CTC-chip, the Toner group released a herringbone CTC capture chip that made use of passive mixing to increase encounters between flowing cells and anti-EpCAM-functionalized PDMS microchannels (73). The creation of microvortices was induced in this “Herringbone-chip” through chevron patterns on a PDMS ceiling, disrupting streamlines and increasing the capture efficiency. Once tethered to the chip through the antibody-antigen interaction, cells could be stained for DAPI, CK, and CD45. The capture efficiency for prostate cancer cells (PC-3) spiked into whole blood was 91.8%, with 14% purity and 95% viability. The device was further tested with metastatic prostate cancer patient samples, with 93%

detection rate. The optical transparency of the glass allowed for further analysis in the form of fluorescence *in situ* hybridization (FISH) to determine androgen receptor copy number in LNCaP cells. Off-chip analysis included RNA isolation for real-time PCR (RT-PCR), allowing the identification of a specific TMPRSS2-ERG translocation. The utility of the Herringbone-chip was demonstrated through its use in a study of the epithelial-mesenchymal transition (EMT) in breast cancer CTCs (74). Using multiple capture antibodies, anti-EpCAM, anti-EGFR, and anti-HER2, CTCs were isolated and subjected to RNA *in situ* hybridization, showing the presence of mesenchymal marker-displaying CTC clusters as well as the epithelial to mesenchymal spectrum of CTCs.

Herringbone micromixers have been optimized in a geometrically enhanced mixing (GEM) chip to increase throughput and purity in anti-EpCAM immunocapture (75). By increasing the width of the grooves within the micromixer, purity was increased to 84% for pancreatic cell line (L3.6pl) cells spiked into whole blood. However, a high number of white blood cells were present when patient samples were analyzed, leaving room for additional optimization. As CTCs were detected in 17 of 18 patients studied, and CTC number corresponded to tumor size in three stage IV metastatic pancreatic cancer patients analyzed over the course of treatment, this technology appears to hold promise for use in the clinical setting.

Another device from the Toner group, the CTC-iChip, took advantage of multiple modes of separation (56). Samples were labeled with magnetic beads before introduction to the chip, at which point running buffer diluted the sample while performing initial separation based on cell size. Remaining cells were then aligned using a focusing channel for ultimate magnetic separation. The device could be operated in either positive or negative selection mode based on the choice of antibody conjugated to the magnetic bead. Positive selection was performed using beads with

antibodies to select CTCs, while negative selection selected for white blood cells, leaving all unlabeled cells for further analysis. Isolated cells could undergo a wide spectrum of analysis including immunofluorescence, hematoxylin and eosin, and Pap staining; FISH; and gene expression analysis. Over the course of the study, patient samples were processed from breast, lung, prostate, pancreatic, colorectal, and melanoma cancers.

The VerIFAST system (76) is another magnetic bead-based microfluidic technology that was designed with an emphasis on practical operation. Following incubation with antibody conjugated paramagnetic particles, magnetically labeled cells could then be dragged through oil pinning wells using a handheld magnet, bringing target cells through to the next stage while blood cells remained in the input well. Following incubation in the staining well, the cells could be moved to a sieve well where magnetic particles were removed and any intracellular staining was conducted. This technique was applied to blood and lavage samples, allowing staining for TTF-1 and EGFR. While limited to staining applications, the VerIFAST used immunomagnetic separation and the lack of interaction between oil and aqueous solutions to streamline the capture and staining process. This technology has since been updated, renamed, and applied to 26 prostate cancer patient samples (77), detecting CTCs in 25/26 patients (range: 0-1213 CTCs/7.5 mL blood). RT-qPCR was performed for 12 genes, and androgen receptor splice variants were detected.

Poly(methyl methacrylate) (PMMA) can serve as an alternative to silicon or polystyrene as a substrate for microfluidic CTC capture and analysis devices due to its low cost and excellent optical transparency. Polymers such as PMMA are advantageous due to their amenability to convenient fabrication techniques such as hot embossing and injection molding. Carboxylic acid groups can be selectively generated on the surfaces of PMMA by UV exposure to explore electroless deposition, protein concentration, and cancer cell capture (78). Increased roughness can

be induced using high intensity light, providing increased surface area for functionalization. Additionally, thermal bonding occurs at low enough temperatures to preserve these microfeatures (79). Using these properties of PMMA, a high throughput microsampling unit (HTMSU) was developed. The HTMSU was functionalized with anti-EpCAM monoclonal antibodies for capture and included a conductivity sensor which enabled enumeration. The device was initially characterized with MCF-7, SW620, and HT29 cells (breast and two colorectal cell lines, respectively), showing the potential for cell release *via* trypsin and cell analysis using the polymerase chain reaction (PCR) and ligase detection reaction (LDR) (79, 80). The benefits of the high aspect ratio features of PMMA are not limited to antibody capture. The anti-EpCAM monoclonal antibodies were exchanged for RNA aptamers against the prostate-specific membrane antigen (PSMA) for tissue-specific recognition (80).

Cyclic olefin copolymer (COC) has the advantages of PMMA in addition to having increased optical transmissivity; the implication of this is increased UV activation-produced carboxyl groups for increased capture antibody presentation, yielding higher capture efficiencies and purities (81). This polymer was used as the substrate for a high throughput (HT) CTC selection module that comprises a component of a CTC isolation and analysis system (82). Following capture in high aspect ratio sinusoidal anti-EpCAM functionalized microchannels, CTCs were released using trypsin. The cells flowed across an impedance sensor embedded in PMMA for enumeration into a 2D array fabricated in PMMA for staining and confined imaging. The capture efficiency for the selection module was dependent on channel length, with an overall average of 83.1% and a maximum of greater than 90%. Collection efficiency of the staining and imaging module was determined by comparing stained cells with numbers generated by the impedance sensor. Fixed cells were collected with higher efficiency than unfixed cells (96% vs. 85%). A lower

collection efficiency of 72% was exhibited by analyzed pancreatic ductal adenocarcinoma (PDAC) patient samples, possibly a result of the 15% misclassification rate inherent in the impedance sensor due to the enumeration of white blood cells. Samples analyzed from metastatic and local PDAC patients averaged 53 and 11 CTCs/mL respectively with a high purity of 86%, although cell viability was negatively affected by trypsinization.

The integration of microfluidics represents a dramatic change in the CTC separation paradigm, allowing for increased purity, yield, and sensitivity when compared to the CellSearch™ system. However, in the interest of increasing these metrics, researchers have increasingly turned to the incorporation of nanomaterials in addition to the use of microfluidics. Through interaction on the scale of extracellular structures, increased capture agent presentations, and the ability to transition to capture agent independent methods, nanomaterials provide the advantages necessary to take these next steps in CTC research.

1.3.3 CTC Devices Incorporating Nanomaterials

1.3.3.1 Magnetic Nanoparticles

Magnetic nanoparticles (MNPs) can be used to take advantage of surface expression as well as innate physical properties of the cell. Following the exchange of blood plasma for dilution buffer, MNPs functionalized with anti-EpCAM were used to bind selected cells in the presence of a magnetic field in a reversibly bonded PDMS chamber using NdFeB block magnets (83). The PDMS was then removed, facilitating microscopy. Cells were stained for CK, CD45, and DAPI and evaluated using computer automation with 90% capture ratios observed for spiked cell lines. An additional example of immunomagnetic separation included a dynamic set-up to minimize cell aggregation and settling while maximizing capture (84). Using a magnet which was positioned in direct contact with the microchannel (with the exception of the inlet, preventing accumulation),

cells labeled with Fe_3O_4 MNPs were separated in up to six devices that were rocked and repositioned during flow. Staining was performed with DAPI, anti-CK, and anti-CD45. Characterization with Colo205, PC-3, and SKBR-3 cell lines yielded 97%, 107%, and 94% capture ratios. Devices tested with patient samples showed comparable results to portions of those same samples exported to CellSearch™ for comparison. Like the Herringbone-chip, cell clusters were found.

The inherent properties of the MNPs themselves have been exploited to characterize CTCs. Through the immunolabeling of three different sizes (10, 12, and 16 nm) of MNP with various biomarkers, a cell expressing those biomarkers can in turn be labeled with these MNP complexes (85). Levels of expression can be detected due to the directly proportional relationship between the magnetic moment of the targeted cell and the number of bound MNPs. Biomarker expression was determined by the magnetization curve representative of the different MNP sizes. Using a micro-Hall detector to detect the magnetic moments of cells in a solution, Issadore *et al.* counted CTCs from patient blood. MNP-complex-labeled cell solutions were processed through a microchannel array featuring a chevron ceiling, focusing the cells toward the bottom center of the channel over the implanted micro-Hall detectors. The four biomarkers (HER2/neu, EGFR, EpCAM, and mucin-1) detected CTCs in all 20 ovarian cancer patients whereas CellSearch™ performed on samples from those same patients only found CTCs in five. This same four-biomarker panel was used with a novel bioorthogonal nanoparticle detection (BOND) strategy to amplify cell labeling by immunolabeled MNP, to allow detection by a micro-nuclear magnetic resonance (μNMR) platform, as described in a recent review (86).

Separation of CTCs from the blood through use of immunomagnetic nanobeads was achieved through lateral magnetophoresis, allowing for high throughput and purity (87).

Microchannels were molded in SU-8 photoresist above ferromagnetic wires. Pre-immunomagnetic nanobead labeled blood and buffer were introduced in two separate inlets and converged in the main channel, flowing above the wire-containing substrate. The application of a magnetic field drew the labeled cells into a separate smaller outlet from the larger outlet into which the blood cells naturally flowed due to the laminar nature of the channels. This setup led to 90% recovery in cell spike solutions and an average of 85% and 83% purities for 3 breast and 3 lung cancer patient samples respectively. Downstream analysis was demonstrated through the RT-PCR detection of thyroid transcription factor-1 (TTF-1) expression levels in the isolated cells.

MNPs were also strategically self-assembled for use in CTC capture, detection, and downstream analysis (88). Layer-by-layer assembly was used to coat nanospheres with alternating layers of poly(ethylene imine) and MNPs. A series of reactions ultimately presented carboxylic acid groups on the surface of the magnetic nanospheres, allowing for NHS/EDC chemistry to be used for functionalization with anti-EpCAM. Characterization with 100 cells/mL spiked into whole blood of EpCAM-expressing cell lines showed capture efficiencies of greater that 92%. 90.5% of captured cells were viable and could be cultured *in vitro*. CK19 and EGFR mutations could be detected through RT-PCR. Varied volumes of blood samples from patients with colon, liver, lung, and breast cancer patients were analyzed, with CTCs being detected in all.

Immunomagnetic labeling was combined with a magnetic sifter for high throughput (10 mL/hr) cell capture and subsequent release (89). In the presence of a magnet, samples prelabeled with anti-EpCAM-conjugated MNPs were drawn to the edge of the 40 μm pores in a silicon nitride membrane that was coated with an 80% nickel 20% iron permalloy; unlabeled cells continued through. Release occurred following the removal of the magnet and a buffer wash, releasing 92.7% of captured cells. Between 31 and 96 CTCs/mL were detected in each of six non-small-cell lung

cancer patients. Using antibodies specific to wild type and mutated EGFR, additional analysis could be performed by applying extracted membrane proteins to a magneto-nanosensor biochip.

Using genetic engineering techniques, Maeda *et al.* were able to harness the cellular machinery of the bacterium *Magnetospirillum magneticum AMB-1* to modify its naturally-produced nanoscale bacterial magnetic particles (BacMPs) (90). The BacMPs were enclosed in a membrane which has a number of integral proteins that can be used in gene fusion to effectively conjugate a desired protein to the BacMP. Maeda *et al.* fused the biotin carboxyl carrier protein (BCCP) as well as Protein G to the bacterial protein Mms13. Streptavidin conjugated with a quantum dot bound the expressed biotin, functionalizing the particle for imaging. To perform cell capture, the solution of interest was incubated with an anti-EpCAM antibody followed by mixing with the nanocomposite, which bound the constant fragment of the antibody with the fused Protein G. A magnetic separation was performed, yielding 92% recovery in experiments using cell lines.

As shown by these examples, the nanoscale affords a breadth of advantages not available to traditional magnetic methods. Cellular internalization, signature size-based characteristic magnetic curves, and natural production and scale-up are several features that can be exploited by operating in the nano regime.

1.3.3.2 Nanopillars, Nanowires, and Nanofibers

The ability of cell surface components to interact with nanofeatures due to their mutual scale is a fundamental asset in the biological application of nanotechnology (91). The fabrication of such elements for cell capture has been performed using multiple materials in several structures.

Silicon was etched or deposited into nanopillars or nanowires to increase surface contact with extracellular features. Wang *et al.* used a silver and hydrofluoric acid etching process to create a surface of silicon nanopillars (SiNP). After attaching streptavidin through NHS/maleimide

chemistry, biotinylated anti-EpCAM was coupled, joining the capture antibody to the SiNP (92). The capture efficiency of SiNP modified substrates (45-65%) was up to ten times higher than that of the flat silicon substrates (4-14%). The effect of SiNP length on capture was tested, resulting in speculation that the optimized lengths corresponded to lengths amenable to interaction with extracellular structures. Having optimized the substrate with MCF-7 cells spiked into whole blood, a SiNP surface was used in conjunction with a chaotic micromixer for both cell line and patient sample CTC capture (93). The results from patient sampling were compared with CellSearch™ analysis, and showed a marked improvement over this established method, detecting CTCs in 20 out of 26 patients while CellSearch™ found CTCs in only 8 of those patients. Using a chemically-etched silicon nanostructured surface with similar dimensions under the name silicon nanowires (SiNW), Hou *et al.* were able to conjugate a temperature sensitive polymer, poly (N-isopropylacrylamide) (PIPAAm), to the high surface area substrate, designated SiNWS, allowing for controlled release of captured CTCs (94). Further conjugated with anti-EpCAM antibodies, the functionalized SiNWS-bound PIPAAm facilitated cell capture at a ratio of over 70% of labeled MCF-7 cells spiked into blood and 90% cell release for 1000 MCF-7 cells/mL with 90% viability.

The role of the antibody as a capture moiety may be assumed by DNA aptamers. These aptamers were conjugated to the elements of a silicon nanowire array (SiNWA) to isolate CD4+ T lymphocytes (95). In addition to showing increased specificity as a result of both the aptamers and the nanostructured surface, the application of exonuclease I allowed for the release of 97% of captured cells with 90% viability. A similar method of rare cell capture and release *via* DNA aptamers of cancer cells was put forth as an update to the NanoVelcro Chip (96). This device was validated using the non-small-cell lung cancer (NSCLC) cell line A549, and release was conducted with the enzyme Benzonase Nuclease. Increased purity was achieved through a second

capture/release pass through the device, resulting in greater than 95% purity. The clinical utility of this method was demonstrated through genetic analysis of the released cells, using PCR and Sanger sequencing to reveal a mutation characteristic of A549 cells, $KRAS^{G12S}$.

Nanofabrication can also be conducted with titanium oxide, which can be electrospun into nanofibers of 100 to 300 nm diameter (97). Horizontally oriented as opposed to the vertical orientation of the nanoposts and nanowires described above, titanium nanofibers (TiNFs) provide a scaffold for CTC capture. Zhang *et al.* fabricated TiNFs from a spun composite of titanium n-butoxide (TBT) and polyvinyl pyrrolidone (PVP). Through 3-mercaptopropyl trimethoxysliane (MPTMS) and N-maleimidobutyryloxy succinimide ester (GMBS), streptavidin was joined to the fiber, with biotin/avidin chemistry being exploited to join a biotinylated anti-EpCAM to the surface to enable cell capture. Performance was verified using samples from gastric and colorectal cancer patients. SEM imaging displayed cell spreading and the interaction of cellular structures with the nanostructures on the substrate surface.

Electrospinning was used to coat a laser microdissection slide with poly(lactic-*co*-glycolic acid) (PLGA) nanofibers, yielding a transparent capture surface with the advantages of a nanostructured surface (98). For melanoma-specific capture, biotinylated anti-CD146 is presented by streptavidin linked to the PLGA nanofibers by NHS chemistry. The device was characterized using the melanoma cell line M229, with an 87% capture efficiency when cell suspensions were flowed at 1 mL/hr, with a slightly higher capture ratio when operated at 0.5 mL/hr. Two patient samples demonstrated the clinical application of this device as well as potential for downstream analysis. Following four biomarker immunocytochemical analysis which detected 43 and 36 CTCs, individual cells could be extracted by laser microdissection for subsequent whole genome

analysis and Sanger sequencing. This allowed for the detection of the $BRAF^{V600E}$ mutation, which is highly relevant in the use of therapeutic BRAF inhibitors.

Through various chemical fabrication methods and coupling chemistries, a wide array of substrate surface structures has become available for use in CTC research. Nanopillar, wire, and fiber geometries exploit both size scale and high surface area to increase the interface between capture substrates and cellular structures, improving upon capture with specific antibodies alone.

1.3.3.3 Nanoroughened Structures

The adhesion preference of CTCs differs from that of blood cells, making nanoroughened surfaces an alternative technique for CTC capture (99). Nanoroughened surfaces increase the surface area available for adhesion, binding, and reactions. Through deposition, molding, and etching, nanoroughened surfaces have been fabricated to facilitate capture and post-processing of rare cells, including CTCs.

The ability of RNA to reveal the tissue of origin or mutations associated with cancer progression makes it an important resource in CTC investigation. As such, its isolation and analysis is an area of interest that can be aided by the use of nanoroughened surfaces. Following the extraction of RNA from magnetic bead-captured CTCs, Ivanov *et al.* were able to recognize the cells as originating from the prostate by using electrodes covered in peptide nucleic acid probes for prostate specific antigen (PSA) RNA (100). The cells were further characterized by including probes for TMPRSS/ERG Type III, a gene fusion commonly found in prostate cancer. To increase the presentation of probes on the surface of the electrodes, a nanostructured surface of palladium was deposited by electroplating. The increase in binding of RNA due to the increased accessibility allowed for a lower detection limit, which is especially desirable given the small population size of CTCs. RNA binding was sensed by the electrodes when the local increase in negative charge

created an electrochemical signal through interaction with an electrocatalytic solution of $Ru(NH_3)_6^{3+}$ and $Fe(CN)_6^{3-}$. The efficacy of this technology was shown using prostate cancer patient samples in an attempt to correlate CTC levels with Gleason score.

The established interactions between cell surface features and nanoscale structures suggest the possibility of capture without the use of a specific capture moiety. Chen *et al.* exploited the selective adhesion of cancer cells to nanotextured surfaces when compared with blood cells by reactive ion etching a glass surface for use in CTC capture (99). Increased roughness correlated with increased capture, while the conjugation of anti-EpCAM to the nanoroughened surface was not shown to make a significant difference in capture for increasingly roughened surfaces. The use of selection by EpCAM expression causes a significant loss of information within CTCs due to the inherent selection of a specific EpCAM-expressing population of cells that may not give a complete picture of the cancer. By using nanoroughened surfaces, the use of capture antibodies is not necessary, showing the potential of nanoscale features to capture a metamorphic population of cells.

When every additional cell captured represents a significant increase in the amount of information that can be obtained, the ability of nanoroughened surfaces to increase capture yield through increased surface area for aptamer and antibody binding and display or through direct capture of the cells *via* extracellular structure interaction shows their promise in the expanding field of CTC research.

1.3.4 Graphene Oxide Chip

Graphene oxide is a promising material as a component in applications such as delivery of water-insoluble cancer drugs (101), biosensors for bacterium assays and DNA detection (102, 103), energy-storage materials (104, 105), paper-like materials (106, 107), and polymer

composites (108, 109). It is a derivative of graphene with oxygen functional groups on its basal planes and edges. Converting graphene oxide to graphene is one method used to manufacture graphene (108, 110). Ruoff's group demonstrated a solution-based approach to obtain individual graphene oxide sheets involving chemical oxidation of graphite to hydrophilic graphite oxide, followed by exfoliation through ultrasonication in water (111). Graphene oxide has certain advantages for biological applications. It is easy to functionalize graphene oxide through polyethylene glycol (PEG)-based chemistry (112). Additionally, graphene oxide particle size can be controlled by sonication time and filtration (113). Furthermore, the optical transparency of graphene oxide is one of its promising characteristics for biological and medical research, allowing for improved imaging (114).

Yoon *et al.* demonstrated the graphene oxide chip for sensitive capture of CTCs (115). Graphene oxide nanosheets functionalized with polyethylene glycol (PEG) were able to self-assemble on a gold-patterned silicon surface through use of a positively charged intercalating agent (116, 117). A series of linker chemistries including crosslinker and biotin-avidin chemistry were then used to ultimately functionalize the substrate with an anti-EpCAM antibody. To characterize the graphene oxide chip, MCF-7, Hs-578T, and PC-3 cell lines were spiked into buffer or blood and flowed through the chip. The captured cells were cultured on the patterned gold surface with graphene oxide sheets, making use of the advantageous virtually two-dimensional capture surface. Blood samples from patients with breast, pancreatic, and early lung cancer were processed on the graphene oxide devices and 2-23 CTCs/mL were captured. Additionally, RNA was purified from breast cancer patient samples and analyzed for relative HER2 expression levels using RT-qPCR. Due to the high sensitivity of this device coupled with its potential for downstream analysis, this device is ideal for the study of CTCs in genitourinary cancers.

1.4 Applications of CTC isolation technologies

While many technologies have been put forth to address the challenge of CTC isolation, their utility will only be fully realized as those technologies are incorporated into medical research and practice, such as use in early detection, serial monitoring of response to treatment and disease progression, and biological study. The collaboration between the technology developers and clinicians is both the foundation of this field and the path to its future. To ensure the clinical utility of subsequent technologies, most new CTC technologies include at the very minimum enumeration analysis of clinical samples from various cancers.

Enumeration of CTCs can serve multiple purposes, including attempts to correlate with progression and surrogate endpoints as in the studies using CellSearch. Another potential application of CTC enumeration is in early disease detection. The GEDI platform has been used to sample for CTCs in three cohorts with the aim of assessing the potential for early detection, including patients with precancerous cystic lesions, patients with pancreatic ductal adenocarcinoma (PDAC), and a control group (118). Using a cut-off of three CTCs/mL, there was no detection in the control, while at least this level of CTCs was detected in 33% of patients with cystic lesions and 73% of patients with PDAC. Based on the disease trajectory of these patients with precancerous lesions, future studies could show the utility of this device for use in a cancer that desperately needs new techniques for early detection.

The relative ease of serial blood sampling compared with multiple invasive biopsies points to the potential value of CTC isolation technologies to serially monitor patient progression and response to treatment. The HTMSU has been used to try to correlate CTC burden with disease burden using a patient-derived xenograft (PDX) mouse model of PDAC (119). CTCs were enumerated pre-and post-treatment, and while there was not a statistically significant correlation

between CTC number and tumor volume, there was a correlation between the change in CTC counts and the change in tumor burden. Additionally, those mice undergoing treatment with BKM120, a phosphatidylinositol-3-kinase inhibitor, showed a decrease in CTC burden. In humans, the GEM chip was not only verified with pancreatic patient samples but was also used to serially monitor CTC burden over the course of multiple treatment cycles in three patients, showing correlation tumor size as measured by CT scans (75). Response to gefitinib treatment in one lung cancer patient was monitored using the NanoVelcro technology, both by assessing the CTC burden and radiographically assessing the tumor size, as well as by conducting whole genome amplification and Sanger sequencing to detect relevant mutations in EGFR (120).

As shown in the last example, enumerating CTCs may only be the tip of the informational iceberg, with genomic, expression, and proteomic analysis likely being able to provide insights into the fundamental mechanisms of how cancer spreads. The Hb Chip functionalized with an antibody cocktail including anti-EpCAM, anti-EGFR, and anti-HER2 has been used to study RNA levels of transcripts associated with various points on the spectrum of EMT in breast cancer patient CTCs (74). RNA *in situ* hybridization (ISH) was used to visualize epithelial transcripts (keratins 5, 7, 8, 18, 19 as well as EpCAM and cadherin 1) and mesenchymal transcripts (fibronectin, cadherin 2, serpin peptidase inhibitor clade E). The varying levels were tracked in patients as they underwent treatment and increased mesenchymal marker expression was associated with clusters of CTCs. Additionally, RNA was sequenced yielding the discovery of enriched transcripts for ECM proteins, therapy resistance signatures, and transforming growth factor β (TGFβ) found in mesenchymal and clustering CTCs. CTCs isolated from a mouse model of pancreatic cancer using the CTC-iChip have undergone single cell RNA sequencing, also showing high expression of ECM proteins such as SPARC (121).

However, a major limitation to the study of CTCs is their rarity, and even 100% efficient separation would still yield few cells. Consequently, an area of emerging investigation is to culture these cells *ex vivo*. A technique to culture isolated cells on-chip has been optimizing using a modified CTC Chip, a mixture of collagen and Matrigel, and fibroblasts for coculture (122). Successful expansion was achieved in 14 out of 19 lung cancer patients assessed for this purpose. Cultured CTCs were released with trypsin for further analysis such as transwell invasion assays and next-generation sequencing. CTCs isolated using the CTC-iChip have also been cultured as spheres under hypoxic conditions in a serum-free media containing growth factors, although this technique only showed success in 6/36 attempts (123). These cells could then be stained using immunofluorescence and IHC and could undergo next-generation sequencing, revealing several relevant mutations. Additionally, these mutations were used to develop a drug testing regime to target these treatments. The use of cultured CTCs for functional testing and therapeutic guidance represents the crossing into the next frontier of CTC research, where the results of CTC analysis can be used to characterize an individual's disease to optimize treatment.

Continuing this thrust of using CTC isolation technologies beyond initial development into the study of CTCs in clinically relevant information, in this thesis, I seek to apply a nanomaterial-based microfluidic device, the GO Chip, to the thorough investigation of CTCs in genitourinary cancers to address current challenges facing those diseases.

1.5 Prostate cancer

Prostate cancer is the second leading cause of cancer death in men in the United States (124). It is the most commonly diagnosed cancer in men other than skin cancer, with 1 in 8 men receiving this diagnosis in his lifetime. The majority of men with prostate cancer are diagnosed based on an elevated levels of prostate specific antigen (PSA) in the serum (125). PSA is a secreted

enzyme that is generally contained within the prostate, but enters the serum when there is damage to prostatic tissue, allowing for a simple blood test. However, there have been calls to decrease the frequency of PSA testing due to the possibility of overdiagnosis, i.e., the diagnosis of clinically indolent prostate cancer that is unlikely to lead to metastasis and/or death (126). Thus, there remains a need for a more informative test for prostate cancer, with an emphasis on the cancer's ability to metastasize, such that severe treatments and invasive surgeries are only undergone by those whose cancers that truly warrant them.

Once the disease progresses to an advanced state, a common treatment for prostate cancer is androgen deprivation therapy (ADT) to decrease proliferation and promote apoptosis in cancer cells, decreasing tumor burden and serum PSA levels (127). However, there is often recurrence due to incomplete androgen ablation, which is potentially coupled with the selection of cells with upregulated androgen receptors or mutations allowing the recognition of anti-androgens by the androgen receptor. Other mutations notable in prostate cancer include PTEN deletions and the TMPRSS2:ERG fusion (128), while the prostate specific membrane antigen (PSMA) represents an additional tissue specific marker (129). Another feature of prostate cancer is the specificity with which it metastasizes to the bone, although the mechanisms of this specificity are not fully understood. This highlights a lack of physiologically relevant models for prostate cancer, as xenograft mice rarely undergo bone metastasis (128). CTCs therefore have the potential to provide a window into both the trajectory of a patient's disease as well as unanswered questions into the biology of the disease.

1.6 Bladder cancer

Bladder cancer is the fourth most prevalent cancer in men, and affects men four times as frequently as it does women (130). It is historically important and the subject of much molecular

characterization due to the discovery of the human *ras* genes in the T24 bladder cancer cell line (131). Instances of the disease may be stratified into two tracts: non-muscle-invasive and muscle-invasive. The intense surveillance in the form of cystoscopies and repeated surgeries to resect the tumors make this disease highly detrimental to both the comfort and quality of life experienced by the victim as well as extremely expensive to the healthcare system (132, 133). A particularly perilous example of invasive disease is carcinoma *in situ* (CIS), which can proceed to invasive disease. While chemotherapy and radiation are used to treat invasive bladder cancer, they do not completely eradicate it (132), and 50% of patients with metastatic bladder cancer die within 5 years (133). Drug resistance is also a common problem with invasive disease (134). For those patients with advanced disease, overall survival has remained unchanged for over 30 years (135), indicating a need for both better prognostic and diagnostic indicators in addition to more therapeutic targets.

There are multiple methods used to diagnose bladder cancer. Endoscopy and transurethral biopsy are invasive procedures that pose obvious discomfort and have been known to miss CIS (131). Additionally, these techniques contribute to the financial burden of bladder cancer, which is projected to be responsible for greater than 3% of cancer-related spending by 2020 (136). A noninvasive exam involves the use of urine cytology, which has the drawback of low sensitivity. Many molecular markers have been identified with the goal of using them to make more informed treatment decisions, better predictions regarding the outcome of the disease, and better understand the underlying biology in hopes of discovering additional therapeutic targets. Biomarker expression in bladder cancer has a spatial component. The urothelium is organized into three layers, each with a corresponding cell type: basal, intermediate, and umbrella (133). An example of localized expression is that of EGFR. In normal urothelium, it is expressed by basal cells, protected from interacting with EGF in the urine by the other two layers (135). If this barrier is

disturbed, EGFR may bind EGF, potentially leading to tumorigenesis. Expression may also be variable between primary tumors and their metastases, such as the over-expression of HER2 in 45% of the metastases from HER2 negative primary tumors. Different stages of bladder cancer may also have varied expression levels. An example is the androgen receptor, which is expressed in bladder cancers in lower levels than in normal urothelium but at higher levels in invasive and high grade tumors relative to noninvasive and low grade tumors (137). The two tracts of urothelial cancer may involve varied molecular mechanisms, with misregulation of RB and other tumor suppressors being of great importance in invasive bladder cancer while issues in the MAPK pathway may be behind papillary disease (132). Biomarkers have applications in clinical decision making, surrogate endpoints, and prognostication, and easy access to tumor related specimens may improve their use and provide opportunities to discover new ones.

Major challenges currently facing bladder cancer include the need for therapies for metastatic disease and better techniques to monitor the disease. CTCs represent a more easily acquired sample of biological tissue that could be used to both monitor the disease as well as serve as a substrate for study potential therapeutic targets.

1.7 Mission statement and hypothesis

CTCs have the potential to address unmet needs in the study of genitourinary cancers. As the population of cells preselected for their ability to enter the bloodstream, they present a clinically relevant population of cells that is simultaneously highly accessible as a liquid biopsy. In the ten years since the publication of the CTC Chip, many CTC isolation technologies have emerged, but it is in their application to the study of patient cohorts where they will prove their worth.

In this thesis, I have applied the highly sensitive GO Chip technology to the study of CTCs in prostate and bladder cancers and have taken steps to improve the technology to further its

clinical utility. Following characterization of prostate CTCs by both immunofluorescence staining and RNA expression analysis, I looked to clinical outcomes to determine which parameters can best inform us about a patient's disease. I then examined specific molecular markers first in prostate cancer, then in bladder cancer, to further investigate the metastatic process. Finally, I explored different techniques to release cells captured on chip to enable further molecular characterization. Through this work, I furthered our lab mission of taking advantage of current technology and applying it to pressing clinical problems.

Chapter 2 Isolation and transcriptome analysis of CTCs in prostate cancer

2.1 Abstract

Rates of progression and treatment response in advanced prostate cancer are highly variable, and there is a clear need for non-invasive methods to assess the molecular characteristics of these tumors in real time. The unique potential of circulating tumor cells (CTCs) to serve as a clinically useful liquid biomarker is due to their ability to inform via both enumeration and RNA expression. We used a microfluidic graphene oxide based device (GO Chip) to isolate CTCs from the whole blood of 41 men with metastatic castration-resistant prostate cancer. CTCs were detected in all 41 samples (median: 20 CTCs/mL, range: 3-166 CTCs/mL). We observed CTCs present in clusters in 26/41 patients (63.4%). The cluster size ranged from 2-8 CTCs/cluster, and the percentage of CTCs present in samples as clusters ranged from 0-54.8%. Additionally, we determined the expression of 96 genes of interest by RT-qPCR. We then conducted multivariate analyses to determine the genes most closely associated with overall survival, PSA progression, and radioclinical progression. Scoring of genes based on relative expression of CD44, CDH1, EPCAM, ERCC1, PIK3CA, STAT3, TGFB1, and ZEB2 produced a score that accurately predicted overall survival (AUC = 0.88). This signature, comprised of high expression of stemness genes and low expression of epithelial and mesenchymal genes, implicates an undifferentiated CTC phenotype as a marker of poor prognosis in this setting.

2.2 Introduction

While men with metastatic castration resistant prostate cancer (mCRPC) have a median survival of approximately 18 months, there is substantial heterogeneity and time-to-progression varies widely (138-140). Additionally, given the evolving treatment landscape, there is a clear need for better biomarkers of progression and treatment response in order to help guide therapeutic decisions. While soft tissue and bone biopsies can provide the necessary molecular information, many men with mCRPC have already undergone multiple prior invasive biopsies, and the tissue-based information is representative of only that single disease site.

A liquid-biopsy based approach offers the potential for repeated, non-invasive measurements and may more widely sample the overall disease state. This could potentially be furnished by circulating tumor cells (CTCs), which are shed from tumors and can be detected in the blood stream (141). In addition to giving insight into the burden of disease, these cells can provide further insight into the overall molecular state and risk of progression through the analysis of gene expression and the phenotypes of the traveling cells (142). However, key obstacles to capturing CTCs include their rarity and the millions of surrounding white blood cells and red blood cells (143). To best interrogate CTCs, they must be detected with high yield and sufficient purity.

This problem has been addressed with a host of isolation technologies (17). Notably, the first FDA approved CTC isolation technology, CellSearch, has been used to establish survival differences based on CTC enumeration (24, 33, 34). This macroscale technology uses a magnetic ferrofluid conjugated with an antibody against the epithelial cellular adhesion molecule (EpCAM) to capture EpCAM-expressing cells from 7.5 mL whole blood (32). For increased sensitivity and flexibility of downstream analysis, microfluidics and nanomaterials (16) have been developed to isolate and study CTCs (77, 144-146). While there exist many CTC isolation technologies that

separate CTCs based on their size relative to white blood cells, the observation in other cancers that CTCs are larger than white blood cells has not held in prostate cancer (44, 147, 148), leading to an emphasis on the use of immunocapture.

The nanomaterial-based graphene oxide chip (GO Chip) affords highly sensitive capture of rare cells with low white blood cell contamination (115). Optimized with cell line spike-in samples with as few as 3-5 cancer cells per milliliter of whole blood, the device showed promise in the capture of PC-3 cells under physiologically relevant conditions and concentrations (115). Coupled with the capability for downstream molecular and morphologic analysis, the GO Chip is poised to enable CTC enumeration, characterization, and RNA expression from the whole blood of patient samples (115). Its efficiency and sensitivity allow for evaluable results from only 1 mL of blood processed on a single chip. Toward the goal of using CTCs to provide clinically relevant molecular information that could eventually be utilized to assist with patient management, we undertook a prospective study of 41 men with mCRPC. We sought to utilize captured CTCs and extracted RNA from parallel GO Chips to determine CTC characteristics associated with progression and survival in advanced prostate cancer.

2.3 Methods

2.3.1 Patient sample acquisition

Blood samples were collected with informed consent from 41 patients with mCRPC recruited under institutional approved IRB (HUM00052405) between August 2013 and November 2016 using EDTA tubes. Processing occurred on the day of blood draw. Four healthy male controls were recruited internally and processed in the same manner as patient samples.

In addition to overall survival, PSA at the time of blood draw, radiographic, and clinical progression events were recorded. PSA progression was defined using the PCWG3 criteria of an

increase of greater than or equal to 25% from the nadir, with a minimum increase of 2 ng/mL (149). Radioclinical progression was also used as a clinical endpoint using the date of whichever happened earliest. Radiographic progression entailed one of three events: 20% or more increase in the sum of the diameters of soft-tissue target lesions based on RECIST criteria applied to CT scans; an increase of at least 5 mm in the short axis of a previously normal lymph node (this lymph node must be at least 1.0 cm in the short axis); or at least two new bone lesions. Clinical progression was defined as worsening disease-related symptoms or new cancer-related complications.

2.3.2 Cell culture

The prostate cancer cell line PC-3 cell line was used to generate a scanning electron microscopy image to demonstrate cell capture on the GO Chip. This cell line was a generous gift from the lab of Mark L. Day following their purchase from ATCC. They were maintained in RPMI 1640 (Gibco) supplemented with 10% fetal bovine serum (FBS, Corning) and 1% antibiotic-antimycotic (Gibco). Cells were maintained in a 37°C incubator with 5% CO_2. The cell line tested negative for *Mycoplasma* contamination as assayed using the Lonza Mycoalert on February 27, 2017.

2.3.3 Device fabrication

Fabrication of the graphene oxide chip (GO Chip) has been described previously (115). Briefly, a suspension was made by probe tip sonicating graphene oxide (CheapTubes.com) and tetrabutyl ammonium hydroxide (TBA, Fluka) in dimethylformamide (Sigma-Aldrich). A phospholipid-polyethyleneglycol-amine (PEG, NOF America Corporation) was added to the resulting suspension and bath sonicated for 1 hour. Silicon wafers with gold features fabricated using photolithography were dipped in the suspension to allow self-assembly of the GO-TBA-PEG onto the gold. This pattern was then enclosed in a polydimethylsiloxane (PDMS, Dow

Corning) microfluidic chamber. The crosslinker N-γ-maleimidobutyryl-oxysuccinimide ester (GMBS, Pierce) was then added to the devices and incubated at which point tubing (Tygon) was inserted. Following a wash, NeutrAvidin (Invitrogen) was added to the devices via syringe pump (Harvard Apparatus). The devices could be stored at 4º C until use, at which time biotinylated anti-EpCAM (**Table 2-1**) in 1% bovine serum albumin (BSA, Sigma) was added prior to sample processing.

Table 2-1 Antibody information.

Antibody	**Conjugate**	**Application**	**Company**	**Catalog number**	**Clone**
Goat anti-human EpCAM	Biotin	Cell capture	R&D Systems	BAF960	Polyclonal
Mouse IgG2a anti-human cytokeratin 7/8	N/A	Primary antibody	BD Biosciences	349205	CAM5.2
Mouse IgG1 anti-human CD45	N/A	Primary antibody	BD Biosciences	555480	HI30
Goat anti-mouse IgG2a	Alexa Fluor 546	Secondary antibody	ThermoFisher	A-21133	Polyclonal
Goat anti-mouse IgG1	Alexa Fluor 488	Secondary antibody	ThermoFisher	A-21121	Polyclonal

2.3.4 Scanning electron microscopy

To fix cells on the device for scanning electron microscopy (SEM) imaging, the PDMS layer was removed and the substrate was fixed in 2.5% glutaraldehyde (Electron Microscopy Sciences) for one hour. The substrate was then washed twice with PBS and dehydrated through successive 10 minute dips in increasing concentrations of ethanol (50%, 70%, 95%, 100% twice). The substrate was dipped twice in hexamethyldisilazane (HDMS, Electron Microscopy Sciences) for 10 minutes each and then dried overnight in a chemical hood. The fixed substrate was then sputter coated with carbon and imaged on a FEI Nova 200 Nanolab.

2.3.5 Patient sample processing

Following blocking with BSA, 1 mL whole blood was introduced into the GO Chip at a flow rate of 1 mL/hr. Devices were then flushed with a total volume of 6 mL phosphate buffered

saline (PBS, Gibco) at 100 µl/min immediately following blood flow. Subsequent steps were determined based on the ultimate application of the device in the work-flow. For devices that would be stained for enumeration, the contents of the PDMS chamber were fixed using 4% paraformaldehyde (PFA, ThermoFisher). These devices were then stored at 4°C until they were stained. On a parallel device, RNA extraction was performed by first flowing RNA extraction buffer (a component of the PicoPure® RNA Isolation Kit, Arcturus). The device and syringe were then incubated for 30 minutes at 42°C, after which DEPC water (ThermoFisher) was flowed. Collected RNA extraction buffer and DEPC water from the device outlet were stored at -80°C until purification.

2.3.6 Immunofluorescence staining

Subsequent to processing and fixation of the sample, immunofluorescence staining was performed on-chip using a syringe pump. Cells were permeabilized using Triton X (Sigma) and then blocked a combination of goat serum (ThermoFisher) and BSA. See **Table 2-1** for all antibody information. Primary antibodies against CD45 and cytokeratin 7/8 were detected using the appropriate secondary antibodies labeled with Alexa Fluors 488 and 546. Antibodies were suspended in 1% BSA while 2-(4-amidinophenyl)-1H-indole-6-carboxamidine (DAPI, Invitrogen) in PBS was used to label cell nuclei. Imaging of fluorescence staining was conducted on a Nikon Eclipse Ti fluorescence microscope using either a 10x or 20x objective. Images were captured using a QImaging cooled mono 12-bit camera and analyzed using NIS-Elements software. Those nucleated cells expressing CK but not CD45 (DAPI+/CK+/CD45- cells), were counted as CTCs.

2.3.7 Quantitative reverse-transcription polymerase chain reaction (RT-qPCR)

Bulk cell lysates extracted during sample processing from 36 patients and four healthy controls were subsequently purified using the remaining components of the PicoPure® RNA Isolation Kit; five patients were processed only for enumeration and not RNA expression analysis (**Table 2-2**). Purification was conducted according to the manufacturer's protocol. Purified RNA was reverse transcribed to cDNA according to the manufacturer's protocol using an Ambion kit (ThermoFisher). The cDNA was pre-amplified after which it underwent RT-qPCR using an Applied Biosystems™ TaqMan® Gene Expression Assay. Using the BioMark HD qPCR platform (Fluidigm), C_T levels were determined for 96 genes of interest (complete list, **Table 2-3**) in the following categories: apoptosis, blood cell, cell cycle, cell junction, cytoskeleton, developmental, DNA repair, extracellular matrix, epithelial, growth factor, hormone, housekeeping, inflammation/immune system, long noncoding RNA, mesenchymal, oncogene, proliferation, stemness, transcription factor, and tumor suppressor.

Table 2-2 Sample flow through study.

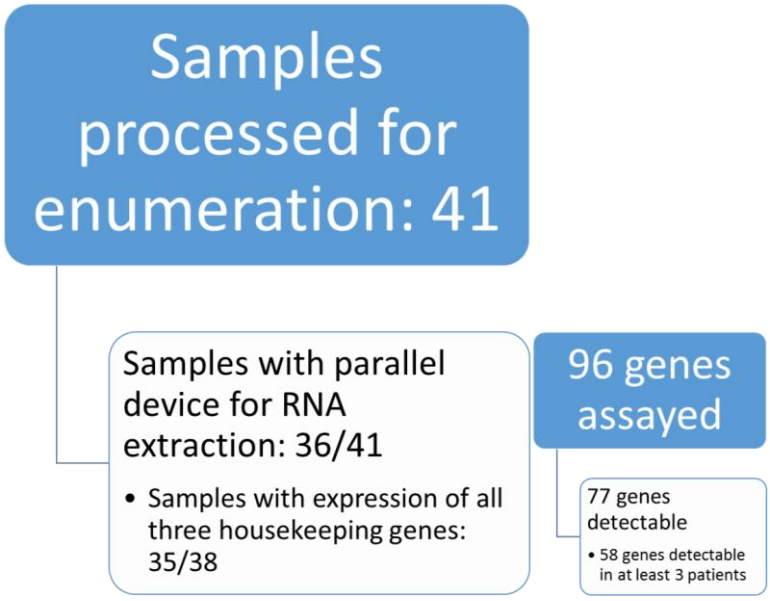

Table 2-3 List of 96 genes analyzed by RT-qPCR.

Gene	Category
BCL-xL	Apoptosis
CASP3	Apoptosis
XIAP	Apoptosis
CD3D	Blood cell
CD11B	Blood cell
CD20	Blood cell
CD45	Blood cell
CD33	Blood cell
CD34	Blood cell
PTPRN2	Cell cycle
CCND1	Cell cycle
CHP1	Cell cycle
KLF4	Cell cycle
PSME3	Cell cycle
DSP	Cell junction
EVPL	Cell junction
JUP	Cell junction
CTNNA1	Cytoskeleton
CTNNB1	Cytoskeleton
CTNND1	Cytoskeleton
PKP2	Cytoskeleton
FOXC1	Transcription factor
FOXC2	Transcription factor
ERCC1	DNA repair
COL1A2	ECM
COL3A1	ECM
LGALS3BP	ECM
MMP2	ECM
MMP9	ECM
SPARC	ECM
TIMP1	ECM
TIMP2	ECM
CDH1	Epithelial
EPCAM	Epithelial
KRT7	Epithelial
KRT8	Epithelial
KRT14	Epithelial
KLK3	Epithelial
EMP2	Epithelial
MUC1	Epithelial
TROP2	Epithelial
FGF18	Growth factor
IGFBP5	Growth factor
TGFB1	Growth factor
AR	Hormone
GAPDH	Housekeeping
ACTB	Housekeeping
UBB	Housekeeping
CXCL16	Inflammation/Immune system
CXCR1	Inflammation/Immune system
IL6	Inflammation/Immune system
IL8	Inflammation/Immune system
MTOR	Inflammation/Immune system
NFKB1	Inflammation/Immune system
PD-1	Inflammation/Immune system

PDL-1	Inflammation/Immune system
XBP1	Inflammation/Immune system
XIST	lncRNA
HOTAIR	lncRNA
CDH2	Mesenchymal
CDH11	Mesenchymal
VIMENTIN	Mesenchymal
KRT5	Mesenchymal
SNAI1	Mesenchymal
SNAI2	Mesenchymal
ZEB1	Mesenchymal
ZEB2	Mesenchymal
CD146	Mesenchymal/endothelial
ERBB2	Oncogene
ERG	Oncogene
FOLH1	Oncogene
ALK	Oncogene
EGFR	Oncogene
KRAS	Oncogene
MAPK1	Oncogene
NTRK2	Oncogene
PIK3CA	Oncogene
MKI67	Proliferation
MLPH	Signal transduction
SERPINB6	Signal transduction
STAT3	Signal transduction
ALDH1A1	Stemness
ALDH1A3	Stemness
CD24	Stemness
CD44	Stemness
CD44v6	Stemness
CD133	Stemness
BMi1	Stemness
ABCG2	Stemness/Drug resistance
ETV1	Transcription factor
TMPRSS2	Transcription factor
ELF3	Transcription factor
TP53	Tumor suppressor
PTEN	Tumor suppressor
RB1	Tumor suppressor
PTCH1	Tumor suppressor

Table 2-4 Detected genes.

Genes detected in one or more patients (C_T < 30)	**Detected in three or more patients?**
ABCG2	Yes
ACTB	Yes
ALDH1A1	Yes
ALDH1A3	Yes
AR	Yes
BCL-xL	Yes
BMi1	Yes
CASP3	Yes
CCND1	Yes
CD11B	Yes
CD146	Yes

CD20	Yes
CD24	Yes
CD33	Yes
CD3D	Yes
CD44	Yes
CD45	Yes
CDH1	Yes
CDH2	Yes
CHP1	Yes
CTNNB1	Yes
CTNND1	Yes
CXCL16	Yes
CXCR1	Yes
EPCAM	Yes
ERBB2	Yes
ERCC1	Yes
FOXC1	Yes
FOXC2	Yes
GAPDH	Yes
IL8	Yes
JUP	Yes
KLF4	Yes
KRAS	Yes
LGALS3BP	Yes
MAPK1	Yes
MKI67	Yes
MMP9	Yes
MTOR	Yes
NFKB1	Yes
PIK3CA	Yes
PSME3	Yes
PTEN	Yes
RB1	Yes
SERPINB6	Yes
SPARC	Yes
STAT3	Yes
TGFB1	Yes
TIMP1	Yes
TIMP2	Yes
TP53	Yes
TROP2	Yes
UBB	Yes
VIMENTIN	Yes
XBP1	Yes
XIAP	Yes
ZEB1	Yes
ZEB2	Yes
CD44v6	No
DSP	No
EGFR	No
ELF3	No
EMP2	No
ETV1	No
EVPL	No
FOLH1	No
IGFBP5	No
IL6	No

KLK3	No
KRT8	No
MLPH	No
MUC1	No
PDL-1	No
PKP2	No
SNAI1	No
TMPRSS2	No
XIST	No

2.3.8 Statistical analysis

The primary outcome of interest was overall survival. Data variables were related to either enumeration or RNA, and in the case of enumeration included CTCs/mL, the presence of clusters, the number of clusters, the percentage of CTCs in clusters, the average number of CTCs/cluster, and the maximum number of CTCs/cluster. The base ten log of the enumeration variables was taken for the purposes of analysis. Analyses were performed using Excel and R (150) with the following R packages: rpart (151), survival (152), and survivalROC (153). The CTC enumeration variables were compared to the clinical metrics using Cox proportional hazards models and Kaplan-Meier survival analysis. The Wald test was used to determine significance for Cox proportional hazards modeling, while the log-rank test was used in the Kaplan-Meier analysis. In other comparisons, statistical significance was determined using the Mann-Whitney test. A nominal p-value of less than 0.05 was considered statistically significant. RT-qPCR results were first normalized to the mean of three housekeeping genes (GAPDH, ACTB, UBB) to obtain a ΔC_t value, and then background corrected by deducting the mean expression level of each in the four healthy controls to obtain a $\Delta\Delta C_t$ value, and subsequently analyzed as $\log_2(2^{-\Delta\Delta C_t} + 1)$. To select genes for the generation of a point-based score, analysis conducted with the rpart package in R was used as a screening mechanism, with nominally significant genes being considered.

2.4 Results

2.4.1 Clinical cohort

We assessed 41 metastatic castrate resistant prostate cancer patients over the course of this study (**Table 2-5**). The median patient age was 73 years (range: 50-84 years), while the median baseline PSA level was 37.9 ng/mL (range: 1.2-6433 ng/mL). The median number of prior treatments other than first-line hormonal therapy was one (range: 0-7), and at the time of CTC collection there were 17 patients receiving abiraterone, four receiving cabazitaxel, two receiving cabozantinib, seven receiving docetaxel, eight receiving enzalutamide, one receiving olaparib, and one receiving pembrolizumab. During the study and follow-up period, 34 patients experienced PSA progression; 37 experienced radioclinical progression as defined by a ≥20% increase in the sum of the soft tissue lesion diameters during computed tomography, ≥2 new bone lesions on bone scan, or symptomatic progression (worsening pain aggravation or new cancer-related symptoms); and 22 patients died. For surviving patients, the median time to last follow-up was 19.1 months (range: 3.3-37.8 months). Median time to death was 17.5 months (range: 2.6-39.6 months).

Table 2-5 Clinical cohort information.

Number of patients	41	100%
Age		
Median (range)	73	(50-84)
Race		
Caucasian	39	95.1%
Black	3	7.3%
Castrate resistant	41	100%
Performance status		
0	15	36.6%
1	22	53.7%
2	3	7.3%
Prostate-specific antigen (ng/mL)		
Median (range)	37.9	(1.2-6433.1)
Metastatic disease	41	100%
Visceral metastases	11	26.8%
Number of prior therapies		
Median (range)	1	0-7
Therapy at time of collection		
Abiraterone	17	41.5%
Cabazitaxel	4	9.8%
Cabozantinib	2	4.9%
Docetaxel	7	17.1%
Enzalutamide	8	19.5%
Olaparib	1	2.4%
Pembrolizumab	1	2.4%

2.4.2 Circulating tumor cell detection, enumeration, and gene expression analysis by RT-qPCR in clinical samples

To investigate the presence of CTCs in clinical samples, we processed 1 mL of whole blood from 41 metastatic castrate resistant prostate cancer patients for CTC enumeration (**Figure 2-1**). CTCs were detected in all 41 samples with the number of CTCs ranging from 3-166 CTCs/mL (median: 20 CTCs/mL, **Figure 2-2**). The median number of CTCs detected in healthy controls was

5 CTCs/mL (range: 3-14 CTCs/mL). CTC counts for patients were significantly higher than those for healthy controls ($p = 0.013$).

For 36 of the patients, we had the opportunity to run a parallel microfluidic device that

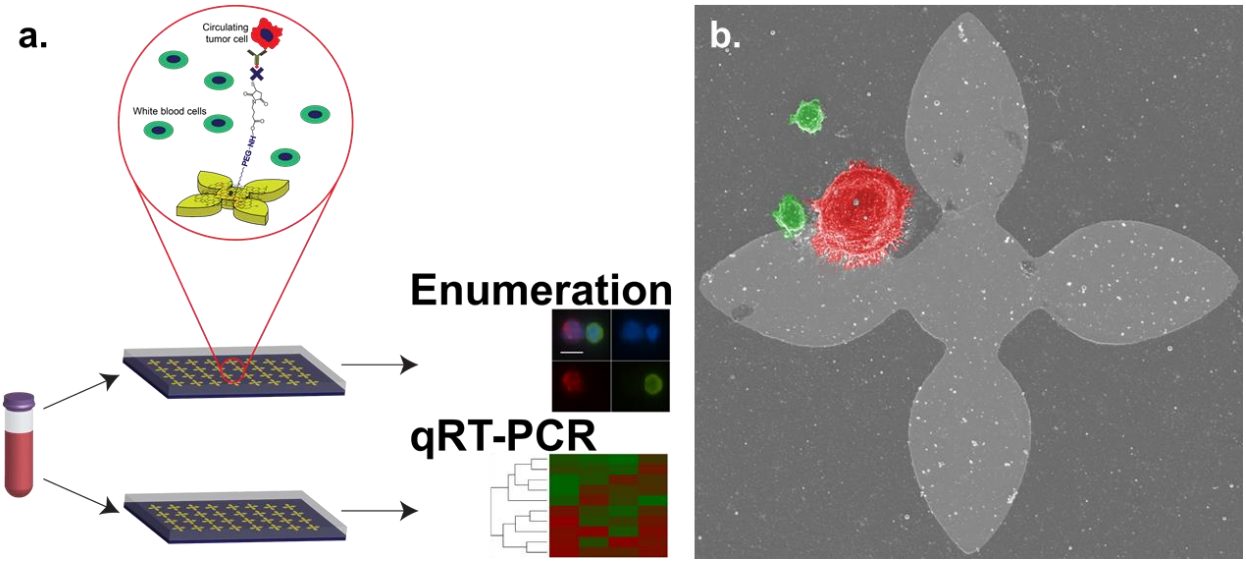

*Figure 2-1 Graphene oxide chip-enabled isolation of prostate circulating tumor cells. (**A**) Sample workflow. Two parallel devices were processed, one each for circulating tumor cell enumeration and RNA extraction. (**B**) Scanning electron micrograph of PC-3 cell (red pseudocolor) and white blood cells (green pseudocolor) on-chip. Flower patter is 100 μm in height and width.*

ultimately yielded RNA following cell lysis and purification, which was used for RT-qPCR (**Table 2-2**). Results from one patient sample were discarded due to insufficient expression of housekeeping genes suggesting lack of sufficient RNA for analysis. In the remaining 35 patient samples, 77 of the 96 genes were detectable ($C_T < 30$) in at least one patient, and 58 genes were detectable at this threshold in at least three patients (**Table 2-3**, **Table 2-4**).

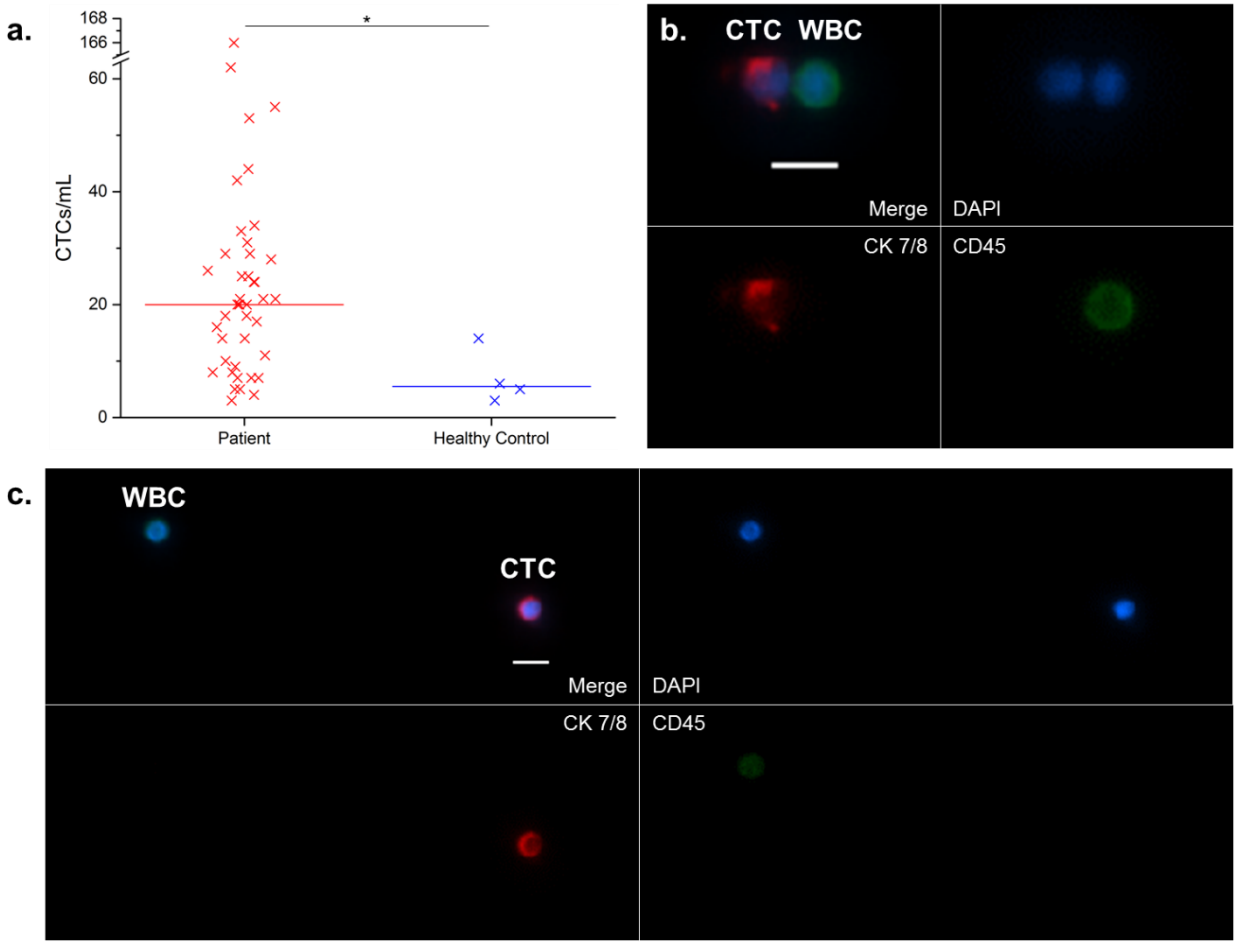

*Figure 2-2 CTC enumeration in mCRPC patients. (a) Circulating tumor cell (CTC) enumeration results for 41 metastatic castrate resistant prostate cancer patient samples (range: 3-166 CTCs/mL, median: 20) and four healthy controls (range: 3-14 CTCs/mL, median: 5). *denotes $p < 0.05$. (b, c) Examples of CTCs captured on-chip as well as non-specifically bound white blood cells (WBCs). Nuclear staining is shown in blue, cytokeratin 7/8 in red, and CD45 in green. Scale bar is 10 μm.*

2.4.3 Circulating tumor cell cluster detection in patient samples

While processing patient samples, we observed groups of two or more adjacent CTCs (**Figure 2-3a, b**), termed CTC clusters. These clusters were only present in patient samples (26/41, 63.4%) and not healthy controls. Both interpatient and intrapatient heterogeneity were evident from the captured clusters, as cells within the clusters showed varying size and cytokeratin expression. Clusters consisted of up to eight CTCs per cluster (**Figure 2-3c**) with the majority of the clusters comprising fewer numbers of cells. The percentage of CTCs captured in the form of clusters also varied greatly among patients from 0 to 54.8% (**Figure 2-3d**).

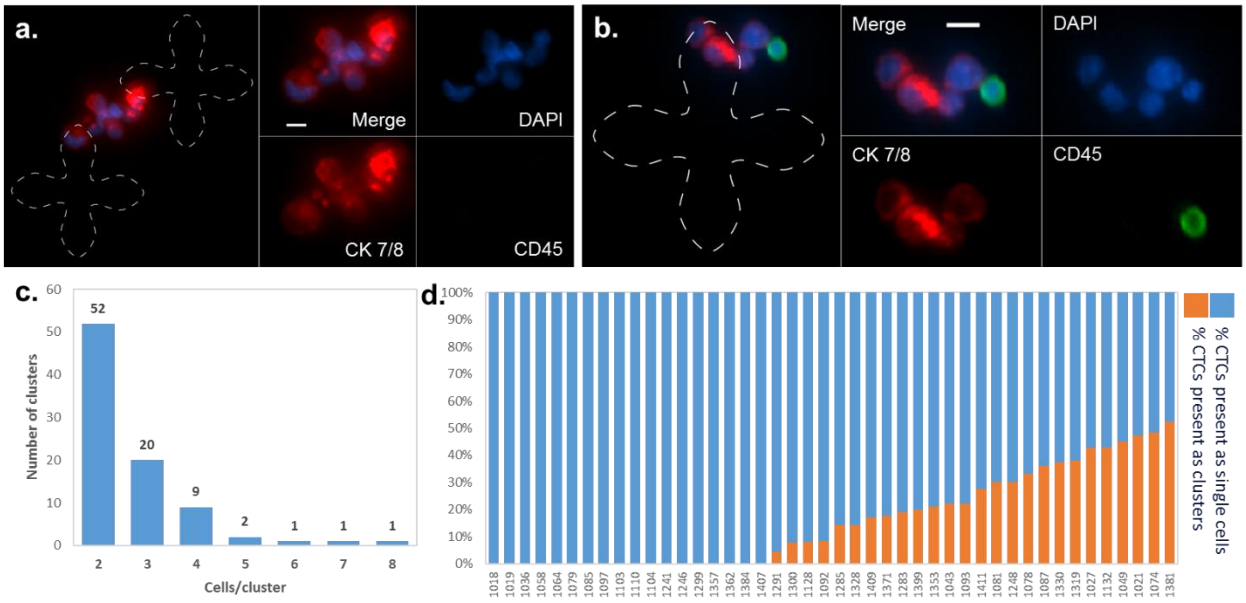

Figure 2-3 CTC clusters in mCRPC patient samples. (a, b) Examples of captured circulating tumor cell (CTC) clusters. CTCs captured within clusters had heterogeneous size and cytokeratin expression. The capture pattern is outlined with a dashed line for visualization purposes; scale bar is 10 μm. (c) Captured CTC clusters ranged in size from two to eight cells per cluster. (d) The percentage of captured CTCs present in clusters ranged from 0 to 54.8%.

2.4.4 Gene-CTC cluster association

We next examined the relationship between gene expression and the measures of clusters to determine potential associations. The association between gene expression and the number of clusters or the percentage of CTCs detected in clusters from each patient sample was examined through linear modeling of these parameters as continuous variables (**Figure 2-4**). If the relationship between the enumeration variable and the gene expression had a negative linear

coefficient, that meant the gene expression decreased as the enumeration variable increased (i.e. as the number of clusters or percentage of CTCs in clusters increased). CTNND1 and ZEB2 were negatively associated with the number of clusters present per sample, and CTNND1 and FOXC1 were negatively associated with the percentage of CTCs found in clusters ($p < 0.05$).

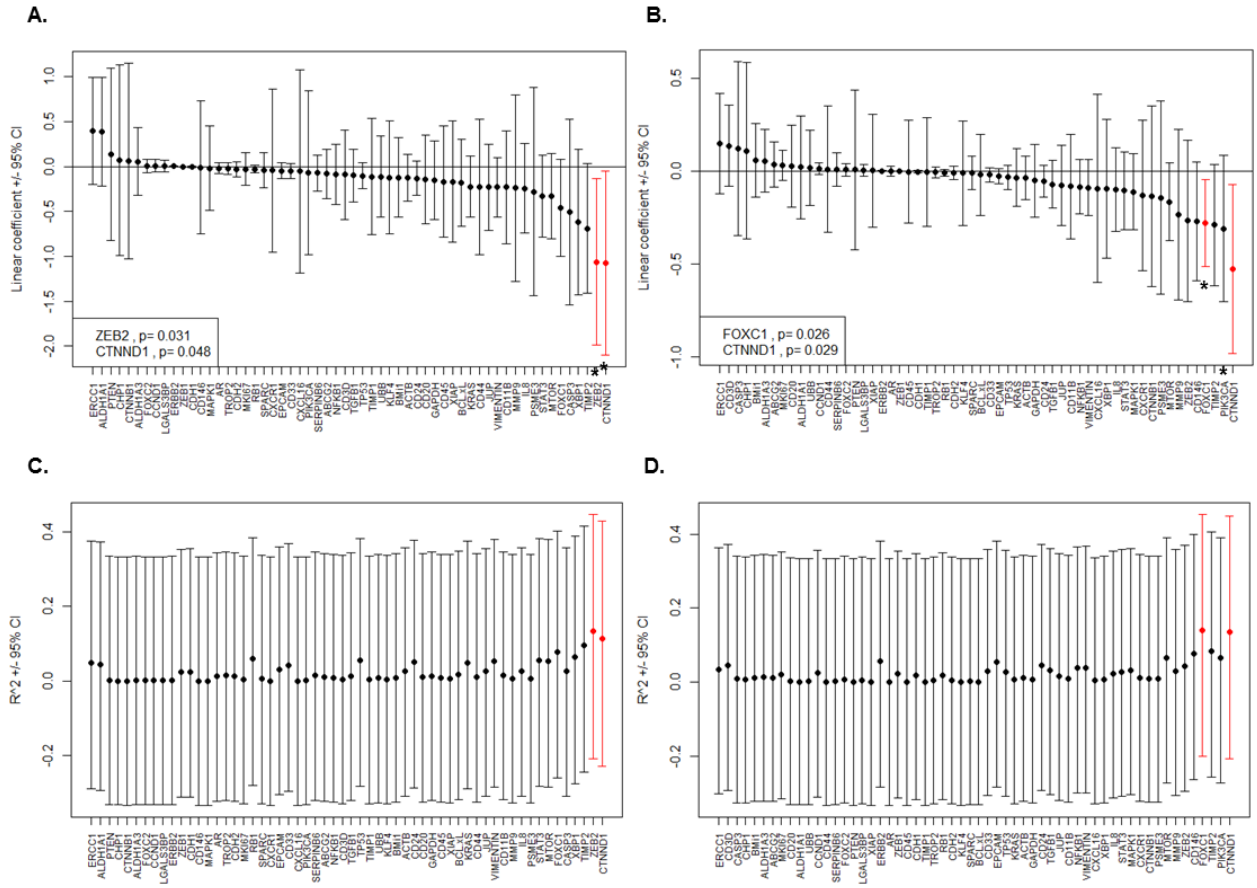

*Figure 2-4 Linear modeling of gene expression based on cluster metrics. (**A**) Linear association of gene expression with number of CTC clusters. Two genes, CTNND1 and ZEB2, showed a significant negative association. (**B**) Linear association of gene expression with percentage of CTCs in clusters versus present as single cells. FOXC1 showed a significant positive association while CTNND1 showed a significant negative association. (**C**, **D**) R^2 values for linear associations of gene expression with number of CTC clusters and percentage of CTCs in cluster versus present as single cells, respectively. Data is plotted as the linear coefficient or R^2 ± the 95% confidence interval; */red denotes $p < 0.05$.*

2.4.5 Exploratory single variable analysis

To assess the clinical relevance of the experimental data obtained, we compared CTC metrics and gene expression with overall survival, PSA progression, and radioclinical progression. While none of the enumeration variables were statistically significant in the

univariable Cox proportional hazards models, patients with a high number of clusters relative to the median had a shorter time to radioclinical progression than those with a low number of clusters in the Kaplan-Meier survival analysis (log rank $p < 0.05$, **Figure 2-5**).

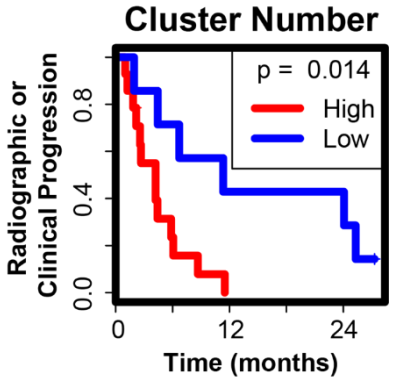

Figure 2-5 Relationship between radioclinical progression and number of clusters as determined through Kaplan-Meier analysis ($p < 0.05$).

To construct a bimodal point-based metric relating gene expression (**Figure 2-6**) to clinical outcomes, we used cut-points to classify patients in to high and low survival groups as determined by subsequent Kaplan-Meier analysis. Cut-points were generated using regression tree analysis from the rpart (recursive partitioning) package in the R software environment. The rpart package uses regression models based on the input data set to find the variable and location that best splits the data into two groups, where best is defined as minimizing the risk of misclassification. In this case, the input data consisted of the gene expression levels and clinical outcomes. Genes associated with overall survival included CD44, CDH1, EPCAM, ERCC1, IL8, PIK3CA, STAT3, TGFβ, TIMP2, and ZEB2. The genes CDH1, CD146, FOXC2, and ZEB2 were associated with PSA progression, while the genes associated with radioclinical progression included ACTB, CDH1, CDH2, CD3D, CD45, CASP3, CD146, CXCR1, KLF4, KRAS, MKI67, MMP9, RB1, SPARC, XBP1, and ZEB2.

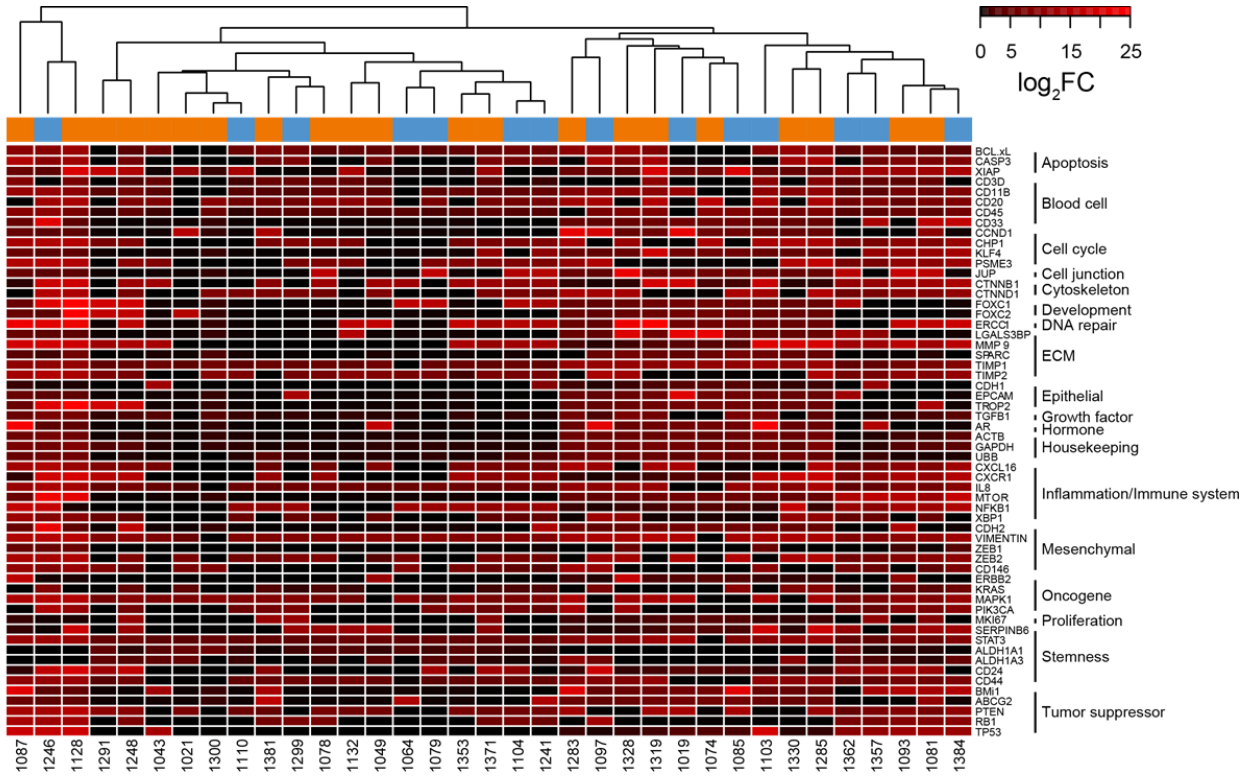

Figure 2-6 Heatmap of log2 fold changes (FC) relative to healthy control background for 58 genes detected in patient samples. Associated gene categories are shown to the right of the gene list.

2.4.6 Multivariate analysis derived from univariate survival and progression analysis

Using these pre-screened genes, we developed a series of prognostic scores to predict survival/progression. Based on gene expression relative to the cut-point, we assigned genes a point value of 0 or 1 based on whether their gene expression value fell above or below the cut-point based on its relationship to shorter survival or progression time. For example, in the case of overall survival, patients expressing greater levels of CD44 than the cut-point were assigned 1 point, while patients expressing lower levels of CDH1 than the cut-point were assigned 1 point. Conversely, patients expressing lower levels of CDH1 than the cut-point were assigned 1 point, while patients expressing higher levels of CDH1 than the cut-point were assigned 0 points. The values for each of the genes were then added in different combinations with all subsets considered and used to generate receiver operating characteristic (ROC) curves, with the scores ranging from 0 to the

number of genes in the score. These curves were then evaluated based on the area under the curve (AUC), with AUCs approaching one having greater discriminatory ability. The 95% confidence interval (CI) was generated by resampling, with 10^4 bootstrap samples. Additionally, the Cox proportional hazard ratio (154) was calculated for each score.

Of the significant genes established for overall survival, a set of eight genes ultimately had the best prognostic power: CD44, CDH1, EPCAM, ERCC1, PIK3CA, STAT3, TGFB1, and ZEB2 (**Figure 2-7a**). The resulting ROC had an AUC of 0.88 (95% CI: 0.69-0.98, **Figure 2-7b**). Assessing the score using the Cox proportional hazard model yielded a hazard ratio of 1.83 (95% CI: 1.33-2.51) for overall survival, representing the increased risk between the patient groups one unit apart on the numerical score. Using the same methods to relate the subsets of significant genes to radioclinical progression produced a five-gene score consisting of CD3D, MMP9, RB1, XBP1, and ZEB2 (AUC: 0.82, 95% CI: 0.67-0.96, **Figure 2-9**). This score carried a hazard of 1.51 (95% CI: 1.19-1.92) for radioclinical progression. Finally, investigation of combinations of genes related to PSA progression resulted in a three-gene score: CDH1, CD146, and ZEB2 (AUC: 0.69, 95% CI: 0.47-0.87, **Figure 2-8**); and a proportional hazard of 1.75 (95% CI: 1.17-2.63).

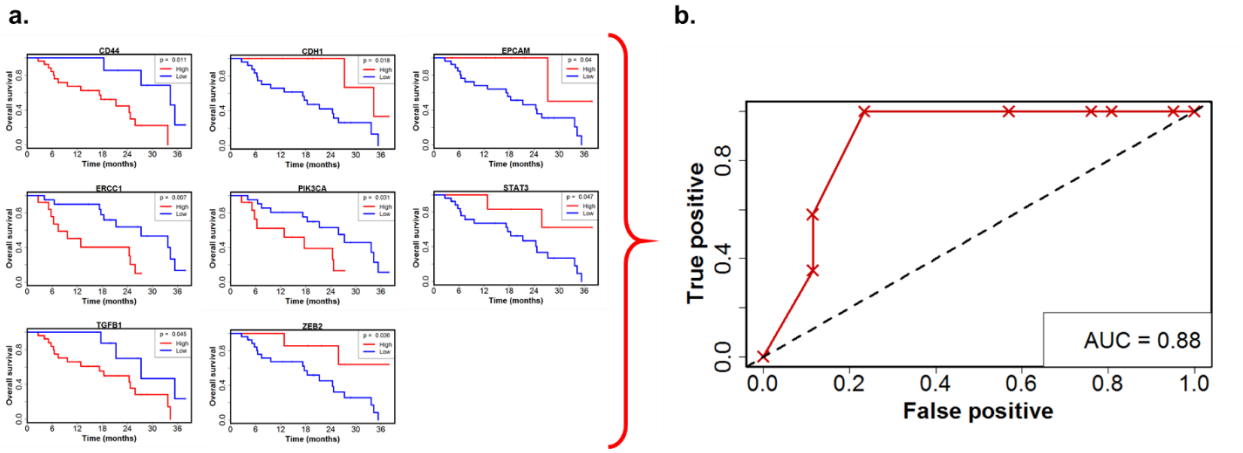

Figure 2-7 Relationship between RNA expression and overall survival. (a) Kaplan-Meier curves for genes with statistically significant relationships with overall survival used to construct the optimized point-based score. (b) Scores were optimized by maximizing the area under the curve (AUC) of the associated receiver operating curve.

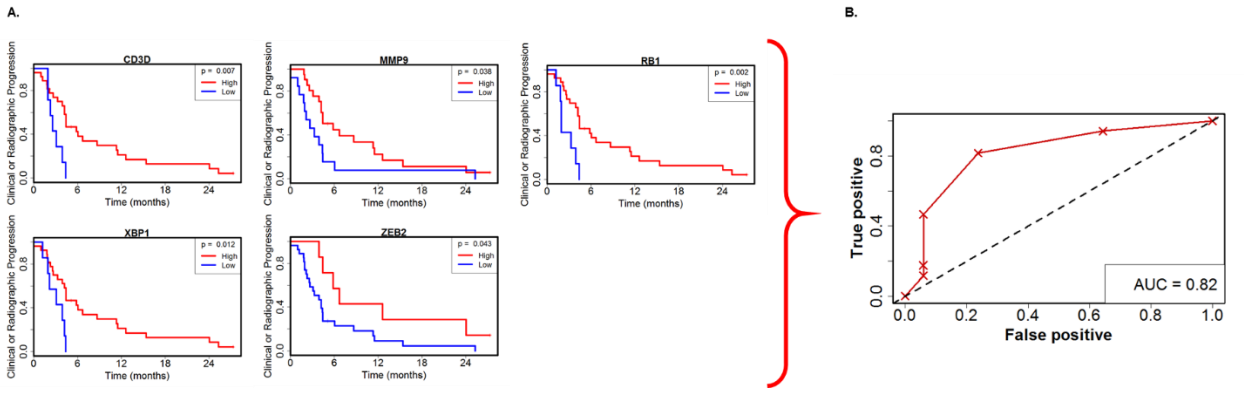

Figure 2-9 Relationship between RNA expression and radioclinical progression. (A) Kaplan-Meier curves for all genes with statistically significant relationships with radiographic or clinical progression used to construct the optimized point-based score. (B) Scores were optimized by maximizing the area under the curve (AUC) of the associated receiver operating curve.

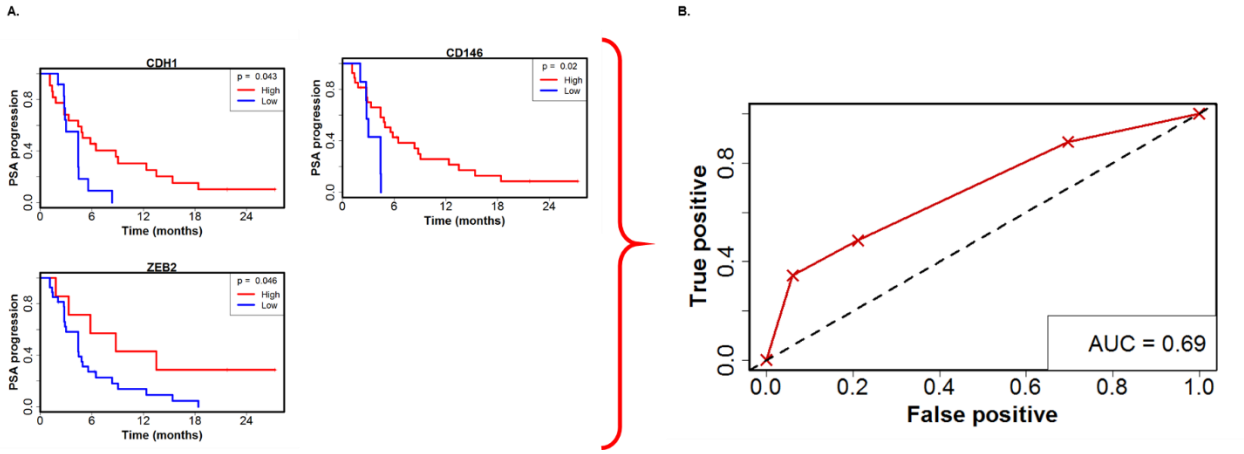

Figure 2-8 Relationship between RNA expression and PSA progression. (A) Kaplan-Meier curves for genes with statistically significant relationships with overall survival used to construct the optimized point-based score. (B) Scores were optimized by maximizing the area under the curve (AUC) of the associated receiver operating curve.

2.5 Discussion

To best study both the underlying biology and disease trajectory of prostate cancer, there is a need for an informative biomarker that is both accessible and capable of capturing tumor heterogeneity. CTCs provide this opportunity as a readily-available liquid biopsy. The incorporation of microfluidics into CTC research offers substantial promise for overcoming the hurdles of low CTC counts and the immense quantity of surrounding normal blood cells. It was

our goal to integrate an ultra-sensitive CTC isolation technology enabling both immunofluorescence characterization and RNA expression analysis in order to investigate the relationship of the CTC-based results with key oncologic outcomes. We detected CTCs from whole blood samples from 41 mCRPC patients, and were additionally able to observe clusters in over 60% of samples. Following qRT-PCR analysis, we compared RNA expression with survival and progression, and in the process, determined a set of eight genes that comprised a score prognostic of overall survival. Our work here is an example of a strategy to incorporate CTC-related metrics with clinical data.

Prior studies have also used cell enrichment technologies coupled with RT-qPCR to study prostate CTCs. For example, mCRPC patients with AR-V7-positive CTCs displayed abiraterone and enzalutamide resistance, indicating the potential for liquid biopsy approaches to provide predictive information (155). The original microfluidic CTC-Chip was used to study prostate CTCs in localized and metastatic patients, with CTCs detected in 23/36 metastatic patients (144). RT-qPCR was also used for further analyses, in this instance, to detect the TMPRSS2-ERG fusion in 9/20 metastatic patients. The next-generation CTC chips such as the Herringbone (HB) Chip (145) and the geometrically enhanced differential immunocapture (GEDI) chip (69) have also been applied to prostate cancer. The HB Chip was used to investigate androgen receptor (AR) signaling through immunofluorescence staining for PSA and PSMA (156), while further immunofluorescence characterization by the GEDI chip examined ERG expression (70). Recently the CTC-iChip was used to reveal the role of noncanonical Wnt signaling through single-cell RNA-Seq of prostate CTCs from 13 patients isolated by negative selection (146). However, the majority of these studies reported on a limited set of genes. To our knowledge, our study is the

first to apply microfluidics-enabled study of CTC enumeration and RNA expression in a cohort of this size using a gene panel of this size.

Another key potential advantage of the approach utilized here is the ability to observe clusters of CTCs, which may provide important prognostic information. CTC clusters have previously been observed in prostate cancer patient samples analyzed using the CellSearch technology, where they have at times been detected in as many as one third of patients (35, 157). CTC clusters have also been visualized using the Epic Sciences platform, some of which have been shown to be AR-V7 positive (43). Additionally, the HB Chip found CTC clusters in 6 out of 64 patients sampled at multiple time points, and detection of CTC clusters at any time point was associated with decreased overall survival (29). This suggests a future direction for our technology, in which serial sampling may provide more prognostic information. Importantly, the fraction of CTC clusters reported in the present study (63.4%) suggests that the GO Chip may be less disruptive to cell-cell interactions and have greater sensitivity for identifying these clusters.

The GO Chip also facilitated RNA extraction from limited numbers of cells for gene expression analysis and subsequent comparison with clinical parameters. We identified a number of genes that were associated with overall survival, PSA progression, and radioclinical progression, and we performed exploratory analyses to determine which set of genes were most strongly associated with these outcomes. In our discovery analysis, we found 10 genes where high or low expression could be correlated with overall survival through Kaplan-Meier analysis. Of these 10 genes, eight comprised a score that produced a highly predictive receiver operator curve with an AUC of 0.88. Three of the genes, CDH1, EPCAM, and ZEB2, are reflective of epithelial or mesenchymal phenotypes. That the low expression of both the epithelial and mesenchymal genes was associated with lower overall survival may suggest the importance of a transitory

phenotype in leading to disease progression. This potentially undifferentiated phenotype is also in concordance with the high CD44 expression associated with shorter overall survival, as CD44 is a cancer stemness marker in prostate cancer (158). Low ZEB2 was also implicated in the scores for PSA progression and radioclinical progression, while low CDH1 was implicated in the score for PSA progression, suggesting an emerging theme. Additionally, STAT3 is activated by AR signaling loss and is associated with cancer stem cells (159). These observations are in line with previous descriptions of stemlike tumor-propagating subpopulations in prostate cancer (160).

In our analysis of the relationship between the number of clusters and gene expression, we found lower expression of ZEB2 and CTNND1 as the number of clusters increased. Overexpression of δ-catenin has been associated with increased proliferation (161). The lower expression and therefore potentially lower proliferation would be consistent with an observed stemlike phenotype within the clusters, which would also be consistent with the lower ZEB2 expression. In addition to CTNND1, FOXC1 was expressed at lower levels as the percentage of CTCs in clusters increased. FOXC1 expression is associated with poor prognosis, androgen independence, and angiogenesis (162), so this result may be indicative of aggressive properties in CTCs present as single cells.

Our study has important limitations. Without question, this work will continue to benefit from longer follow-up and validation in larger cohorts, and recruitment of additional controls will be important to examine background levels of cytokeratin positive cells. This false positive rate, a marker of the balance between assay sensitivity and background noise, will need to continue to be refined. Furthermore, our current study makes use of bulk RNA extraction. While we have taken steps to subtract “background” signal from white blood cells in the form of processed healthy

control samples, we plan to integrate single-cell techniques into future work to better assess intrapatient heterogeneity.

In addition to establishing the presence of CTC clusters in blood samples taken from mCRPC patients, we examined RNA expression signatures with respect to clinical outcomes. Using multi-gene scoring paradigm, we have identified a number of CTC-based genes associated with progression and death in our training cohort. Further work to validate this approach in larger cohorts and to explore the implications of CTC stemness is ongoing.

Chapter 3 Interrogation of the role of HER2 and EGFR in prostate cancer metastasis

3.1 Abstract

Activation of the EGF receptors EGFR (ErbB1) and HER2 (ErbB2) drives the progression of multiple cancer types through complex mechanisms that are still not fully understood. In this study, we report that HER2 expression is elevated in bone metastases of prostate cancer independently of gene amplification. In examining the role of EGFR in tumor-initiating cells (TICs), we found that EGFR expression was required for primary and secondary sphere formation of prostate cancer cells. EGFR expression was also observed in circulating tumor cells (CTCs) during prostate cancer metastasis. Dual inhibition of HER2 and EGFR resulted in significant inhibition of tumor xenograft growth, further supporting the significance of these receptors in prostate cancer progression. Overall, our results indicate that EGFR promotes survival of prostate TICs and CTCs that metastasize to bone, whereas HER2 supports the growth of prostate cancer cells once they are established at metastatic sites.

3.2 Introduction

Significant roles for the ErbB family receptors [EGFR (HER1), HER2, HER3, and HER4] have been suggested in prostate tumorigenesis and progression for a number of years, but the molecular mechanisms by which ErbB family members support the disease progression and metastasis is not fully understood. Aberrant activities of HER2 and EGFR have also been associated with development of castration-resistant disease, possibly due to compensation for the loss of androgen signaling (163-166). Like prostate cancer, breast cancer is a hormone-

sensitive/refractory disease, and both share common sites of metastases, such as bone. Importantly, adjuvant treatment with HER2 inhibitors has reduced the recurrence rate by more than 50% in women suffering from breast cancer (167). On the basis of our findings here that ErbB receptor proteins are overexpressed in metastatic prostate cancer, it may be prudent that patients suffering from advanced disease are screened for treatment with ErbB-specific inhibitors.

Although the role of HER2 in prostate cancer remains controversial (168), HER2 protein has been reported to be overexpressed during prostate cancer progression, and HER2-dependent signaling may support the development of castration-resistant prostate cancer (CRPC) by activating androgen receptor signaling through androgen ligand–independent mechanisms (166). Recent evidence supporting HER2 function in prostate cancer comes from a comprehensive immunohistochemical (IHC) evaluation of HER2 protein in a tumor array composed of 2,525 prostate cancer samples (169). This study revealed significant associations between HER2 staining and advancing stage and grade of disease and tumor recurrence with only 1 in 2,525 (0.04%) cases exhibiting HER2 gene amplification. It is also known that EGFR overexpression is associated with the development of CRPC in patients (165). However, EGFR expression is not significantly associated with tumor differentiation, positive margins, extra-prostatic invasion, or preoperative prostate-specific antigen (PSA; (165)), suggesting that EGFR expression only increases during disease progression and in the development of castration-resistant disease.

The intermediate state between primary and metastatic tumors and their ultimate metastases are circulating tumor cells (CTC), those cells that are shed and present in the blood stream (2). The clinical significance of CTCs has been shown in multiple cancers, including prostate cancer, in which the prognostic values of CTC counts above and below the cutoff of 5 CTCs/7.5 mL whole blood have been associated with overall survival (141). Beyond enumeration,

novel CTC isolation technologies have also enabled further characterization, including protein expression by immunofluorescence (17, 115).

HER2 expression has been investigated in CTCs, largely in work conducted in breast cancer. Using the FDA approved CellSearch, HER2-positive CTCs have been sought out by immunofluorescence, oftentimes identifying discordant HER2 status between CTCs, primary tumors, and metastases. Graded as having weak, moderate, and strong HER2 expression, HER2-positive CTCs were detected in 14/58 breast cancer patients with CTCs in the GeparQuattro clinical trial, some of whom had HER2-negative primary tumors; HER2-positive CTCs were also associated with higher tumor stage (170). Another study defined HER2 CTC positivity as having at least 50% of CTCs displaying HER2 expression, with 7 of the 96 metastatic breast cancer patients with CTCs meeting that criterion (171). The expression of HER2 as well as other molecular markers associated with endocrine therapy resistance have been investigated in CTCs using CellSearch to generate an endocrine therapy index (172). This study also observed discordance between CTC HER2 status and the status of primary or metastatic tissue. Other studies have examined both CellSearch and the RT-PCR detection based assay AdnaTest on breast cancer cohorts. In one such study, CTC HER2-status concordance with the primary tumor was observed in 59% of samples, while CTC HER2-status concordance with metastatic sites was observed in 67% of samples (173). Another study compared the two tests, detecting HER2-positive CTCs in 41% of metastatic breast cancer patients by CellSearch and 47% of patients by AdnaTest (174). That same study detected HER-positive CTCs in patients with HER2-negative primary tumors in 32% of patients by CellSearch and 49% of patients by AdnaTest.

HER2 expression in CTCs has also be assessed using microfluidic technologies. HER2-positive CTCs were discovered in 84% of 19 ER+/HER2- breast cancer patients as determined

through immunofluorescence and FACS of cells isolated by the CTC-iChip (175). CTC cultures derived from patients in this study exhibited HER+ and HER2- subpopulations which were available for drug testing (175). Antibodies against HER2 have been using for CTC isolation in immunocapture. In addition to using anti-HER2 along with anti-EpCAM and anti-EGFR for capture, a study using the Herringbone-chip also using RNA ISH for HER2 to confirm that captured mesenchymal cells were of tumor origin (74). A micropost chip functionalized with HER2 has been used to capture CTCs from five breast cancer patients along with five gastric cancer patients (71).

There has also been a great deal of interest in EGFR expression in CTCs, with much of the investigation taking place in lung cancer facilitated by microfluidic technologies. As early 2008, CTCs captured using the original CTC Chip were investigated for EGFR-activating mutations (detected in 11/12 non-small cell lung cancer (NSCLC) patients (68)). A PDMS CTC chip was used to culture CTCs captured from NSCLC patients, with some of the subsequent analysis focusing on EGFR (122). EGFR expression was detected both through RT-qPCR and immunofluorescence, showing expression at both the RNA and protein level. EGFR mutations in CTCs isolated from an NSCLC patient were also assessed serially and in conjunction with treatment in a study performed using the NanoVelcro substrate (120). Tumor cells isolated from both blood and lung lavage samples from NSCLC using the VerIFAST platform were measured for EGFR expression using immunofluorescence (76). In addition to immunoaffinity methods, inertial sorting has also been used to isolated CTCs from NCLC patients and then interrogated for EGFR-activating mutations using mass spectrometry (176). CTCs isolated through CellSearch have been assessed for EGFR through immunofluorescence staining in breast (177), lung (178), and prostate cancer as well (33).

In this study (4), we evaluated the expression of HER2 protein in metastatic samples obtained from patients with prostate cancer and investigated the functional significance of HER2 and EGFR overexpression in the osseous growth of human prostate cancer cells *in vivo*. The role of EGFR was also examined in the tumor-initiating population of prostate cancer cells, where it may support their survival and promote self-renewal in the bone microenvironment. In addition, results from patient samples suggest that EGFR may also have a role in the survival of CTCs in the metastatic progression of prostate cancer.

3.3 Methods

3.3.1 Cell culture and inhibitors

LNCaP, MCF7, BT-474, and SK-BR-3 were purchased from ATCC. C4-2B and C4-2B luciferase transduced (C4-2B^{Luc}) cell lines were obtained as previously described (18). All cell lines, including luciferase and knockdown cell lines, were fingerprinted (IDEXX RADIL). Cell lines were cultured in DMEM (Lonza), RPMI-1640 (Mediatech), 50% DMEM/50% RPMI, or T-Medium (Gibco), supplemented with 10% FBS (HyClone), penicillin/streptomycin/Fungizone, and l-Glutamine (Gibco). Cells were kept in a 37°C, 5% CO_2-humidified incubator. Lapatinib and afatinib were purchased from LC Laboratories. Cetuximab and trastuzumab were obtained from the Cancer Center Pharmacy, University of Michigan (Ann Arbor, MI).

3.3.2 Generation of lentiviral vectors and stable cell lines

3.3.2.1 ERBB2 knockdowns

C4-2B cells were transduced with a panel of 4 lentiviral constructs containing short-hairpin HER2 or shVector and incubated for 6 hours. Four shHER2 oligos (MISSION^{TM} SHGLY) were obtained from SIGMA Co and tested in MCF7, LNCaP, C4-2B, and C4-2B^{Luc} cell lines. Western blot analysis was used to identify HER2 protein knockdown cells as compared to shVector

expressing cells. The sequence that showed the highest downregulation of HER2 protein expression was characterized in stable cell lines (C4-2B and MCF7) following selection in Puromycin. The shHER2 construct reported here contained the following target sequence: TGTCAGTATCCAGGCTTTGTA. Other shHER2 sequences tested include CAGTGCCAATATCCAGGAGTT, GCCATCAAAGTGTTGAGGGAA, and CAGCTCTTTGAGGACAACTAT. These oligos were utilized in prostate and breast cancer cells (12).

3.3.2.2 EGFR knockdowns

A series of oligos (MISSION^{TM}) was directed against EGFR: GCTGGATGATAGACGCAGATA, GCTGCTCTGAAATCTCCTTTA, GCCACAAAGCAGTGAATTTAT, CCTCCAGAGGATGTTCAATAA, CAGCATGTCAAGATCACAGAT. These oligos were tested in LNCaP, C4-2B and C4-2B^{Luc} cells. Knockdown was validated by western and found to be lethal after two passages in culture.

3.3.3 Animal models and treatment

All experiments began with 8-week-old male NOD/SCID mice from Jackson Laboratories. Mice received (right) tibia injections of 5×10^5 C4-2B cells containing either shVector (n = 10) or shHER2 (n = 10). After 3 weeks, the mice were sacrificed and tibiae (right and left) were removed and fixed in 10% formalin. For the inhibitor experiments, each mouse (n = 30) received an intratibial injection of 1×10^6 C4-2B^{Luc} cells in their right tibia. Drug treatments started the following day for lapatinib (n = 10) and trastuzumab + cetuximab dual treatment groups (n = 10). Untreated control mice (n = 10) had the same tibia xenografts. Lapatinib was given orally at 100 mg/kg 5 times per week. The inhibitor cocktail [trastuzumab (10 mg/kg) + cetuximab (3 mg/kg)] was given by intraperitoneal (i.p.) injections 3 times per week. After 7.5 weeks of treatment, the

mice were sacrificed and tibiae collected in 10% formalin. These experiments were based on reports of dose escalation of lapatinib (179-181) and on combinations of inhibitors (182). All animal experiments were approved by the Institutional Animal Care and Use Committee.

3.3.4 IHC and tissue microarrays

Prostate cancer tissue microarray (TMA) slides were designated TMA 85 (primary and bone) and TMA 142 (primary, lymph node, and liver). TMAs were prepared as previously described (183, 184). Formalin-fixed, paraffin-embedded (FFPE) tissue blocks with tumor samples were previously identified by a pathologist and processed as instructed by the IRB. Prostate tissue samples were taken from the radical prostatectomy series and the University of Michigan SPORE Rapid Autopsy Program (185). Tumors were staged and graded using the Gleason system (186). All tissue sections were reviewed by 2 board-certified genitourinary pathologists (R. Shah, L.P. Kunja) and scored for stain intensity (0–3), percent positivity, and subcellular location.

The tibiae from the mice were decalcified in Decalcifier II (Leica Biosystems) for 3 hours before paraffin embedding. Antigen retrieval was performed for NeoMarkers' staining by pretreating with citrate at pH 6 with microwaving for 10 minutes, cooled for 10 minutes, and washed with water for 10 minutes. There was no pretreatment for Dako staining, which was stained using the Dako AutoStainer. All tissue sections were cut to 4-μm thickness. Hematoxylin and eosin (H&E) staining was analyzed, followed by IHC for the following biomarkers in serial sections: anti-HER2 (NeoMarkers Ab-17 1:100), anti-HER2 (Abcam EP1045Y 1:100), anti-HER2 (Dako A0485 manufacturer spec.), anti-EGFR (Life Technologies 31G7 1:100), anti-CK8/18 (Epitomics ac-9002RUO 1:100), anti-pHist3 (Abcam ab5176 1:500), anti-RANK (R&D Systems 80707 1:500), anti-Ki-67 (Dako MIB-1 1:200), and anti-E-cadherin (ThermoFisher HECD-1 1:200).

3.3.5 Tissue imaging

All photomicrographs were taken on an Olympus BX51 with a DP72 camera system using the CellSense software for analysis. Three different fields of cells were counted using 600x magnification for a total of at least 500 cells/ analysis of positive staining (RANK and Ki-67).

3.3.6 Cell viability assay

Five thousand C4-2B cells were seeded per well into 96-well plates, and 24 hours later, lapatinib was added to reach the indicated concentrations. The Titer Blue reagent (CellTiter-Blue Cell Viability Assay, Promega) was used to detect cell viability at 1, 24, and 48 hours of treatment using a fluorescent plate reader (Molecular Devices tunable SpectraMax M5). This assay was conducted as per the manufacturer's instructions.

3.3.7 Western blotting

Protein isolation and Western blotting were carried out as previously described (187), with these primary antibodies: anti-HER2 (NeoMarkers Ab-17) anti-HER2 (Abcam EP1045Y), anti-EGFR (NeoMarkers H9B4), anti-α-tubulin (Upstate DM1A), and anti-E-cadherin (ThermoFisher HECD-1). Mouse and rabbit HRP-conjugated secondary antibodies (Bio-Rad) were used and illuminated by ECL (Advansta). One Western blot assay utilized IRDye 680 goat anti-mouse and IRDye 800 goat anti-rabbit secondary antibodies (LI-COR).

3.3.8 Quantitative flow cytometric analysis

Cell surface HER2 and EGFR were quantified using the Dako QIFIKIT according to the manufacturers' protocol. Three different passages of C4-2B cells were grown in complete T-medium without phenol red and detached with TrypLE Express (Gibco). A total of 1×10^5 C4-2B cells were analyzed in triplicate. HER2-binding sites were saturated with anti-HER2 (R&D Systems 191924; 10 μg/mL) and EGFR sites with anti-EGFR (LSBio 225; 10 μg/mL) as primary

antibodies. Alexa Fluor 488 goat anti-mouse IgG (H+L) (Invitrogen; 1:400) was utilized as the secondary antibody. The median fluorescence intensity (MFI) was analyzed by flow cytometry (Accuri BD analyzer) and the number of molecules per cell calculated by FlowJo and subsequent extrapolation of the samples' MFI into a standard curve on the basis of the calibration beads MFI.

3.3.9 Cell staining and prostate tumor sphere (prostasphere) formation

C4-2B cells were prepared as described for "QIFIKIT analysis" and profiled by FACS with fluorescent-labeled anti-EGFR FITC (Abcam ICR10 1:40), anti-HER2 APC (B.D. Neu24.7 1:133), and anti-RANK PE (Abcam 9A725 1:17) antibodies. Live cell staining of 1×10^6 cells (per analysis) was carried out in staining buffer (RPMI no phenol red with 2% FBS) in a final volume of 200 μL. Cells were stained for 1 hour on ice plus 10 minutes at room temperature, washed with 2 mL of staining buffer, filtered through cell strainer–capped tubes (Falcon 352235), and then resuspended in 250 μL of staining buffer with DAPI. FACS was carried out as described previously (188), and cells were sorted directly into T-Medium. The MoFlo XDP instrument was utilized for the analysis. DAPI was added for selection of viable (vs. DAPI-negative) cells where DAPI-positive cells (no antibody staining) were sorted as viable controls for sphere formation. For positive cell staining: $EGFR^{high}$ (top 5%), $EGFR^{low}$ (bottom 5%), and $HER2^{high}$ (top 5%), $HER2^{low}$ (bottom 5%) cells were collected and seeded in triplicate at 200 cells/200 μL (96-well plates) in complete MammoCult medium (STEMCELL Technologies). Primary prostaspheres were grown for 10 days followed by disruption with trypsin and then reseeded (200 cells/200 μL of MammoCult medium) to develop secondary spheres after another 10 days of growth. Spheres were viewed using an Olympus CKX41inverted microscope.

3.3.10 FISH

An *ERBB2* BAC probe, which encoded for the entire gene sequence of the *ERBB2* gene (introns and exons), was utilized for gene copy number analysis. Labeled probe was generated by DNase treatment of the *ERBB2* gene and Nick translation incorporated Dig-dUTP nucleotides into dsDNA. *ERBB2* cDNA was denatured by heat treatment at 75°C to produce single-strand DNA probe. Fixed tissues (on slides) were denatured with formamide at 42°C prior to hybridization with labeled probe. Fluorescent antibody to Dig-dUTP was employed for imaging and analysis.

3.3.11 In vivo tumor imaging with firefly luciferase bioluminescence

Mice received intraperitoneal injections of 2-mg D-luciferin and were anesthetized. Ten minutes after the injection, the luciferase signatures were captured using a PerkinElmer IVIS Spectrum with Living Image software (v4.2).

3.3.12 CTC isolation using graphene oxide chip

CTCs were isolated from whole blood samples taken from consented patients with prostate cancer under IRB: HUM52405. Procedures for microfluidic chip fabrication and CTC isolation using the microfluidic graphene oxide (GO) chip have been described elsewhere (115). Briefly, tetrabutyl ammonium hydroxide–intercalated GO nanosheets grafted with phospholipid-polyethyleneglycol-amine were assembled on gold-patterned silicon substrates and enclosed in a polydimethylsiloxane (PDMS, Dow Corning Sylgard) chamber. Components of a functionalization chemistry could then be introduced to the assembled device via Harvard Apparatus syringe pump to ultimately present an antibody against the epithelial cellular adhesion molecule, anti-EpCAM (R&D Systems). Whole blood was flowed through the device to enable CTC capture, after which the device was washed and the cells were fixed. Cells were then permeabilized and stained on-chip with primary antibodies against cytokeratin 7/8 (CK, BD

Biosciences CAM5.2), CD45 (Santa Cruz 3H1363), and EGFR (Invitrogen 31G7) with the appropriate secondary antibodies (Invitrogen) and the nuclear stain DAPI (Invitrogen). Devices were scanned using a Nikon TI inverted fluorescence microscope. Nucleated $CK^+/CD45^-$ entities were enumerated as CTCs.

3.3.13 Statistical analysis

Results of *in vitro* experiments are presented as mean ± SD or mean ± SE. The Student *t* test was used to compare continuous variables when there were 2 groups. A paired *t* test was used for paired data comparisons. Mouse tumor xenografts experiments are presented with means and SEs of the mean. Pairwise comparisons were made using ANOVA within the models at cross-sections and the Bonferroni multiple comparisons adjustment was used for pairwise tests. Analyses were completed using SAS 9.3 (SAS Institute). The mean values between prostasphere groups were compared in ANOVA by Tukey multiple comparisons using GraphPad Prism 6.0 (GraphPad Software, Inc.). Alpha of 0.05 determined statistical significance.

3.4 Results

3.4.1 Assessment of HER2 in organ-confined, localized, and metastatic prostate cancer

It is known that EGFR is overexpressed in metastatic and CRPC (165); however, the evaluation of HER2 protein at this stage of prostate cancer has not been investigated. Mechanisms of HER2 overexpression have historically been explained in the context of gene amplification, whereas transcriptional and posttranscriptional mechanisms leading to increased HER2 protein have not been critically evaluated. We utilized two distinct HER2 antibodies: the first, a cytosolic-specific polyclonal antibody (Dako); and the second, two monoclonal antibodies that recognize two cytosolic epitopes (NeoMarkers). Both antibodies were used to evaluate HER2 protein in FFPE sections of normal prostate, localized prostate cancer, and metastatic prostate cancer. We

evaluated H&E-stained serial sections (**Figure 3-1a, i-ii**) followed by staining with the indicated HER2 antibodies (**Figure 3-1a, iii-vi**). A direct comparison of both antibodies revealed that the Dako antibody does not detect HER2 protein in normal prostate, but that the NeoMarkers antibody detects low levels of HER2 located at the basal–lateral junctions of luminal epithelium (**Figure 3-1a, iii and v**). Both HER2 antibodies detected elevated protein in prostate cancer tissue (**Figure 3-1a, iv and vi**), and we found that EGFR was expressed in moderate levels in localized (primary) cancer (**Figure 3-1a, vii and viii**).

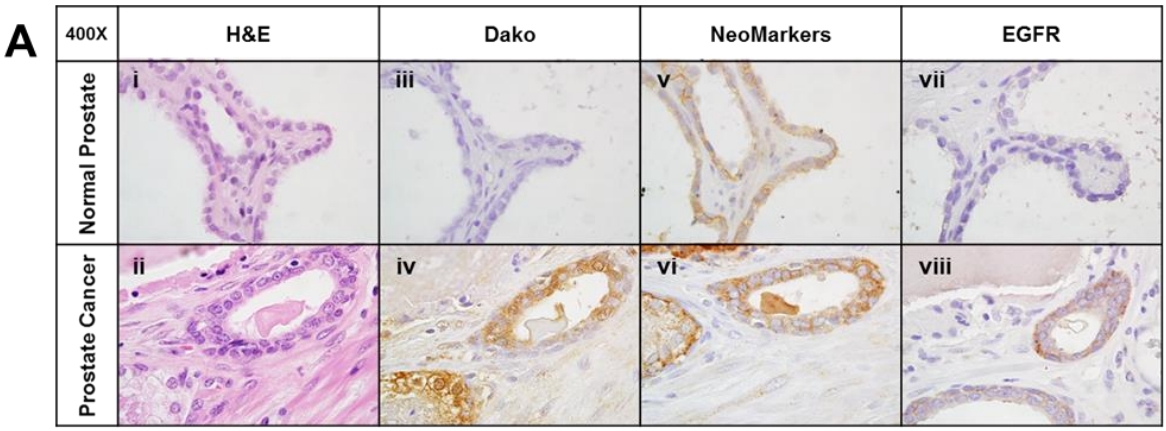

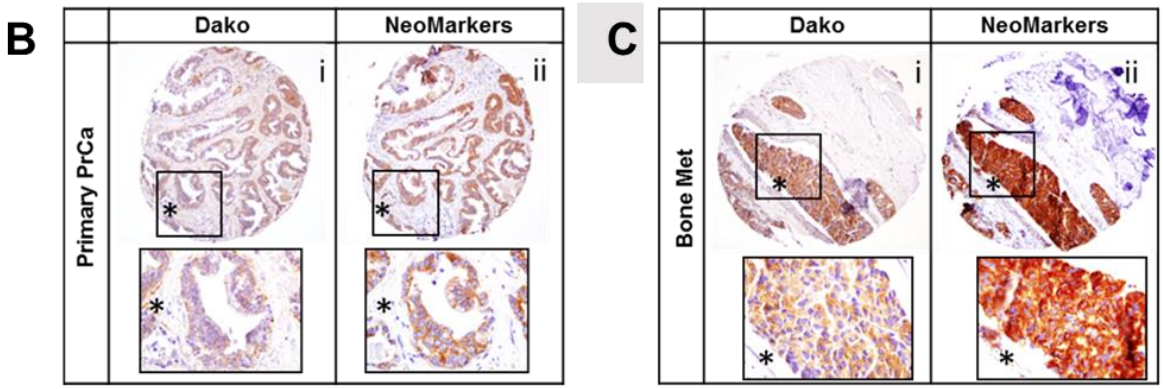

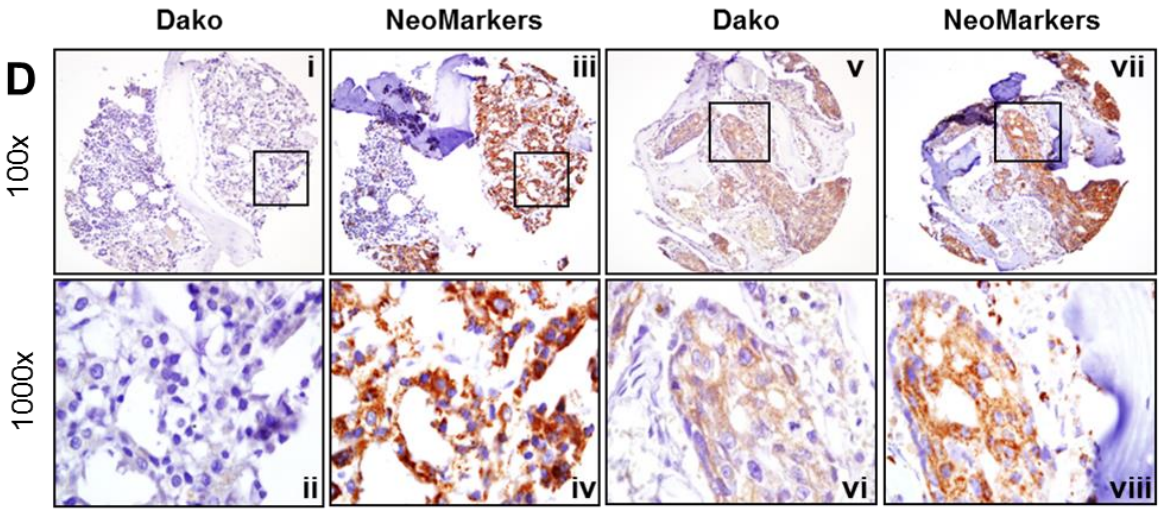

E

Dako			NeoMarkers		
Cytoplasmic	Membranous	Both	Cytoplasmic	Membranous	Both
57.70%	7.70%	34.60%	34.10%	0.00%	65.90%

Figure 3-1 Assessment of HER2 in organ-confined, localized, and metastatic prostate cancer. a) Serial sections of normal prostate (i, iii, v, vii) and prostate cancer (ii, iv, vi, viii) were stained with H&E, Dako (Rb.pAb anti-HER2), NeoMarkers (MAb anti-HER2), and ab-15 (MAb anti-EGFR). b) IHC staining of primary prostate cancer. c) Bone metastases from serial sections of TMA 85 with Dako and NeoMarkers antibodies. d) Two different patients' bone cores from TMA 85 stained with Dako and NeoMarkers antibodies. Inset boxes (ii, iv, vi, viii) are 1,000 magnification of 400 images (i, iii, v, vii). e) Tabulated summary of cellular distribution of HER2 staining on TMA 85 (4).

A 17-patient prostate cancer metastasis TMA (TMA 85) was stained with the Dako and NeoMarkers HER2 antibodies **(Figure 3-1b, c)**. An intensity score (0–3) was assigned to the stained core by 2 board-certified genitourinary pathologists (R. Shah and L.P. Kunja). Shown in **Figure 3-1d** (core 1: i–iv and core 2: v–viii) are serial sections of two representative patients with bone metastasis from the metastasis array to characterize the cellular location of HER2 staining with these antibodies. Cellular localization of HER2 staining in the bone metastasis cores is described as cytoplasmic, membranous, or as a combination of both (**Figure 3-1e**). The Dako antibody exhibited primarily cytosolic staining in organ-confined disease (**Figure 3-1b**) and retained this pattern in bone metastasis (**Figure 3-1c, d**). Interestingly, the staining for the NeoMarkers antibody changed from a predominantly membrane pattern in early-stage disease (**Figure 3-1b**) to an intense cytosolic pattern in bone metastasis (**Figure 3-1c, d**). As in previous experiments, the NeoMarkers antibody appears more sensitive for the detection of HER2 *in situ* than the Dako antibody. FISH analysis was performed on TMA 85 and TMA 142, another prostate cancer array with 49 patients, to determine whether *ERBB2* gene amplification was present. In agreement with the FISH analysis of radical prostatectomy specimens reported by Minner and colleagues (169), all 35 patients' TMAs had normal *ERBB2* copy numbers, thus

eliminating gene amplification as a mechanism of HER2 and EGFR protein overexpression (**Figure 3-2**).

ERBB2 Fluorescence In Situ Hybridization (FISH)									
ERBB2 Probes		Total Cores	Analyzed Cores	5' Del	3' Del	Amp	5' Dup	3' Dup	Summary
TMA 85	*ERBB2* locus/control	44	5	0	0	0	0	0	TMA 85 No cases Amplified
TMA 142	*ERBB2* locus/control	54	40	0	0	0	0	0	TMA 142 No cases Amplified

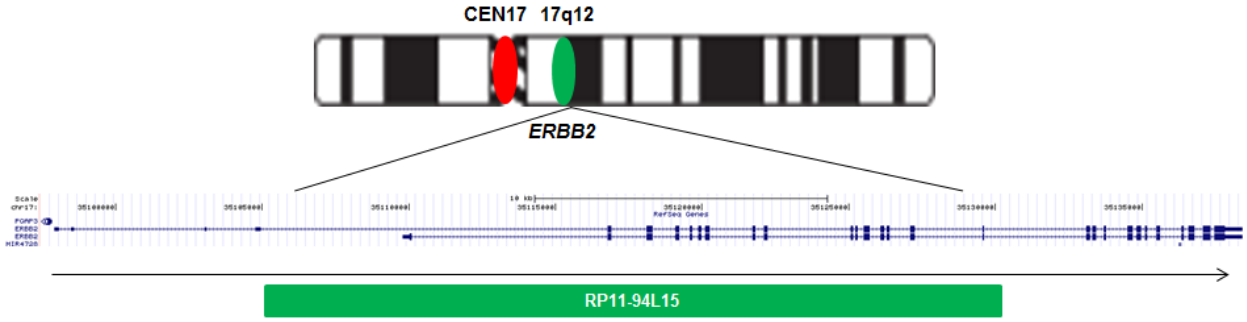

Figure 3-2 Fluorescence in situ hybridization analysis of ERBB2. Schematic diagram depicts the genomic organization of ERBB2 on chr17q12: deletions (Del), amplifications (Amp), duplications (Dup). The red dot indicates the location of Chr. 17 centromere probe and the green dot is the location of ERBB2 locus on Chr17q12. BAC clone RP11-94L15 spanning 161kb on chr17q12 contains ERBB2 gene (4).

3.4.2 The requirement of HER2 for osteoblastic growth

To determine whether HER2 protein is required for the osseous growth of prostate cancer cells, we knocked down ERBB2 mRNA in C4-2B cells using lentiviral constructs containing ERBB2-specific shRNA sequences (shHER2) or scrambled HER2 sequences (scrVec). Reduction of ERBB2 was confirmed by Western blot analysis of shHER2 C4-2B cells compared with scrVec and parental (no transduction) control cells (**Figure 3-3a**). scrVec or shHER2 C4-2B cells were injected into the tibia of male SCID mice and allowed to grow for 5 weeks, at which time the tibiae were prepared for IHC analysis. The NeoMarkers antibody in scrVec and shHER2 tumors confirmed that the loss of HER2 expression was maintained in the knockdown xenografts *in vivo* (**Figure 3-3b**). EGFR levels were unchanged in these tumors. However, levels of the proliferation

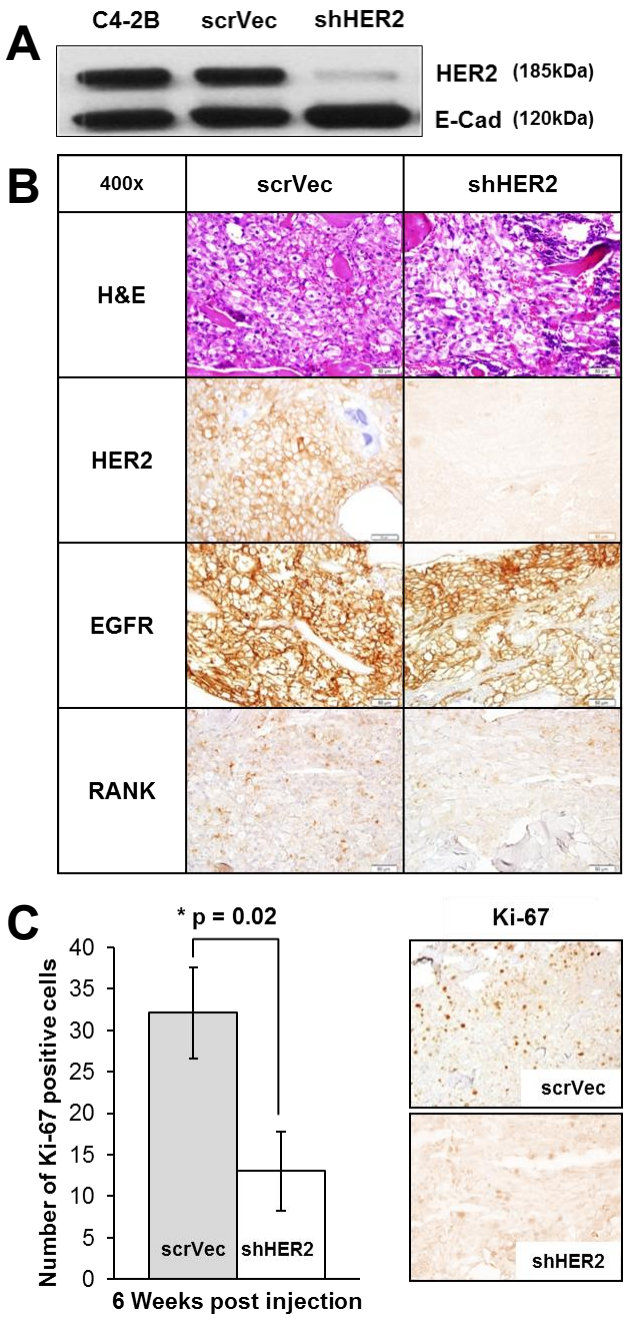

*Figure 3-3 Characterization of HER2 knockdown in C4-2B prostate cancer intratibial xenografts. a) Western blot analysis of HER2 expression in C4-2B parental, scrVec, and shHER2 cells. E-Cadherin was used as a loading control. b) SCID mouse model of tibiae injections of shHER2 versus scrVec C4-2B cells. Representative IHC of the tibiae at 3 weeks post injection using H&E, anti-HER2 (NeoMarkers), anti-EGFR, and anti-RANK. c) From these same mice tibiae, Ki-67 staining was assessed by counting 5x100 cells and using the average percent positive. *, P = 0.02 (4).*

marker, Ki-67, were reduced in parallel with the reduction in HER2 protein expression (**Figure 3-3c**), indicating reduced cellular proliferation in these bone xenografts.

3.4.3 The role of EGFR and HER2 in prostasphere formation

To determine whether HER2 or EGFR plays a regulatory role in the tumor-initiating component of prostate cancer metastasis, we quantified HER2 and EGFR cell surface expression in C4-2B cells by flow cytometry (**Figure 3-4a**). The amount of EGFR (260,000 molecules/cell) on the cell surface was 10-fold higher than HER2 (27,000 molecules/cell) on C4-2B cells. This difference could be visualized by weak cell surface immunofluorescence using an HER2-specific antibody (**Figure 3-4b, i**) compared with strong cell surface immunofluorescence using an EGFR-specific antibody (**Figure 3-4b, ii**). We next examined sphere formation in cells that were selected from the top 5% of EGFR or HER2 surface expression in comparison

with cells selected for the lowest 5% of EGFR or HER2 surface expression. Only high EGFR expressing cells were able to produce primary spheres compared with the DAPI-negative or viable control cells (**Figure 3-4c, d**). In addition, the ability of C4-2B cells to form primary spheres was only reduced in low EGFR-expressing cells. There was no independent requirement for HER2 expression for primary sphere formation, as $HER2^{low}$ cells were fully capable of sphere formation (**Figure 3-4c, d**). To confirm that high EGFR expression was important for the tumor-initiating potential of C4-2B cells, we performed secondary sphere formation assays, which validated the association of high EGFR protein on cell surface and the ability to form secondary spheres (**Figure 3-4c, d**). Because sphere-propagating cells have been associated with tumor-initiating or stem cell–like properties in prostate cancer cells (189-192), our findings support the idea that EGFR may mediate prostate cancer metastasis by supporting the TICs.

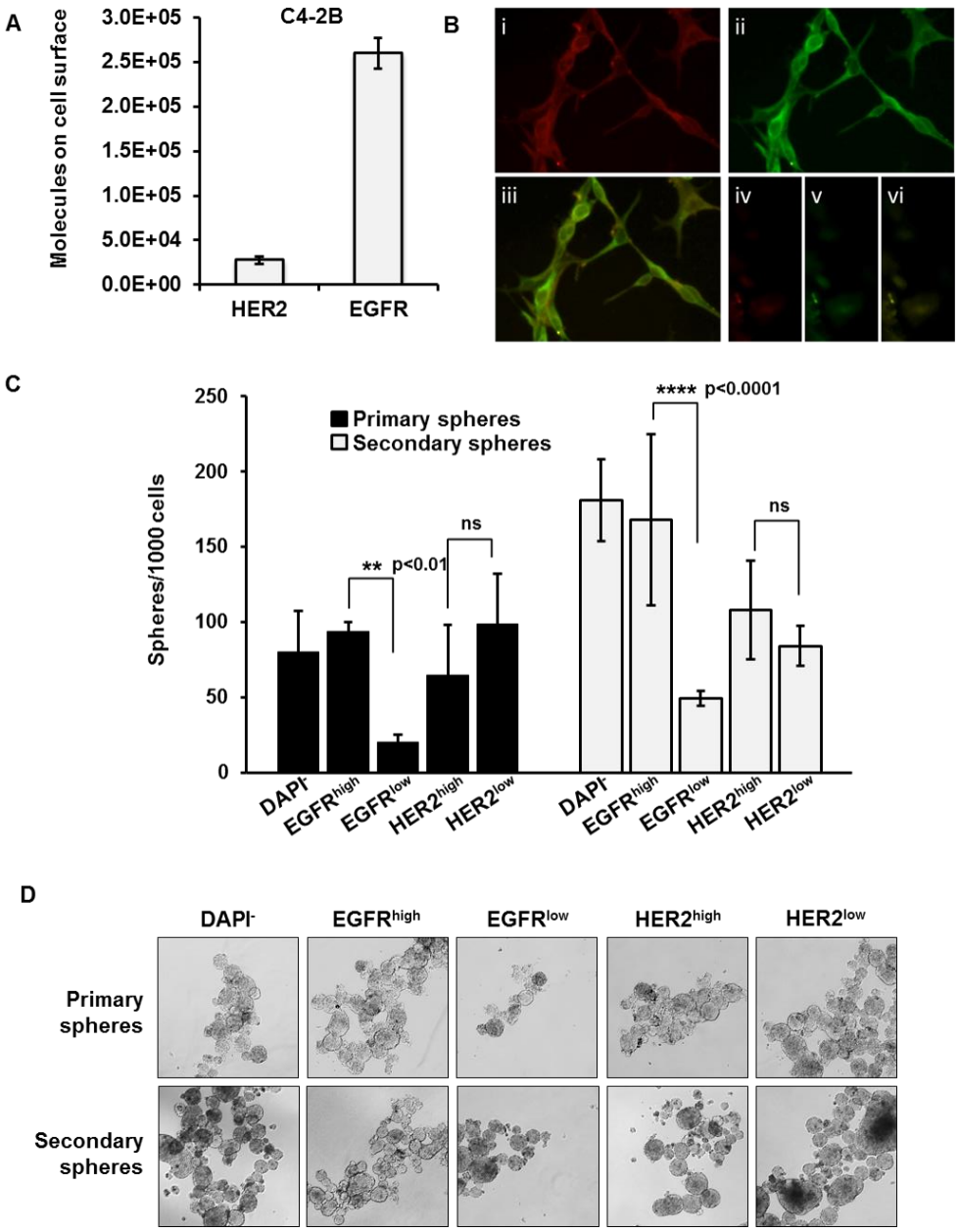

*Figure 3-4 The impact of EGFR and HER2 levels on prostate sphere formation. a) Flow cytometric quantification of EGFR and HER2 molecules on the surface of C4-2B cells under normal growth conditions. b) Fluorescent microscopy of costained C4-2B cells: i, anti-HER2; ii, anti-EGFR; iii, EGFR and HER2 colocalization; and iv–vi, the respective staining backgrounds. c) C4-2B cells were sorted via flow cytometry for high or low expression of EGFR or HER2 (independently). The sorted cells were grown as primary and secondary prostate spheres and then quantified. Cells expressing low levels of EGFR were significantly inhibited in their capacity to form primary and secondary prostaspheres than cells expressing high levels of EGFR. The results represent the mean (n = 3) of 1 of 3 independent experiments. **, $P \leq 0.01$; ****, $P \leq 0.0001$; ns, not significant ($P > 0.05$). D, Brightfield photographs (x10) of the primary and secondary C4-2B prostaspheres as analyzed in C (4).*

3.4.4 EGFR is expressed on CTCs from patients with bone metastasis

CTCs may share important characteristics with cancer stem cells, such as the capacity for dormancy and the expression of a variety of growth factor receptors, including HER2 and EGFR (33, 170, 171, 177). To determine whether EGFR is expressed on CTCs in patients with prostate cancer bone metastasis, we isolated CTCs from whole blood samples taken from consented patients with prostate cancer using the microfluidic GO chip (115). An antibody against the epithelial cellular adhesion molecule (anti-EpCAM, R&D Systems) was used for CTC capture, and captured CTCs were then stained on-chip with primary antibodies against cytokeratin 7/8 (CK), CD45, and EGFR (**Figure 3-5c-e**). The clinical characteristics of the 10 patients are described in **Figure 3-5a**. All patients exhibited metastatic disease with significant bone involvement. CTCs were present in all 10 patients and EGFR staining was detected on CTCs in 9 of 10 patients. A median of 35.5% of CTCs were positive for EGFR staining (**Figure 3-5b**).

A

	N	%
Number of patients	10	100%
Age		
Median (range)	67.5	(57-77)
Castrate Resistant	10	100%
Prostatectomy	4	40%
Prostate-specific antigen		
Median (range)	7.25 ng/mL	(0.09-346.7 ng/mL)
Gleason score		
Median (range)	7	(6-9)
Disease involvement		
Bone only	8	80%
Bone plus soft tissue	2	20%
Hormonal therapies	10	100%
Targeted agents	2	20%
Chemotherapy	3	30%
Radiation	9	90%

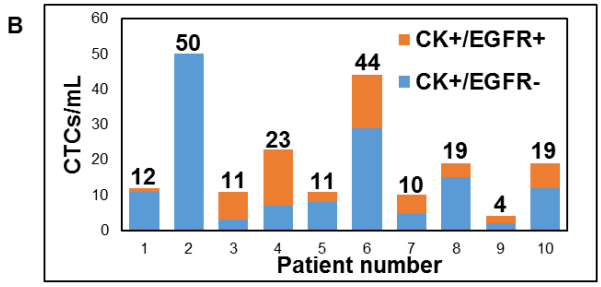

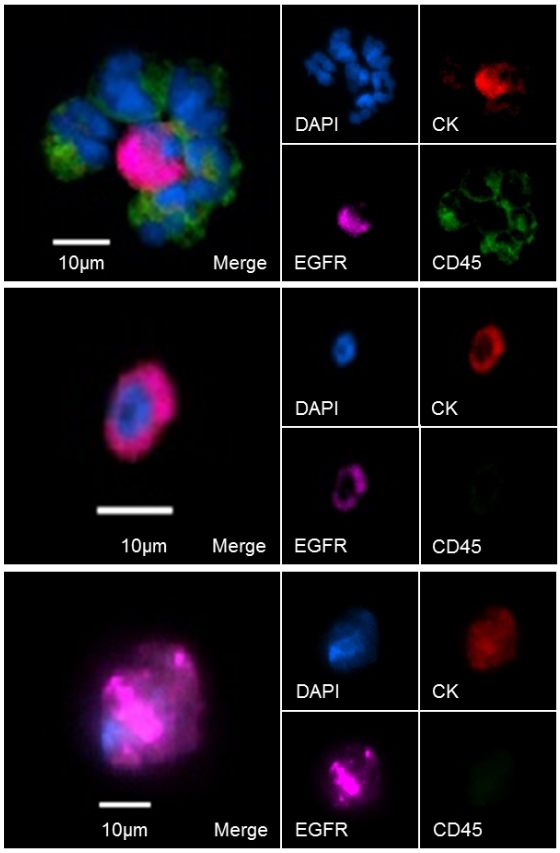

Figure 3-5 Analysis of CTCs from 10 patients with metastatic prostate cancer. a) Clinical history of patients with prostate cancer analyzed for CTCs. b) Number of $CK^+/EGFR^+$ and $CK^+/EGFR^-$ CTCs isolated per 1 mL whole blood. Numbers above the columns indicate the total number of CTCs isolated from patients 1–10. c) Cluster of white blood cells surrounding a $CK^+/EGFR^+$ CTC from patient 3. White blood cells stained positive for CD45. d, e) Other representative images of $CK^+/EGFR^+$ CTCs from patients 3 and 5 respectively (4).

3.4.5 Dual inhibition of EGFR and HER2 is cytotoxic to C4-2B cells in culture and in intratibial xenografts

The observation that EGFR protein expression was unchanged in viable HER2-knockdown cells coupled with the finding that reduction of EGFR expression was lethal in C4-2B cells suggested a role for EGFR in the survival of prostate cancer cells. C4-2B cells exhibited dose-dependent sensitivity to the pan-ErbB tyrosine kinase inhibitor lapatinib over 48 hours (**Figure 3-6a**). The efficacy of lapatinib and afatinib, a related EGFR/HER2 tyrosine kinase inhibitor, on the C4-2B cells was associated with a reduction of both HER2 and EGFR protein following treatment (**Figure 3-6b**). To further assess a dual role for HER2 and EGFR in survival, C4-2B

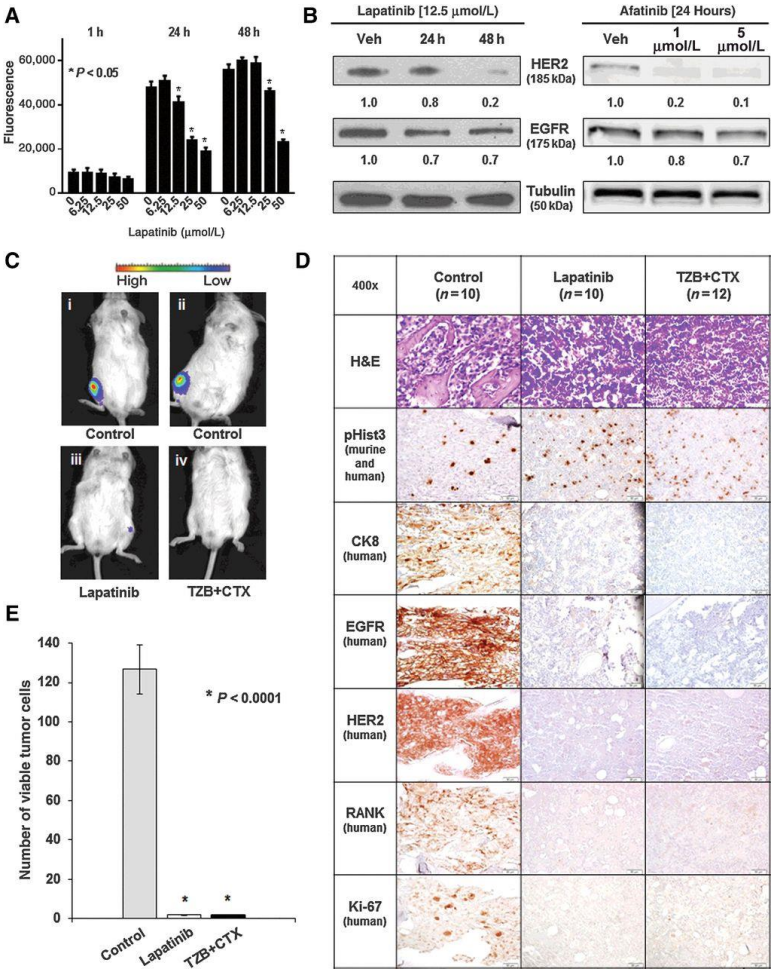

*Figure 3-6 Pharmacologic inhibition of HER2 and EGFR is cytotoxic to prostate cancer in vitro and prevents cancer growth in vivo. a) C4-2BLuc cell viability measured by Titer Blue following lapatinib treatment for 1, 24, and 48 hours. *, P < 0.05 compared with vehicle control. b) Left, Western blot analyses of HER2 and EGFR expression in C4-2B cells following incubation with vehicle or 12.5 μmol/L lapatinib at 24 and 48 hours. Right, Western blot analysis of C4-2BLuc cells after incubation with vehicle, 1 μmol/L, or 5 μmol/L afatinib for 24 hours. Tubulin was used as a loading control. Left, densitometry was performed with ImageJ. Right, fluorescence was measured using the Odyssey CLx (LI-COR) and quantified using Image Studio v3.1.4 software (LI-COR). Both, normalized to tubulin, values shown under respective lanes. c, d) C4-2BLuc cells were injected into mouse tibiae 1 week prior to treatments. Untreated mice (Control, n = 10), treated with lapatinib (n = 10), or treated with a combination of trastuzumab and cetuximab (TZB + CTX, n = 12) biweekly for 6 weeks. c) Bioluminescence of representative mice at the end of the study where i and ii are control, while iii and iv received dual inhibitor treatments. d) Serial sections of representative tibia stained with H&E, anti-pHist3, anti-CK8, anti-EGFR, anti-HER2, anti-RANK, and anti-Ki-67. e) Quantitation of viable tumor cells was performed by counting three fields of anti-CK8–positive cells in areas that exhibited Ki-67 positivity in three animals per group. No viable human tumor cells could be found in the lapatinib or in the TZB + CTX groups at 7.5 weeks. *, P < 0.0001 (4).*

luciferase–expressing xenografts were established in NOD/SCID mice. Thirty-four mice were randomized into 3 treatment groups and monitored by bioluminescence over 7 weeks. Treatment with lapatinib or a combination of cetuximab (anti-EGFR) and trastuzumab (anti-HER2) resulted in smaller tumors at 7.5 weeks posttreatment (**Figure 3-6c, e**). Significant changes in the expression of several relevant biomarkers were also noted in the drug-treated xenografts (**Figure 3-6d)**. A reduction in HER2 and EGFR staining reflected target-specific cytotoxicity of the C4-2B cells, whereas loss of CK8 and RANK revealed that these human tumor cells were completely depleted in the tibiae. We observed a near-complete reduction of cellular proliferation in the shHER2 C4-2B bone xenografts as

reflected by loss of Ki-67 staining (**Figure 3-6d, e**). Positive staining for murine phospho-Histone H3 (pHist3) indicates that after treatment, there are still proliferating mouse cells in the marrow. The lack of EGFR- and HER2-positive cells suggests that ErbB targeting agents have very pronounced efficacy on prostate cancer in the tibia xenograft model.

3.5 Discussion

Metastatic prostate cancer is a deadly disease that initially responds to docetaxel-based chemotherapy and drugs that suppress androgen signaling. While these treatments may offer temporary relief, relapse is inevitable, and therapeutic options for treating patients who fail primary treatment are very limited. Thus, the search for new therapeutic strategies to treat advanced prostate cancer remains of paramount importance. A promising area of investigation focuses on inhibiting specific growth factor signaling pathways that directly support the metastatic progression of prostate cancer. Alterations in growth factor receptors or their downstream signaling components have been implicated in all human cancers; however, the role of these signaling pathways in the progression of prostate cancer has not been fully established. Agents that target these molecules with a high degree of specificity have been developed and tested in preclinical models and in clinical trials for prostate cancer with varying degrees of success.

Previous studies of HER2 overexpression in multiple cancers have reported ranges from 0% to 100% in IHC studies (193-196). These conflicting sets of data are most likely due to the use of different IHC assays and antibodies. Historically, HER2 overexpression has been determined solely by gene amplification and, because of this, protein levels of HER2 have not been extensively explored and characterized in prostate cancer progression. The histopathologic findings from this study demonstrated that the overexpression of both HER2 and EGFR proteins is associated with

prostate cancer progression and bone metastasis. While *ERBB2* gene amplification does not appear to play a role in the etiology of localized prostate cancer progression (169), this had not been examined in metastatic prostate cancer. Hence, FISH analysis was used on both TMAs showing no instances of *ERBB2* gene amplification, although the amplification of *EGFR* in prostate cancer metastasis remains unreported. Therefore, overexpression of HER2 protein may be sufficient to support the osseous metastasis of human prostate cancer.

In addition, we found that EGFR was overexpressed in prostate cancer cells and that high EGFR-expressing cells preferentially formed prostaspheres. The knockdown of HER2 in C4-2B cells did not affect the levels of EGFR expression. Our attempts to knockdown EGFR were lethal to prostate cancer cells, which is not surprising, as these lethal EGFR knockdowns have been observed in a number of studies (197-199). Taken together, this suggests that EGFR may function in various aspects of prostate cancer progression including tumor maintenance and self-renewal. Several lines of evidence support this view, including the previous observations that the addition of EGF to defined media promotes stem cell maintenance (200) and that the activation of EGFR increases prostasphere formation (201).

Recent studies suggest that CTCs may contain a highly enriched proportion of CSCs or at least exhibit many of the same characteristics (202). It will be critical to establish the molecular basis of the relationship between CTCs and CSCs. Of particular interest to us was the relationship between the role of EGFR in prostate TICs and survival of prostate CTCs. It is likely that diverse signaling pathways are required to maintain the cells in circulation and support them as they reestablish their growth at distant sites. There is an increasing body of evidence suggesting that EGFR and HER2 may play such a role (203, 204). This is supported by the finding that not only is EGFR protein expressed in metastatic prostate cancer (165) but also that it is required for sphere

formation in culture. Because of the described microfluidic isolation technology, we were also able to demonstrate that EGFR is expressed in CTCs of men with metastatic prostate cancer.

The pivotal role of EGFR family members in multiple cancers has led to the development of targeted therapies, including therapeutic antibodies and small-molecule inhibitors. Targeting HER2-overexpressing breast cancers with trastuzumab, the therapeutic monoclonal antibody against HER2, has been proven efficacious. Treatment of HER2-expressing CRPC with trastuzumab had little response (clinical trial report NCT00003740). However, trials using cetuximab, erlotinib, and lapatinib have shown a variety of benefits in patients with prostate cancer who express these targets (NCT00728663, NCT00272038, NCT00103194; (205-207)). Low patient accrual, late stage of disease, and formation of various EGFR family dimers (affecting inhibitor binding) are some of the variables that may mask the true effectiveness of these drugs. Although some of the ErbB-specific therapeutics used in this study previously failed in the clinical setting, our results warrant further consideration for repurposing these compounds in combination with other modalities or in the selection of candidates based on ErbB status.

In summary, we found that HER2 protein was elevated in CRPC bone. In addition, we observed that EGFR expression in bone metastasis was independent of HER2 status and was critical for sphere formation in the TIC component of these tumors and was present on the CTCs of patients with metastatic prostate cancer. The importance of HER2 and EGFR in the metastatic progression of prostate cancer was reflected in the mouse studies where only dual inhibition of both receptors inhibited tumor growth.

Chapter 4 Isolation of CTCs from metastatic bladder cancer patient samples

4.1 Abstract

Bladder CTCs have the potential to serve as an alternative monitoring technique in a cancer that currently relies on cystoscopy. They could also provide details about potential therapeutic targets in a disease that has seen little improvement in the prognosis for late stage patients. However, their study has been limited by low detection sensitivity by the currently used technology. We proposed to isolated bladder using the graphene oxide chip with a combination of capture antibodies and to further probe these cells by staining for additional molecular markers of interest. These antibodies were optimized by first using bladder cancer cell lines and then by testing patient derived blood samples using optimized protocols. We detected CTCs in all five patients (range: 5-499 CTCs/mL), and additionally discovered clusters ranging in size from 2-39 cells/cluster. We have observed EGFR+ and CD31+ CTCs, though no HER2+ or ADAM15+ CTCs. Future directions will involve accruing a larger cohort.

4.2 Introduction

Bladder cancer represents 5% of all new cancer diagnoses in the United States (208). Like prostate cancer, as the disease spreads, the five-year survival rate decreases (208). Staging and monitoring of the disease is difficult, with cystoscopy currently the gold standard (209). However, this technique has several major issues including the possibility of understaging the disease (210) and contributions to the high financial cost of bladder cancer (136). While there are a number of soluble protein biomarkers (209) as well as a *fluorescence in situ hybridization* based urine

cytology assay (211), they still cannot supplant cystoscopy (212). There remains a need for a non-invasive biomarker than can better inform disease progression. Circulating tumor cells (CTCs), which are accessible by "liquid biopsy," could represent this alternative.

Prior work in isolating and analyzing bladder CTCs mostly has been conducted using the macroscale CellSearch technology. An initial study was unable to detect CTCs in nonmetastatic patients and only had a 57.1% detection rate in metastatic patients (median: 2 CTCs/7.5 mL, range: 0-79 CTCs/7.5 mL, (213)). A subsequent study was more successful. The overall success rate was 36.4% (median: 2 CTCs/7.5 mL, range: 1-372 CTCs/7.5 mL), with CTCs detected in all five metastatic patients processed (214). Patients without CTCs showed significantly higher overall and progression free survival, while non-metastatic patients with CTCs had shorter disease specific survival. Other studies found that bone disease was more common in patients with CTCs and that patients with CTCs had short median survival, though the overall detection was still low: 27% (215). In general, low detection is a common thread amongst subsequent CellSearch studies, posting 18% (216), 21% (217), and 23% (218) in various cohorts. The last study also assessed HER2 expression on the isolated CTCs (218). Of the 22 patients with detectable CTCs, 14 exhibited concordant HER2 expression with the primary tumor, though CTC HER2 status was not significantly associated with clinicopathologic features or outcomes. The RT-PCR based technique CELLection Dynabeads has been compared with the CellSearch technology, detecting CTCs in 44.4% of high-risk non-muscle-invasive bladder cancer patients in contrast with CellSearch's detection rate of 19.8%. The presence of CTCs was significantly associated with both time to first recurrence and time to progression for both technologies (219).

In addition to serving as a potential biomarker for monitoring, CTCs could also provide additional material to study with regards to molecular markers and pathways responsible for

metastasis. Of particular interest are leads on therapeutic targets as there has been little progress on improving the survival rates for advanced disease in over 30 years (135). Based on our previous work in prostate cancer (Chapter 3, (4)), we are particularly interested in the role of the epidermal growth factor receptors, specifically HER2 and EGFR, in bladder cancer progression. HER2 and EGFR have previously been associated with poor prognosis in bladder cancer (135) and preclinical results of an irreversibly inhibitor of the tyrosine kinase domains of EGFR, HER2, and HER4 have been promising (220). The analysis of CTCs may reveal in which steps of metastasis these receptors play a role, as well as whether different receptors are implicated in different steps.

Given the severe consequences when the disease spreads, we are also interested the mechanisms by which cancer cells enter and leave the blood stream as well as their interactions with cells in the blood. ADAM15 (A Disintegrin And Metalloproteinase) has emerged as an opportunity for intervention given its overexpression at the mRNA level in invasive and metastatic bladder cancer, strong staining in tissue arrays, and role in tumor cell invasion as shown through knockdown (221). Additionally, its multiple domains provide several promising targets for therapeutics (222), and preliminary cell line and xenograft experiments using novel ADAM15-specific sulfonamide inhibitor have been highly successful (221). It is also worth noting that the metalloproteinase component of ADAM15 releases cell-bound ligands that ultimately bind to EGFR.

Another potential contributor to the intermediate steps of metastasis is CD31 (also known as PECAM1). CD31 is more typically associated with endothelial cells (223), and, in the context of cancer, angiogenesis, however recent experimental results from the lab of Professor Mark L. Day have raised questions about its role in cancer cell migration. This led us to question the potential expression of CD31 in CTCs.

We sought to apply a highly sensitive nanomaterial based technology to the isolation of bladder CTCs to overcome previous issues of low detection exhibited by the CellSearch system. To further improve capture and increase sensitivity, we used antibodies against two cell surface markers: EpCAM and EGFR. Given that we used an image-based detection modality rather than PCR detection (as with CELLection Dynabeads), we also had the opportunity to investigate markers potentially associated with the steps of metastasis.

4.3 Methods

4.3.1 Cell culture

The bladder cancer cell lines UM-UC-5, UM-UC-9, and UM-UC-18 were generously provided by the Day lab. Cells were maintained in DMEM (Gibco) supplemented with 10% fetal bovine serum (FBS, Sigma) and 1% antibiotic-antimycotic (Gibco). All cell lines were maintained in a 37°C incubator with 5% CO_2.

4.3.2 Preliminary antibody testing

Antibodies were tested by staining cell lines deposited onto microscope slides. Cells were cytospun onto polylysine coated slides (Thermo Scientific) using a Cytospin 4 (Thermo Scientific). Four percent paraformaldehyde (PFA, Thermo Scientific) was applied to the slides using Cytospin as well. Slides were then permeabilized with 0.05% Triton X (Sigma) in phosphate buffered saline (PBS, Gibco) and blocked with 10% goat serum (Invitrogen). Most primary antibodies (**Table 4-1**) were incubated overnight at 4°C, though some of the tests of the HER2 antibodies were performed using a 1 hr room temperature incubation. After three washes, the secondary antibodies were applied, after which the slides were washed again three times. Coverslips were then mounted with ProLong Gold antifade reagent with DAPI (Molecular Probes).

4.3.3 Cell spike experiments and patient sample processing

To verify our ability to capture bladder cancer cells on the GO Chip, cell spike experiments were performed using GO Chips fabricated and functionalized as previously described (115). All materials were introduced to the chip using a syringe pump (Harvard Apparatus). Following a PBS wash, an antibody solution of anti-EpCAM (R&D Systems) and anti-EGFR (Ray Biotech) in 1% bovine serum albumin (BSA, Sigma) was added to the chip, incubated, and washed off. The chip was then blocked with 3% BSA.

For cell spike experiments, cells pre-labeled with CellTracker dye (Invitrogen) were spiked into whole blood provided by a healthy volunteer and flowed through the chip at 1 mL/hr. Following capture, the device was vigorously washed. Cells were fixed and permeabilized using Cytofix/Cytoperm (Fisher Scientific) and stain for their nuclei using 4',6-diamidino-2-phenylindole (DAPI, Thermo Fisher).

For patient samples, whole blood was collected from metastatic bladder cancer patients with informed consent under IRB HUM42401. Blood was flowed through the chip at 1 mL/hr. Two parallel chips were run for each patient to allow staining for all the markers of interest. The devices were then washed after which cells captured on-chip were fixed using 4% PFA.

4.3.4 Staining

0.2% Triton-X in PBS was used to permeabilize cells, after which blocking was conducted using 2% goat-3% bovine serum. Cocktails of primary antibodies (**Table 4-1**) were incubated on-chip for 1 hr at room temperature, followed by the appropriate secondary antibodies, which were incubated for 1 hr at room temperature in the dark. Nuclei were labeled with DAPI.

Table 4-1 Antibodies used in capture and staining of bladder CTCs. Bold indicates antibodies used in chip staining, while black boxes indicate those used in the second round of staining.

Purpose	Antigen	Host/Isotype	Company	Catalog No.	Fluorophore
Capture	EpCAM	Goat IgG	R&D	BAF960	N/A
Capture	EGFR	Mouse IgG2b	Ray Biotech	MD-02-0006	N/A
Staining 1°	**CD45**	Mouse IgG2a	BioRad	MCA87GA	N/A
Staining 1°	**CD45**	Rat IgG2b	Santa Cruz	Sc-70699	N/A
Staining 1°	**CK 8/18**	Guinea Pig	Abcam	ab194130	N/A
Staining 1°	**CK 7/8**	Mouse IgG2a	BD	349205	N/A
Staining 1°	**EGFR**	Mouse IgG1	ThermoFisher	2800005	N/A
Staining 1°	HER2	Rabbit	Abcam	ab134182	N/A
Staining 1°	HER2	Rabbit	Santa Cruz	sc-284	N/A
Staining 1°/2°	HER2 (preconjugate)	Mouse IgG1	BD	340554	APC
Staining 1°	**HER2**	Rabbit	Cell Signaling	2165	N/A
Staining 1°	CD31	Mouse IgG1	R&D	BBA7	N/A
Staining 1°	ADAM15	Rabbit	Day Lab	N/A	N/A
Staining 1°	**ADAM15**	Rabbit	Abcam	ab124698	N/A
Staining 2°	**Mouse IgG2a**	Goat	ThermoFisher	A-21131	AlexaFluor 488
Staining 2°	**Rat IgG (H+L)**	Goat	ThermoFisher	A-11006	AlexaFluor 488
Staining 2°	**Guinea Pig IgG (H+L)**	Goat	ThermoFisher	A-11075	AlexaFluor 568
Staining 2°	**Mouse IgG2a**	Goat	ThermoFisher	A-21133	AlexaFluor 546
Staining 2°	**Mouse IgG1**	Goat	ThermoFisher	A-21240	AlexaFluor 647
Staining 2°	**Rabbit IgG (H+L)**	Goat	ThermoFisher	SA5-10035	Dylight 755

4.3.5 Imaging and analysis

Imaging was conducted on a Nikon Eclipse Ti fluorescence microscope. Images were captured using a QImaging cooled mono 12-bit camera. Devices were first scanned at 10x for preliminary analysis, with 20x imaging conducted for locations requiring further clarification.

Analysis was conducted using NIS-Elements software. Those nucleated cells expressing CK but not CD45 (DAPI+/CK+/CD45- cells), were counted as CTCs. Cells were also analyzed for their expression of EGFR and HER2 on one chip and ADAM15 and CD31 on the other.

4.4 Results

4.4.1 Cell line spike experiments

Given the high expression of EpCAM by intermediate and high grade bladder tumors (224) and our interest in EGFR, we performed capture with antibodies against those two moieties tethered to the GO Chip. To test the potential of the device to capture bladder CTCs, bladder cancer cell lines with differing expression patterns were fluorescently labeled and spiked into whole blood to simulate patient samples. Of the three cell lines tested (**Figure 4-1**), UM-UC-5 and UM-UC-9 showed higher capture (average captures of 88.5% ± 8.2% and 90.7% ± 14.9%, respectively) than UM-UC-18 (average capture of 12.6% ± 3.3%). This is consistent with the higher expression of

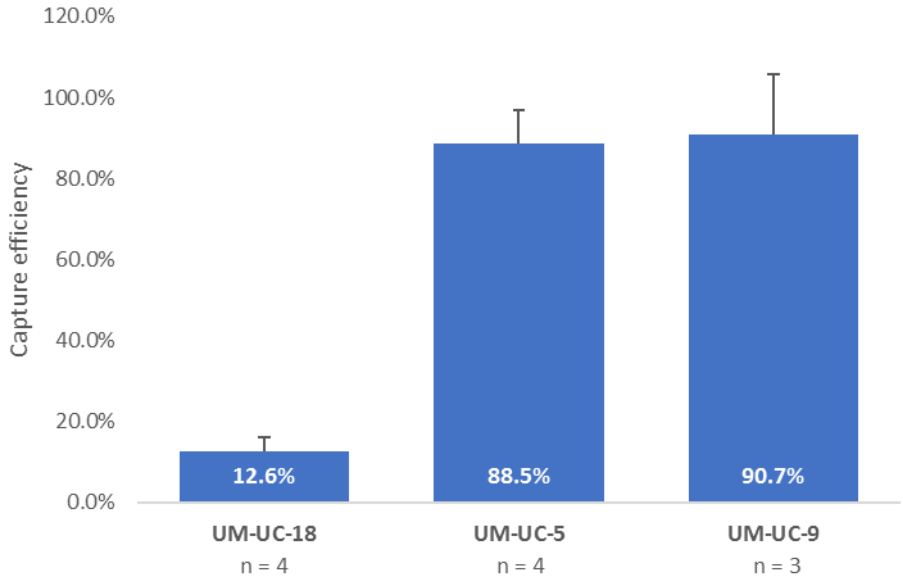

Figure 4-1 Capture efficiencies for bladder cancer cell lines on the GO Chip. Cell lines spiked into whole blood were captured at efficiencies consistent with their levels of antigen expression.

EpCAM and EGFR by UM-UC-5 and UM-UC-9 and the highly heterogeneous expression by UM-UC-18.

4.4.2 Staining optimization

To test antibodies for their ultimate application on-chip, staining was conducted on the three cell lines on microscope slides (example images, **Figure 4-2**). Combinations were selected that ultimately complied with the necessary combinations of isotypes and secondary antibodies and showed staining patterns consistent with previous cell line characterization.

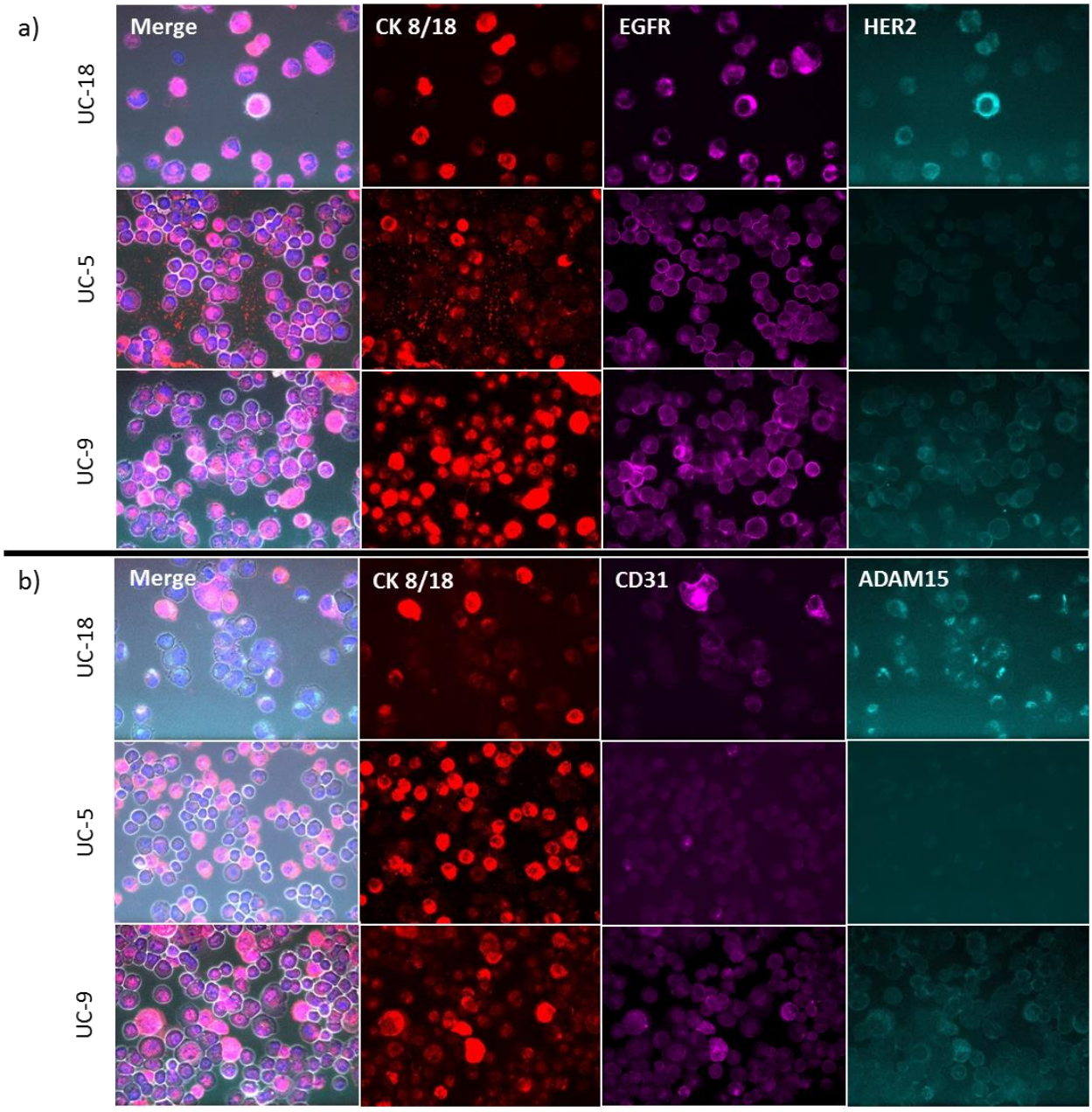

Figure 4-2 Examples of slide staining for antibody optimization. a) Staining for cytokeratin (CK) 8/18, EGFR, and HER2. b) Staining for CK 8/18, CD31, and ADAM15. CD45 staining not shown as these cell lines are negative for CD45.

4.4.3 CTC capture from bladder cancer patient samples

A total of five patients (**Table** 4-2) and one healthy control were processed to determine CTC counts and a false positive threshold respectively (**Figure 4-3**, **Table 4-3**). The first three patients were stained for CK 8/18, CD45, and either EGFR and HER or CD31 and ADAM15.

CTCs were detected in all three patients (range: 5-499 CTCs/mL, **Table 4-3**). CD31+ CTCs were detected in a small percentage of cells in all three samples, while EGFR+ CTCs were detected in 1/3 samples (**Figure 4-4a, b**). ADAM15 and HER2 were not observed to be expressed in any of the captured CTCs. Clusters were observed in 2/3 samples, with one sample (9058) showing a particularly high number and size of clusters (**Figure 4-4c-e**, **Figure 4-5**). Between 0 and 42% of CTCs were present in clusters (median: 9%).

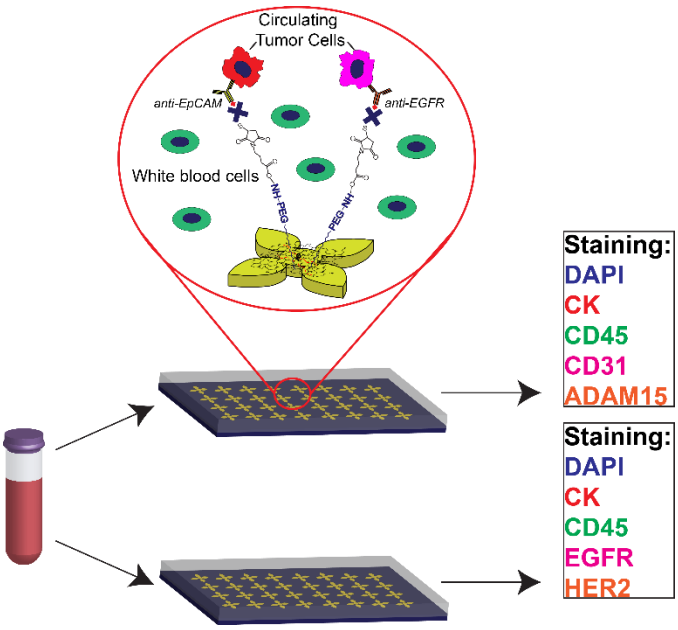

Figure 4-3 Experiment schematic for bladder cancer CTC capture and staining workflow.

However, the high presence of 25 CK+ cells/mL in the healthy control was a concern, leading us to shift to staining for CK 7/8 due to possible issues with CK 18 expression by white blood cells. Two subsequent samples were stained using CK 7/8 with a different CD45 to account for the change in host/isotype of the cytokeratin antibody, as well as with the same antibodies for EGFR, HER2, CD31, and ADAM15 (**Figure 4-7**, **Figure 4-6**). Once again, CTCs were captured from both samples, with CD31+ and EGFR+ CTCs observed. Only one cluster, a doublet, was observed across the four chips.

Table 4-2 Bladder cancer clinical cohort. C = carboplatin. G = gemcitabine. P = pembrolizumab. MVAC = methotrexate/vinblastine/doxorubicin/cisplatin.

Number of patients	5	100%
Age		
Median (range)	73	(70-78)
Sex		
Male	4	80%
Female	1	20%
Race		
Caucasian	5	100%
Performance status		
0	0	0%
1	4	80%
2	0	0%
3	1	20%
Cystectomy	2	40%
Metastatic disease	5	100%
Lymph node metastases	3	60%
Visceral metastases	4	80%
Bone metastases	1	20%
Therapy		
Atezolizumab	1	20%
C/G	1	20%
C/G/P	1	20%
MVAC	1	20%

Table 4-3 Patient sample enumeration in metastatic bladder cancer patient samples.

Staining, round 1 (CK 8/18)					
Sample	**Total**	**CK+/CD31-/ADAM15-**	**CK+/CD31+/ADAM15-**	**Single cells**	**Cells in clusters**
8668	143	142	1	143	0
9057	29	27	2	27	2
9058	410	370	40	262	148
Sample	**Total**	**CK+/EGFR-/HER2-**	**CK+/EGFR+/HER2-**	**Single cells**	**Cells in clusters**
8668	5	5	0	5	0
9057	38	38	0	34	4
9058	499	491	8	287	212
Staining, round 2 (CK 7/8)					
Sample	**Total**	**CK+/CD31-/ADAM15-**	**CK+/CD31+/ADAM15-**	**Single cells**	**Cells in clusters**
9059	3	3	0	3	0
9060	8	7	1	8	0
Sample	**Total**	**CK+/EGFR-/HER2-**	**CK+/EGFR+/HER2-**	**Single cells**	**Cells in clusters**
9059	5	4	1	8	0
9060	7	7	0	5	2

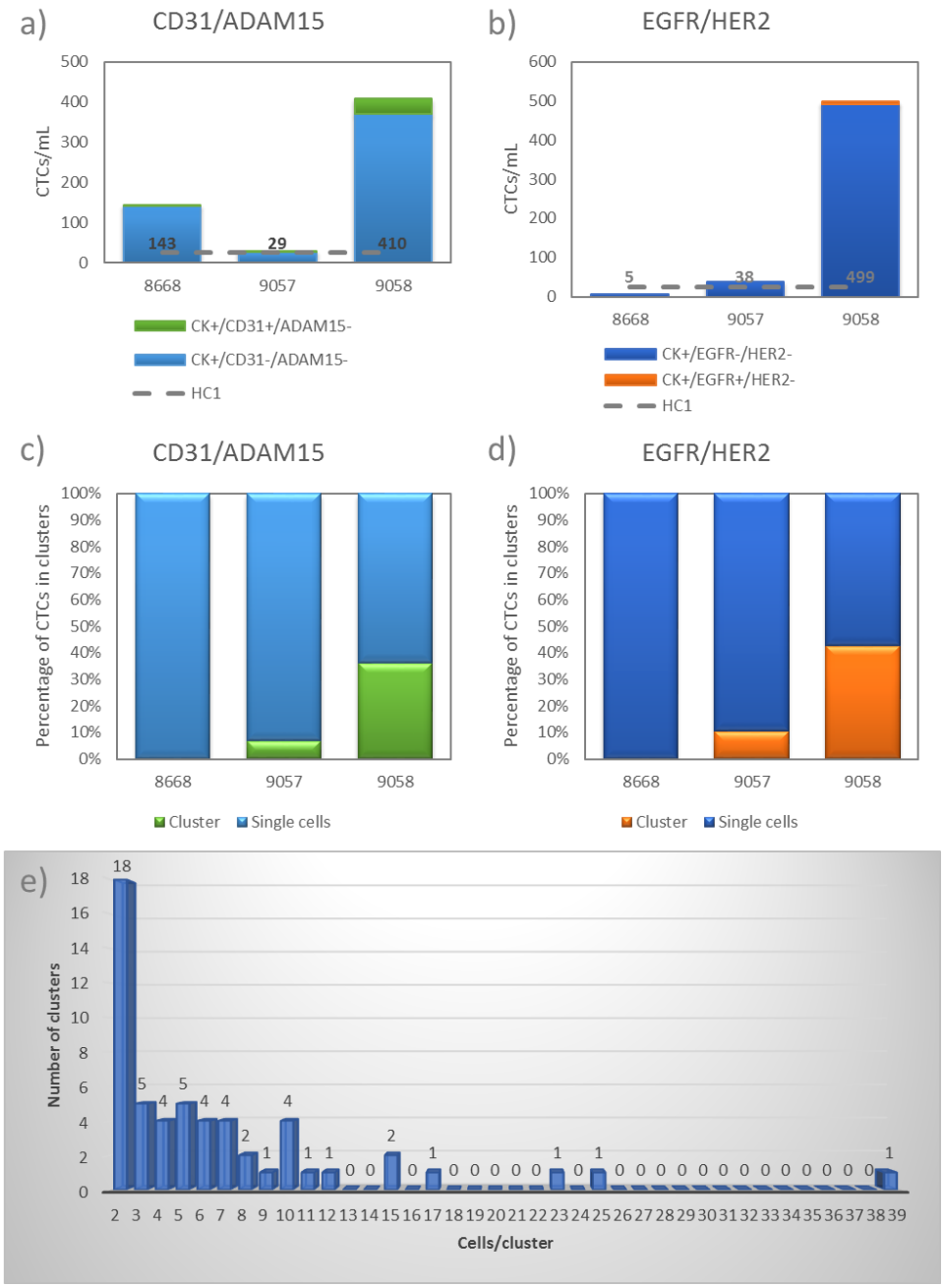

Figure 4-4 Enumeration results from the first round of chip staining. Devices from three patient samples were stained for CK 8/18 and CD45 as well as either CD31 and ADAM15 (a, c) or EGFR and HER2 (b, d). CTCs were enumerated based on their staining patterns (a, b). The percentage of CTCs present as clusters was also determined (c, d). e) Clusters across the six stained chips ranged in size from 2 to 39 cells/cluster, with the majority of clusters comprising lower numbers of cells.

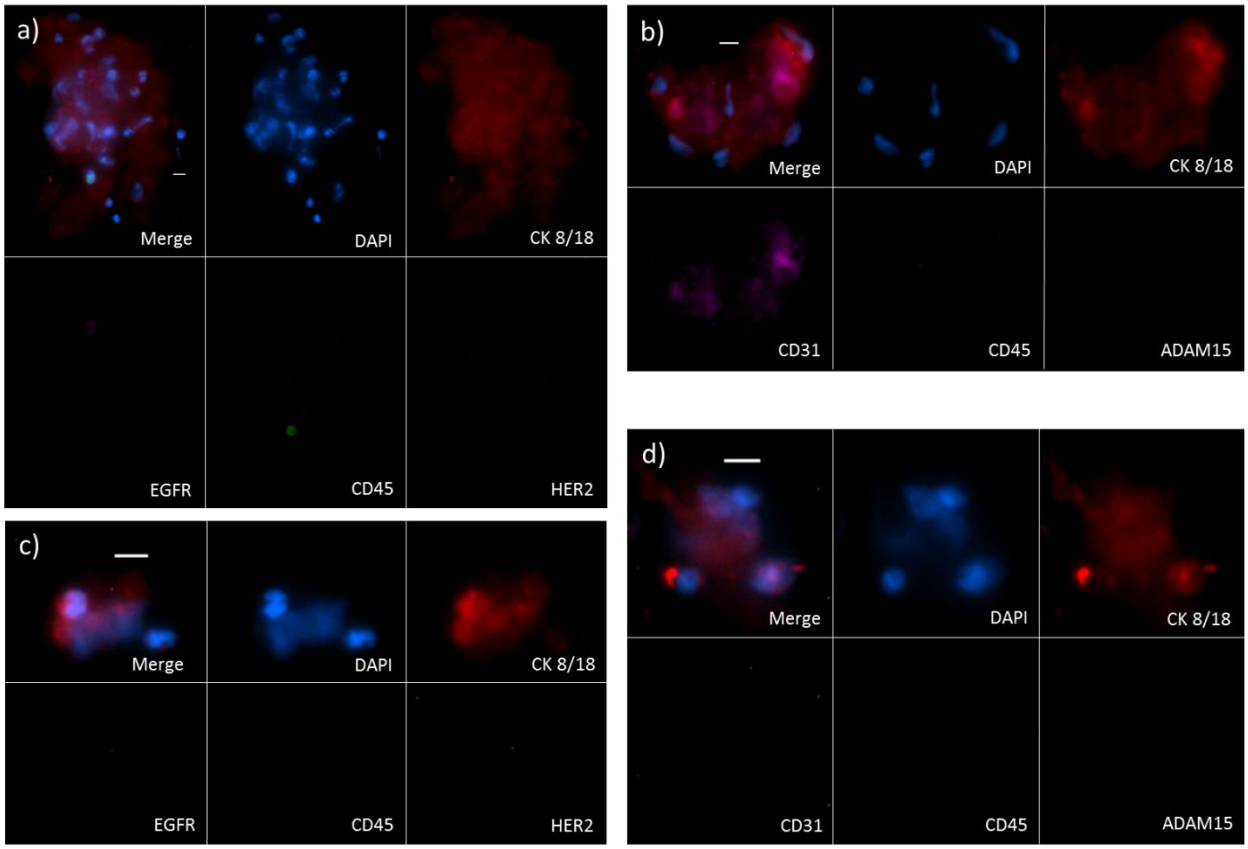

Figure 4-5 Examples of clusters from the first round of staining. Scale bar = 10 μm.

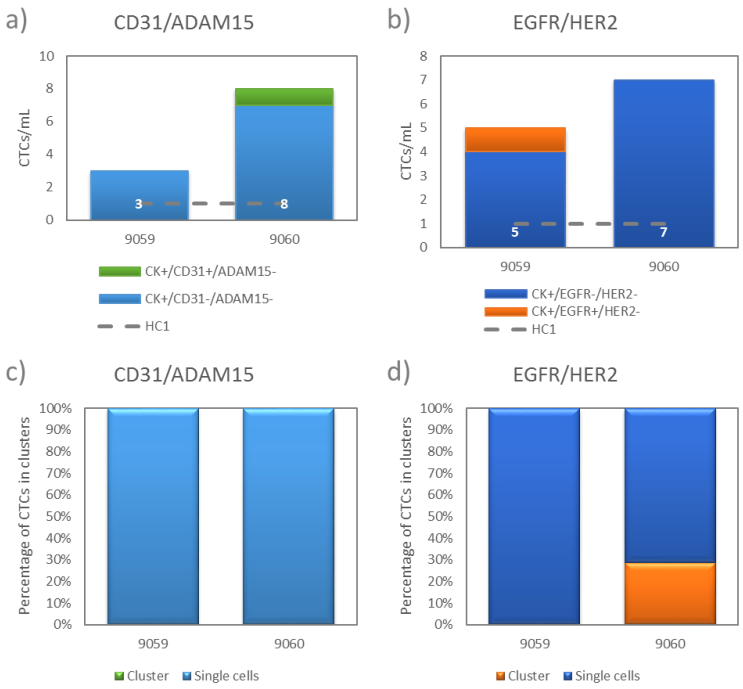

Figure 4-7 Enumeration results from the second round of chip staining. Three patients were stained for CK 7/8 and CD45 as well as either CD31 and ADAM15 (a, c) or EGFR and HER2 (b, d). CTCs were enumerated based on their staining patterns (a, b). The percentage of CTCs present as clusters was also determined (c, d).

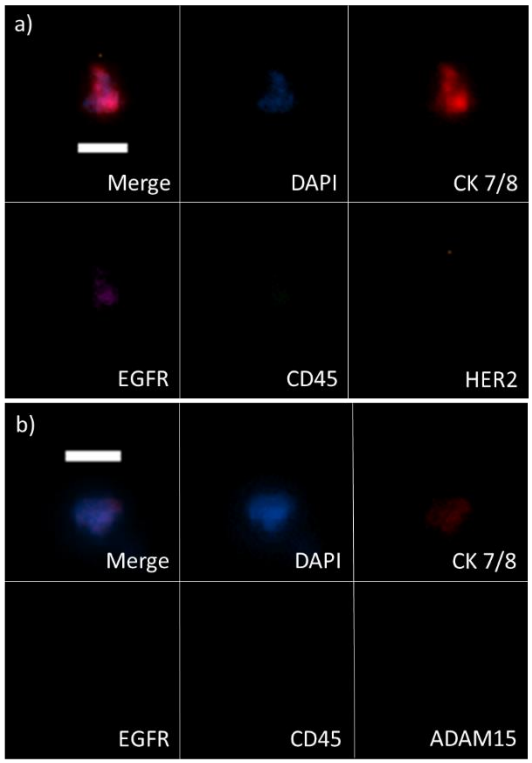

Figure 4-6 Example CTCs from the second round of staining. Scale bar = 10 µm.

4.5 Discussion

The interrogation of CTCs in bladder cancer has been thus far limited by insufficient detection sensitivity. By using a highly sensitive microfluidic technology, CTCs were detected at higher than healthy control threshold on 9/10 chips processed. These preliminary results suggest that further investigation is warranted into these cells on the path to metastasis.

In addition to detecting CTCs, recent equipment upgrades have allowed us to ask specific questions about molecular markers potentially implicated in metastasis. In contrast to our previous work in prostate cancer, we were able to assess the presence of both HER2 and EGFR rather than picking only one of the markers. Interestingly, only EGFR was observed in the CTCs captured from two of the five patients processed here. This is consistent with previous hypotheses that EGFR may be responsible for tumor initiation and survival in transit while HER2 plays more of a role in cell proliferation at established sites (4), though it conflicts with previous reports of HER2 positive CTCs in bladder cancer (218). Given previous reports and other staining results, we will continue to explore antibodies for HER2. However, given the existence of many therapies that target EGFR, this is a promising observation due to the need of therapeutic options for advanced bladder cancer patients.

To our knowledge, this is the first example of the isolation of CD31 positive CTCs. CD31+ cells have been previously isolated from colorectal cancer patients using a filtration-based technology, though those cells were determined to be endothelial cells (225). However, the cells isolated in our study were required to stain positive for cytokeratin, allowing us to make this distinction. Investigation into these tumor cells may shed light on the metastatic process as well as cellular interactions in transit.

We have optimized the protocols and reagents best able to study our hypotheses regarding the role HER2, EGFR, CD31, and ADAM15 in metastasis and processed five patient samples thus far. To draw significant conclusions, more patient samples will need be processed. The data drawn from that study may be used for comparison with cell line and animal models of bladder metastasis.

Chapter 5 GO 2.0: strategies to release captured CTCs from the GO Chip

5.1 Abstract

Challenges to clinical applications of CTC include limitations placed on downstream analysis. In particular, immunocapture techniques offer high sensitivity, but are often hamstrung by the tethering of cells to capture surfaces. Two techniques are discussed to improve on one such immunocapture technology, the GO Chip, by incorporating graphene (GO) oxide into microfluidic devices in conjunction with polymers than may either be degraded or dissolved. Early attempts to build polymer-GO films through layer-by-layer (LbL) assembly failed to simultaneously retain the high capture efficiency and low nonspecific binding of the GO Chip. Ultimately, a microfluidic device incorporating a drop-cast thermosensitive polymer-GO film as the substrate for antibody capture allowed for sensitive capture (up to 95.21%) and efficient release (91.56% in blood-based samples). Clinical applicability of the device was demonstrated through processing 10 breast cancer patient samples and 3 pancreatic patient samples. Potential for downstream analysis was exhibited by performing fluorescence *in situ* hybridization to detect HER2 amplification in CTCs from one breast cancer patient. The validation of this device represents preliminary steps to resolving a current drawback in many CTC isolation technologies.

5.2 Introduction

CTCs not only provide biological insight into primary and metastatic tumors but also have the potential to serve as real time biomarkers for making treatment decisions and monitoring drug efficacy (15). Indeed, over 270 clinical trials have now been proposed using CTCs as surrogate

biomarkers (226). However, to date, CTCs have not been incorporated into clinical practice for management of patients with cancer. The main challenges to this field include: (i) reaching the sensitivity needed to isolate these extremely rare cells from the surrounding blood cells (1 in 1 billion), (ii) minimizing processing to preserve the viability of cells, and (iii) achieving the specificity necessary to acquire pure population to enable meaningful genomic and functional analysis.

A graphene oxide (GO) based CTC capture device, the GO Chip, took advantage of the increased surface area afforded by graphene oxide for highly sensitive and selective cell capture (as described in Chapter 2, Chapter 3, (227)). However, most immunoaffinity based technologies conjugate capture antibodies to either a substrate surface, as is the case with the GO Chip, or three dimensional features. Consequently, the purified CTCs remain within these technologies after capture. This limits post-capture analysis because of difficulty in releasing viable cells from the capture substrate.

5.2.1 Previous release technologies

A number of different methods have been tried for the release of captured cells. Substrates coated with a "sacrificial layer" of hydrogel have been used to release cells upon the degradation of the surface to which the cells are adhered. An early generation of this method used cation chelation to disrupt an alginate hydrogel (228), but this prevented the processing of blood that had been stored in the presence of the anticoagulant EDTA. Cross-linked alginate hydrogels that could be degraded with alginate lyase allowed the processing of EDTA treated blood (229), However, the major drawback of this device was flow rate at which blood was processed (2 μL/min), making it unsuitable for routine implementation for analyzing clinical specimens. A method for the efficient and clinically compatible sample processing followed by cell release is still lacking. An

alternative approach for cell release is the temperature sensitive deconstruction of a biotinylated gelatin-streptavidin layer-by-layer (LbL) film (230). The capture agent was ultimately conjugated through a layer of nanoparticles, and this system allowed both the bulk release of cells by raising the temperature to 37°C or the release of individual cells through stimulation with a frequency-controlled 80-μm microtip. This technology demonstrates the promise of temperature sensitive materials for use in cell release.

Hou *et al.* used a thermoresponsive copolymer of N-isopropyl acrylamide and 3-aminoethyl methacrylate grafted on to a silicon nanowire substrate and carrying anti-EpCAM antibodies as cell capturing agent for the capture and stimulated release of CTCs (231). This methodology was then incorporated in a microfluidic system that could subsequently be used to process blood samples (120). The system was optimized with respect to capture and release efficiency, but the throughput is not yet high enough and requires two rounds of sample processing to yield sufficient purity to conduct efficient whole genome amplification for downstream genetic/mutational analysis. Additionally, the process of fabricating nanofeatures on the silicon substrates is again a rate limiting step and requires access to expensive tools and clean room facilities. Liu *et al.* developed a similar approach for cell capture through hydrophobic interactions which could be thermally switched between capture and release mode (232). However, the limitations include static capture rather than a flow through system, time consuming surface grafted polymerization, and the need for experiments to be conducted at 37° C.

These previously-explored approaches all feature performance limitations in throughput (233), purity requiring additional processing (120), the ability to process blood collected by standard conditions (234), immense fabrication facility requirements (120, 231), time-consuming

chemistry (235), and inconvenient experimental temperature conditions (235). There remains a need for a manageable and convenient yet high performing CTC capture/release technology.

5.2.2 Strategies for cell capture/release devices incorporating graphene oxide

5.2.2.1 Layer-by-Layer (LbL) fabrication enabled GO Chip (LbL GO Chip)

While the graphene oxide (GO) Chip affords excellent sensitivity and selectivity, its utility in CTC analysis is hindered by the opaque capture surface and inability to release captured cells. Altering this device to eliminate the gold-patterned silicon foundation would remove an obstacle to superior imaging. This modification would also eliminate many expensive clean room fabrication steps, and greater functionality would be enabled through the incorporation of a degradable polymer.

Layer-by-Layer (LbL) is a self-assembly method by which layers are sequentially deposited on a surface, and the integrity of the resulting composite is a function of the interactions between the layers. Various forces between layers of differing composition have been exploited and include electrostatic interactions, hydrophobic interactions (236), van der Waals forces (237), hydrogen bonding (238), acid/base reactions (239), and a host of chemical reactions such as click chemistry (240). Films feature both lateral and vertical growth during assembly, and there is interpenetration between layers, creating a composite that draws from the properties of the individual layers. There is precedent for the use of graphene oxide in LbL films (241-244), inspiring our approach to use this method as the basis for a transparent graphene oxide circulating tumor cell capture/release device.

Device construction largely followed the techniques used to build the GO Chip (115). To make the original GO Chip, GO is assembled on the substrate when a gold-patterned piece of silicon is dipped in a GO suspension. The mechanism behind this involves the electrostatic

attraction of the TBA to a monolayer of hydroxide ions formed on the gold patterns (245). The similarity between this process and LbL self-assembly inspired the protocol used for the fabrication of the transparent GO cell capture/release device. To make the LbL GO Chip, alternating layers of cationic and anionic polymer or graphene oxide based suspensions were deposited, also assembling based on electrostatic attraction. Graphene oxide suspensions were preparing similarly to that used in the original GO Chip, allowing them to serve as the basis for the same conjugation chemistry. Through this analogous process, it was hypothesized that device featuring the advantage of the original GO Chip could be fabricated while simultaneously addressing its disadvantages.

5.2.2.2 Incorporation of a thermosensitive polymer

Thermoresponsive polymers, a class of stimuli-responsive polymers that respond to temperature changes by undergoing conformational changes, have found wide applications in drug delivery (246), tissue engineering (247), controlling cell adhesion (248) and bacterial growth (249), protein encapsulation (250), and the release of captured CTCs from the surface of such capturing devices (231, 232).

Graphene- and graphene oxide (GO)-based polymer composites are a new class of materials which combine the excellent properties of graphene, such as high surface-to-volume ratio, high Young's modulus, and high thermal and electrical characteristics (251), with the easy processability of polymers. Such composites have found uses in fields ranging from energy storage (252) and electronic devices (253, 254), to biomedical applications such as drug and gene delivery (255, 256), cancer therapy (257), cell differentiation (258, 259), coating of biomedical implants (260, 261), and bio-imaging (256).

The combined advantages of a biocompatible functionalized nanomaterial with a thermoresponsive polymer that promotes effective cell release could address the challenge of sensitive capture while simultaneously allowing viable cell release. This could lead to improvement in downstream analysis such as fluorescence *in situ* hybridization (FISH), molecular analysis, and single cell analysis. This chapter ultimately presents a tunable thermal-sensitive polymer-GO Chip for highly efficient capture and subsequent release of CTCs incorporated into a microfluidic device (3).

5.3 Methods

5.3.1 LbL device methods

5.3.1.1 Materials and solutions

LbL consists of alternating layers of anionic and cation suspensions, different combinations of which were used throughout this study. Anionic or negatively polar solutions included graphene oxide (GO, cheaptubes.com)-phospholipid polyethylene glycol amine (PEG, NOF America), sodium hyaluronate, and heparin. Cationic solutions included GO-tetrabutyl ammonium (TBA, Sigma-Aldrich) poly(ethyleneimine) (PEI, Sigma-Aldrich), and poly(diallyldimethylammonium chloride) (PDDA, Sigma-Aldrich).

To prepare the GO-PEG suspension, GO powder was probe tip sonicated in 10^{-3} M NaCl at a concentration of 0.1% w/v GO for 1 hour, after which it was allowed to settle for two days. The supernatant was removed and centrifuged for 40 minutes at 3000 rpm. To make the GO-TBA suspension, 10 mg GO was added to 10 mL DI water along with 300 μl 40% TBA hydroxide and was probe tip sonicated for 30 minutes. For both suspensions, PEG was then added at a concentration of 3.75 mg/mL and bath sonicated for one hour, after which the suspension was centrifuged for three minutes at 12000 rpm; the supernatant was reserved for use in LbL.

All solutions were prepared through dilution and/or pH adjustment. PEI stock was diluted to 0.5 wt% PDDA was diluted to 2.0% (w/v). Hyaluronate was dissolved in 0.15 M NaCl to a concentration of 1 mg/mL; the solution pH was then adjusted to 4.5 using acetic acid. Heparin was dissolved in DI water to a concentration of 1 mg/mL.

5.3.1.2 Film formation and device fabrication

The LbL protocol was largely based on previous methods (241). Glass slides were first cleaned by sonication in a solution of HCl and Nochromix®. A polydimethyl siloxane (PDMS) reservoir was then reversibly attached to the clean glass slide and a preliminary layer of cationic solution was pipetted into the reservoir. The solution was incubated for 15 minutes and then washed out of the reservoir. The reservoir was then filled with an anionic solution and incubated for 15 minutes. This was again followed by a wash. This protocol was repeated until the desired number of layers was deposited **(Figure 5-1)**. The reservoir was removed and the substrate was dried with house air. A PDMS chamber was then bonded on to the slide using a corona discharge and incubated on a hot plate at 85°C for 10 minutes. To functionalize, N-γ-maleimidobutyryloxy succinimide ester (GMBS, Thermo Scientific) was injected into the devices and incubated for 30 minutes. Tubing was inserted to allow the performance of all subsequent steps by syringe pump. The device was washed with ethanol, then NeutrAvidin (Thermo Scientific) was flowed and incubated for 40 minutes. The device was then stored at 4°C until use.

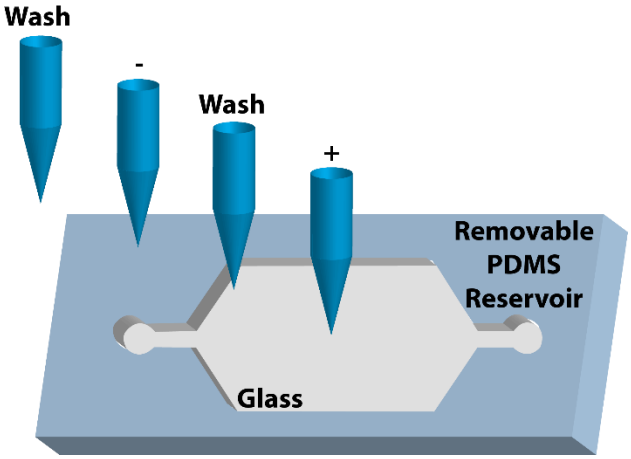

Figure 5-1 LbL protocol schematic.

5.3.1.3 Alternative conjugation chemistry

As an alternative to the GMBS crosslinker, N-(3-Dimethylaminopropyl)-N′-ethylcarbodiimide hydrochloride (EDC, Sigma-Aldrich) N-hydroxysulfosuccinimide (sulfo-NHS, Thermo Scientific) chemistry was attempted. 40 mM EDC in 2-(N-morpholino)ethanesulfonic acid (MES) buffer was added to the PDMS reservoir after film formation and incubated for 15 minutes on an orbital shaker. Then 10 mM sulfo-NHS in MES buffer was added and incubated for 15 minutes on an orbital shaker. After three five-minute phosphate buffered saline (PBS, Gibco) washes on the orbital shaker, NeutrAvidin was added at a concentration of 100 μg/mL and incubated for three hours, followed by three additional five-minute PBS washes.

5.3.1.4 Cell spike experiments

Prior to sample flow, devices were coated/functionalized with anti-EpCAM (R&D systems) and were blocked with 3% bovine serum albumin (BSA, Sigma) in PBS. Cancer cell line cells prelabeled with CellTracker^{TM} dye (ThermoFisher Scientific) were counted and spiked into blood or buffer to evaluate the ability of the device to capture different cell types at various concentrations. Buffer experiments allow the determination of accurate capture efficiencies through mass balance while blood experiments provide purity metrics. The formulated samples were flowed through the devices at 1 mL/hr, followed by washing and fixation. For blood-based samples, cells were also permeabilized and labeled with 4,6-diamidino-2-phenylindole (DAPI, ThermoFisher Scientific). Devices were then scanned using a Nikon Eclipse Ti fluorescence microscope for subsequent counting and analysis.

5.3.2 Thermoresponsive polymer-GO device methods

5.3.2.1 Polymer synthesis

N-acryloyl piperidine was synthesized through reaction between acryloyl chloride (Fluka) and piperidine (Aldrich) (262). In short, 0.11 mol of piperidine and 0.12 mol of triethylamine were dissolved in 100 mL of dichloromethane maintained at 0-5° C. A solution of acryloyl chloride (0.10 mol) in 15 mL of dichloromethane was added drop-wise to the above solution over two hours under constant stirring. After complete addition, the reaction mixture was stirred at room temperature for 24 hours and was extracted with water and purified by column chromatography (hexane:ethyl acetate, 1:1) to yield colorless to light yellow liquid. *N*,*N*-diethylacrylamide (TCI America) was passed through a basic alumina column (Aldrich) prior to polymerization. AIBN (Aldrich) was recrystallized from methanol before use. In a typical polymerization reaction, the required amount of monomers was dissolved in anisole (Aldrich) and 0.3 mol% (of total monomer content) of AIBN was added to the solution. The reaction flask was completely sealed and the solution was purged with Argon for 20 minutes. The reaction was carried out at 65° C for 20 hours. After the reaction, all the solvent was evaporated at high temperature under vacuum to obtain white solid residue. The residue was re-dissolved in chloroform and then twice precipitated in ethyl acetate to obtain white solid mass. The precipitate was recovered and dried at 60° C under vacuum for 2-3 days.

5.3.2.2 Polymer characterization

The synthesized polymers were characterized by gel permeation chromatography (GPC, Waters Inc., 1515 Isocratic HPLC pump and 2414 RI detector) using three Styragel columns – HR2, HR3 and HR4 – in series maintained at 35° C with chloroform as eluent (flow rate: 1 mL/min,

total elution time: 40 min). The instrument was calibrated with polystyrene standards. LCST was ascertained by measuring UV-vis transmittance (Varian Cary 50 Bio) of a 0.1 wt.% aqueous solution of polymers as a function of temperature. A thermocouple was used for real-time measurement of temperature, with the metal junction dipped in the cuvette during the measurement. For effective measurement, the polymer solution was cooled down to 2-3° C along with the metal cuvette holder to slow down the heating up of sample in ambient condition. $CaCl_2$ was placed inside the UV-vis spectrophotometer chamber to ensure humidity-free environment. This was necessary to prevent atmospheric water vapor from condensing on the cold cuvette walls. UV-vis spectrum was measured from 200-800 nm at every 0.2-0.5° C with more frequent measurements near the transition temperature. Transmittance at 400 nm was plotted against temperature and the temperature for 50% transmittance was noted as the LCST. Molecular weights and LCSTs of different polymer batches were noted (**Table 5-1**).

Table 5-1 Molecular weights, polydispersity index (PDI), and lower critical solution temperature (LCST) of different batches of synthesized polymers used in the study (3)

Polymer	M_n (kDa)	M_w(kDa)	PDI	LCST (°C)
P1	209.246	308.086	1.47	13.6
P2	151.332	253.380	1.67	12.7
P3	175.085	255.778	1.46	12.0
P4	173.019	303.009	1.75	11.8

5.3.2.3 Determination of amine surface availability

To show the surface availability of the amine groups from the GO-PEG in polymer-GO composite films, the drop-cast films were incubated with 0.25 mM aqueous solution of an amine reactive dye, 5-(and-6)-carboxyfluorescein, succinimidyl ester (FSE; Life Technologies) for 30 minutes at 40° C and then washed with copious amount of DI water. The dye treated films were then imaged with fluorescence microscope (Olympus BX51 coupled with Olympus DP71 camera and EXFO X-cite Series 120 light source).

5.3.2.4 Device fabrication

The glass slides (Fisher) were sequentially washed with chloroform, acetone, and isopropanol via sonication for 5 minutes each. The glass slides were then air dried and treated in a UV-ozone generator for 30 minutes to remove any carbon contamination and to obtain a high density of surface hydroxyl groups. The cleaned substrates were patterned using Kapton polyimide tape (Cole Parmer) by masking the active device area. Kapton tape was chosen for its impermeability to silane vapors and good stability at high temperatures. The patterned substrates were then cleaned with wipes dipped in ethanol to remove any adhesive residue and treated with (Heptadecafluoro-1,1,2,2-tetrahydrodecyl)trichlorsilane (HFTCS, Gelest Inc.) via vapor phase surface modification at 100°C for 30 minutes. HFTCS treatment resulted in hydrophobic fluoroalkyl groups on the unmasked peripheral regions of the substrates. After HFTCS treatment, the Kapton tape mask was removed and the glass slides were washed with copious amounts of ethanol to remove any physisorbed silane as well as any adhesive residue. The second surface modification was done in liquid phase by immersing the glass slides in 3.35 mM 2-methoxy(polyethyleneoxy)propyltrimethoxysilane (PEG-silane, Gelest Inc.) in ethanol for 12-15 hours. Poly(ethylene glycol) (PEG) is well known to render surfaces non-fouling (263). The PEG monolayer was necessitated to avoid recapturing of the released CTCs on the glass substrate. Subsequently, the glass slides were again washed with ethanol to remove any physisorbed silane. A polymer-GO blend solution containing 10 mg/mL of polymer in 975 μL DMF and 25 μL of GO-PEG solution (functionalized using a previously described chemistry (115)) was then drop-cast in requisite amount on the surface modified glass substrates and allowed to dry at 60°C in an oven for 2-3 hours to yield 3-4 μm thick composite film. The PDMS chamber was assembled on the glass substrate with the polymer-GO composite film through corona discharge to produce a

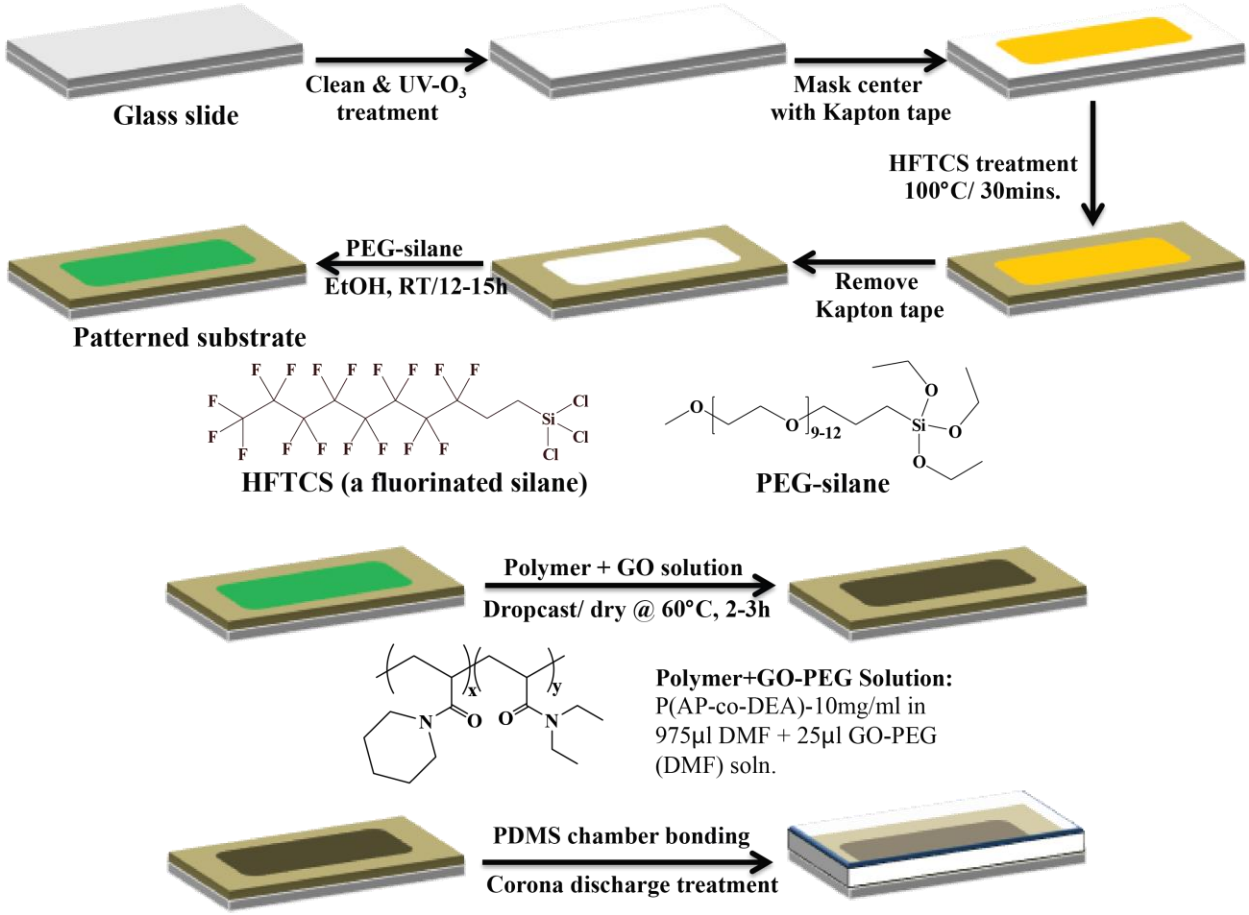

Figure 5-2 Schematic for CTC device fabrication (3).

microfluidic device (**Figure 5-2**). The device was functionalized by immobilizing anti-EpCAM on the surface available GO-PEG through a cross-linker (N-γ-maleimidobutyryl-oxysuccinimide ester, sulfo-GMBS) and avidin-biotin mediated bio-conjugation, providing cell capture/release functionality (**Figure 5-3**).

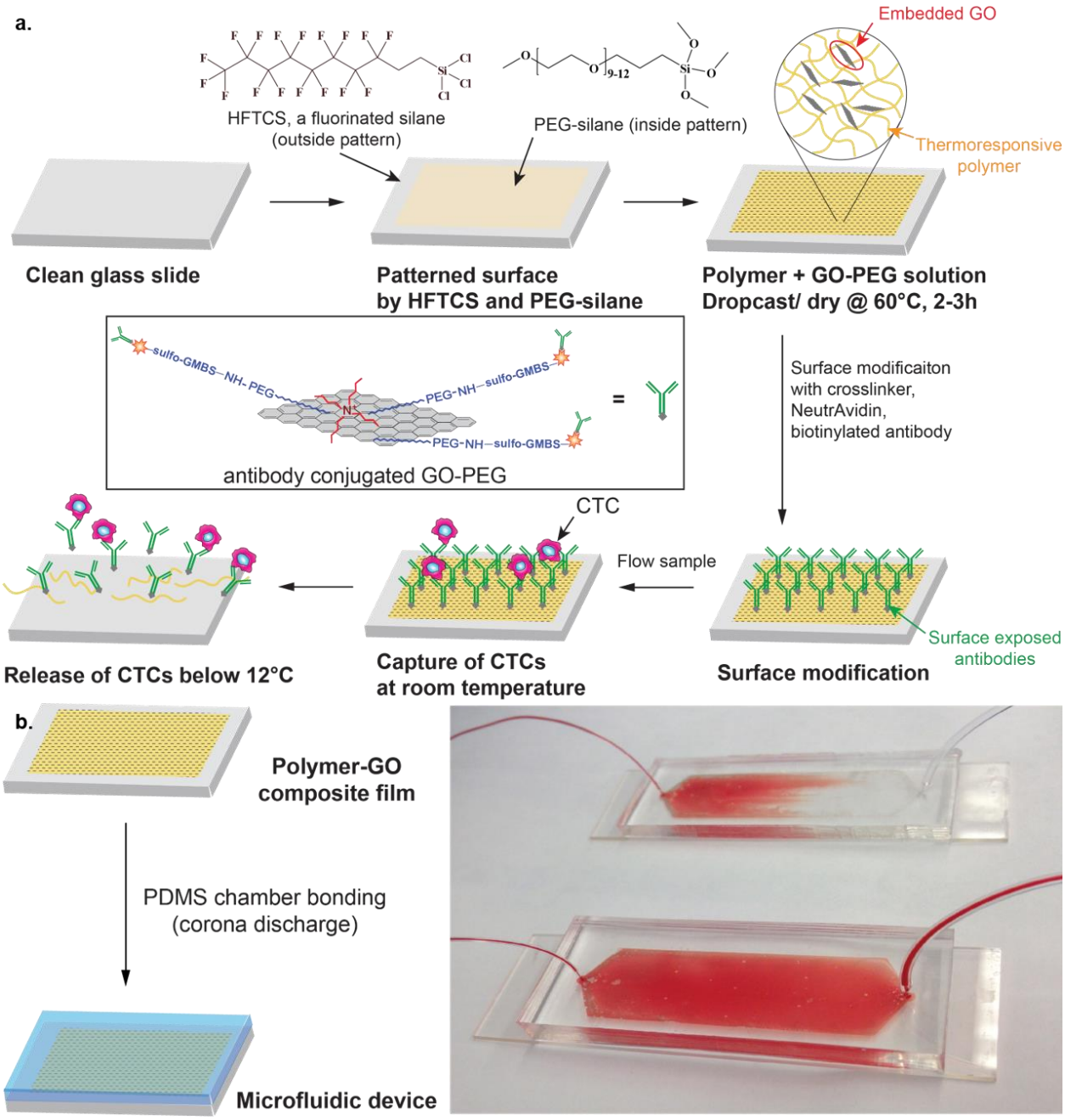

Figure 5-3 Thermosensitive polymer-GO CTC capture/release device. a) Schematic concept of a polymer-GO microfluidic device for the capture/release of CTCs. b) Enclosure within polydimethylsiloxane chamber and photograph of patient blood samples being processed by the polymer-GO devices (3).

5.3.2.5 Fluorescent biotin assay

To verify the ability to immobilize biotinylated antibody to the polymer-GO film surface, surface coverage by a fluorescently labeled biotin (Biotin (5-fluorescein) conjugate, Sigma Aldrich) was assessed (**Figure 5-4**). Three polymer-GO films underwent the entirety of the

conjugation chemistry (i.e. treatment with the GMBS cross-linker and NeutrAvidin; termed "Condition") with fluorescent biotin addition as the terminal step. To account for non-specific binding, three polymer-GO films were treated only with the fluorescent biotin to serve as a control in an analogous fashion to an isotype control (termed "Control"). ImageJ was used to quantify the fluorescence.

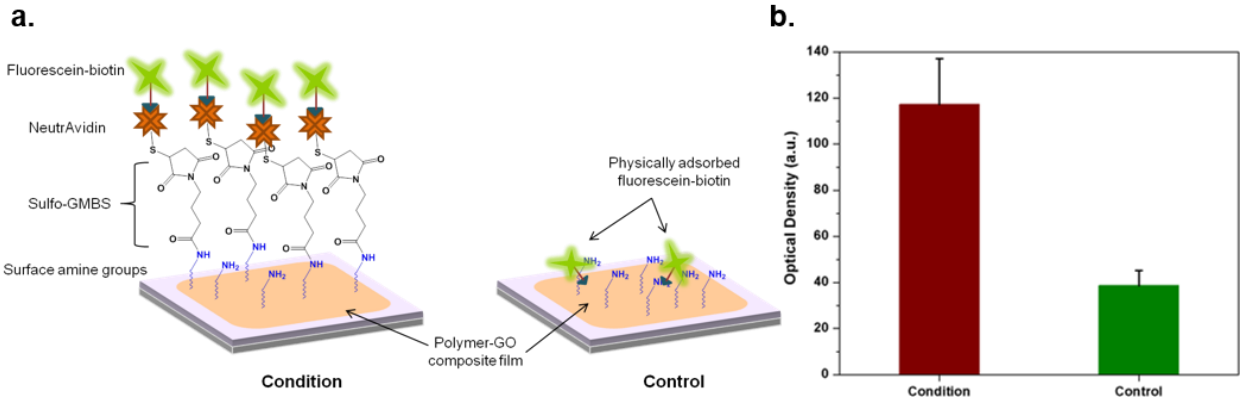

Figure 5-4 Fluorescent biotin assay. a) Schematic represents fluorescent biotin assay and negative control. b) The full conjugation chemistry features statistically higher fluorescence than the negative control as assessed via optical density (p = 0.019 (3)).

5.3.2.6 Sample processing

Following the introduction of anti-EpCAM to the device and blocking with 3% BSA, cell spike samples or patient samples were flowed on the chip. After washing with room temperature PBS, captured cells were released from the device by maintaining the device on ice and flowing cold PBS at a flow rate of 100 µl/min.

To prepare cells for staining, the effluent could be cytospun onto Polysine Microscope Adhesion Slides (Thermo Scientific). Slides were stained for 4,6-diamidino-2-phenylindole (DAPI), anti-cytokeratin 7/8 (BD), and anti-CD45 (BD). Primary antibodies were labeled with fluorescence tagged secondaries (AlexaFluor 546 and AlexaFluor 488, Invitrogen).

To prepare the cells for fluorescence *in situ* hybridization (FISH), CTCs released from the chip were subsequently made into "cell blocks" by first fixing them with ethanol and then embedding them in Histogel (Thermo Scientific). Blocks were then formalin fixed and stored in

70% ethanol until slide preparation. Blocks were paraffin embedded and sectioned at the University of Michigan Histology Core. FISH was conducted using probes for HER2 (BAC clone RP11-94L15) and chromosome 17 control probe (BAC clone RP11-100E5). FISH hybridization and image capture were performed essentially as previously described (264).

5.4 Results

5.4.1 LbL results

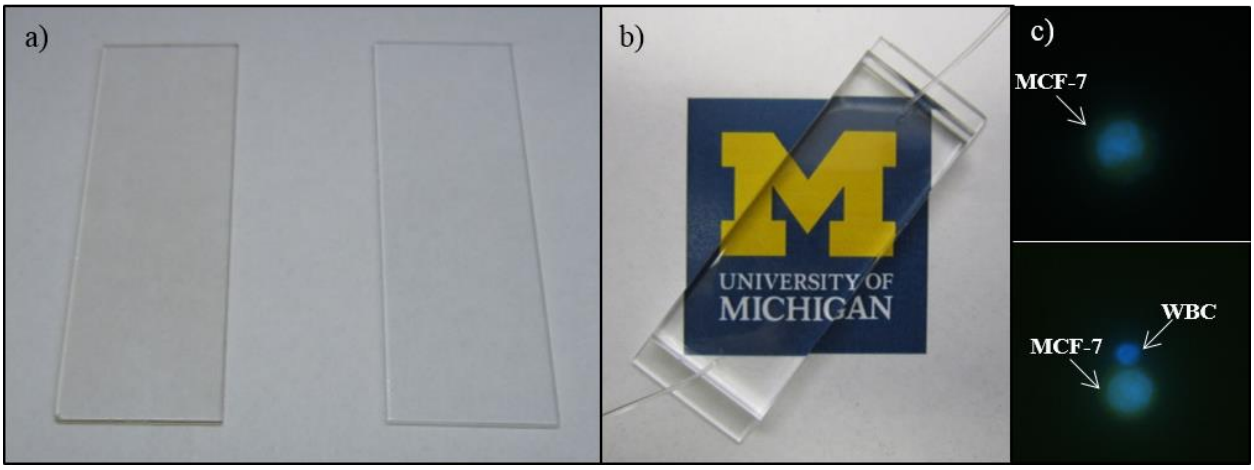

Figure 5-5 The LbL device. a) A ten layer PDDA/GO-PEG coated glass slide (left) contrasted with an uncoated glass slide (right). b) Example of an assembled device. c) Examples of captured cells on-chip. Cells exhibiting green fluorescence and blue nuclei are spiked in MCF-7 cancer cells, while cells with only the nuclei labeled are nonspecifically bound white blood cells.

While films of various compositions with various numbers of layers produced from this combination initially showed good capture results (**Figure 5-5**), these results were difficult to repeat (**Table 5-2**). Additionally, running spike experiments using the preliminary films incorporating PDDA in whole blood rather than buffer revealed issues of nonspecific binding for some conditions. In this instance, high nonspecific binding was defined as too high for the device to be useful for downstream genetic analysis. Oftentimes it was too high to be counted by the computer software, which in addition to being highly indicative of the failure of the device to be useful made it difficult to obtain reportable purity metrics. To combat these initial issues, conditions were attempted that included polymers chosen for their prior incorporation in anti-adhesive coatings, hyaluronate and heparin (265). While use of NaHyaluronate in the anionic

solution mitigated the nonspecific binding issues, devices with that film composition failed to reliably capture cells at a sufficient efficiency for further investigation. Additionally, devices frequently leaked due to bonding issues.

Table 5-2 Attempted experimental parameters for the LbL device. PDDA = poly(diallyldimethylammonium chloride), PEI = poly(ethyleneimine), PEG = phospholipid-polyethylene glycol-amine, TBA = tetrabutyl ammonium.

Anionic solution	Cationic solution	PEI	Numbers of bilayers	Maximum capture efficiency obtained	Nonspecific binding
GO-PEG	PDDA	As final layer for some trials	1, 3, 5, 10	102% (higher than GO Chip control)	High
NaHyaluronate	GO-PEG-TBA	Used to precoat slides for some trials	1, 3, 5, 10, 15	88.3% (unable to repeat this result)	Low
Heparin	GO-PEG-TBA	None	1	69%	High

Due to the upfront issues with achieving the required balance of high capture efficiency and low nonspecific binding during the capture step, this project did not make it to the phase during which release would have been attempted.

5.4.2 Thermoresponsive polymer-GO device results

5.4.2.1 Tunable thermoresponsive polymer

To create a tunable thermal responsive polymer, copolymer poly(*N*-acryloyl piperidine-*co*-*N*,*N*-diethyl acrylamide) was synthesized via free radical polymerization using AIBN as an initiator and was characterized for its molecular weight and LCST (**Figure 5-6a**). LCST was modulated by employing a copolymerization technique using two acrylamide monomers with different degrees of hydrophobicity: *N*-acryloyl piperidine (AP) and *N*,*N*-diethyl acrylamide (DEA). The homopolymers poly(*N*-acryloyl piperidine) (PAP) and poly(*N*,*N*-diethyl acrylamide) (PDEA) have LCSTs of 4° C and 25° C respectively (266). The required capture/release modulation temperature for the CTC device can be achieved by changing the ratio of the two monomers in the copolymer. For example, a copolymer synthesized with 7:3 molar ratio of AP:DEA showed a critical temperature of around 12-13^{o}C, which was used in this study (**Figure 5-6b**).

5.4.2.2 Film characterization

To determine surface availability of the amine groups within the polymer-GO composite, films were incubated with a fluorescent amine fluorescent dye. While polymer-GO composite films showed bright green fluorescence from the surface tethered dye, polymer-only films showed very low to no fluorescence (**Figure 5-6d**). Though the possibility of physically adsorbed dye molecules cannot be completely ruled out, it is most likely that the dye molecules were primarily tethered to the surface through covalent bonding between the amine groups on film surface and succinimidyl ester groups on the dye, as suggested by large contrast in fluorescence intensity from polymer-GO and polymer-only films.

Time dependence of dissolution of polymer-GO composite films in cold water was also determined. Dye treated films were dipped in cold water for different lengths of

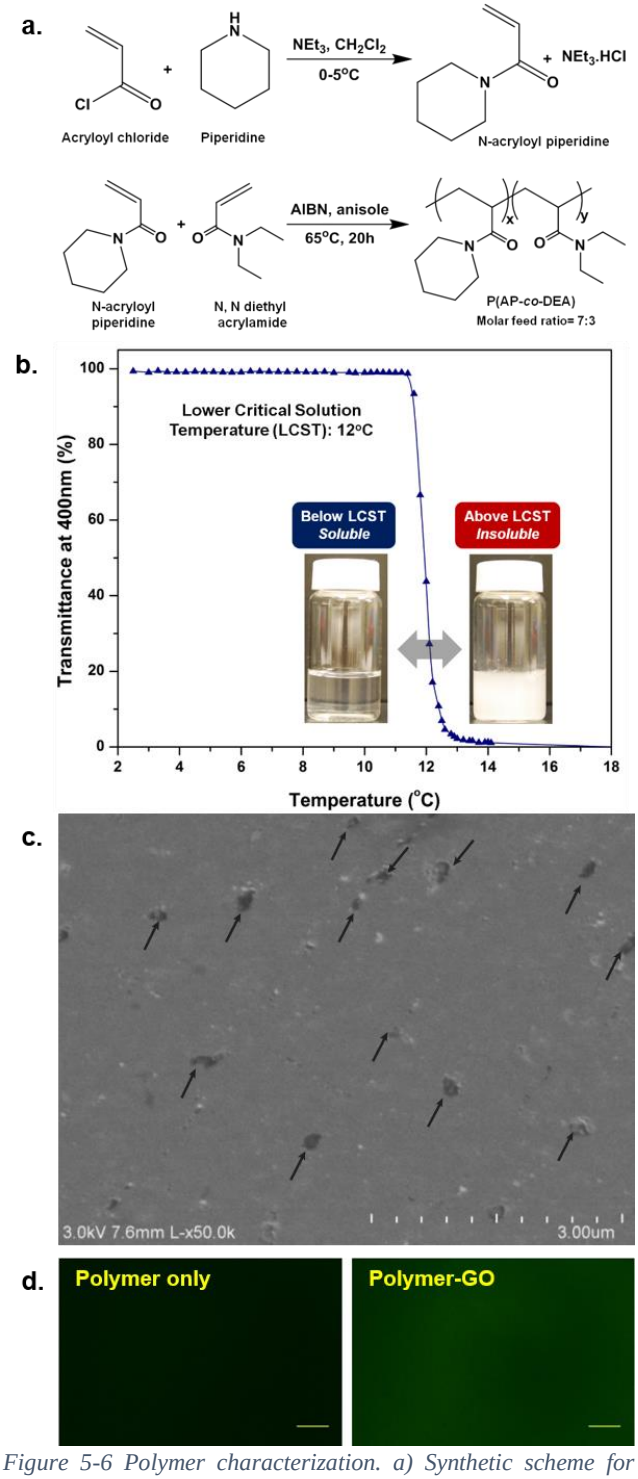

Figure 5-6 Polymer characterization. a) Synthetic scheme for copolymer. b) UV-vis transmittance vs temperature plots for the copolymer showing LCST of ~12° C. c) SEM image of polymer-GO composite surface. Arrows indicate suspended GO present on the surface of the film. d) Fluorescence images of polymer-only and polymer-GO films. The films were incubated with an amine-reactive dye (FSE, 0.25 mM aq. solution) for 30 minutes at 40° C. Scale bar: 20.0 μm (3).

time and the fluorescence images before and after dipping were compared. Films were dipped in cold water (5°C) for 5, 10, 20, and 30 minutes, and in room temperature water (20°C) for 30 minutes. The beakers with the dipped films were kept on an orbital shaker to weakly simulate conditions in microfluidic devices where the films are subjected to shearing by the flowing fluids. While the film was completely dissolved and washed off in 20 to 30 minutes under cold condition, as evident from gradual disappearance of green fluorescence, it remained stable and intact at room temperature even after 30 minutes (**Figure 5-7**). It is to be noted that in the actual device, the dissolution time is much shorter at 10 minutes, most likely due to the shear of the constant flow rate.

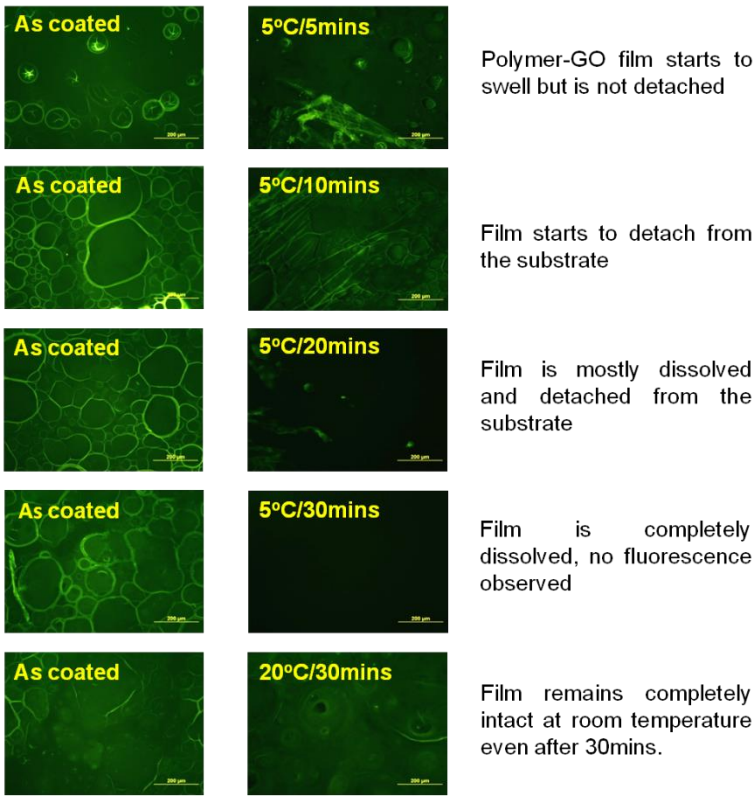

Figure 5-7 Fluorescence microscopy images of polymer-GO films incubated with FSE dye. Left: before and right: after being dipped in either cold (5°C) or room temperature (20°C) water for the specified time durations. Scale bar: 200 µm (3).

5.4.2.3 Device performance characterization

To verify the steps of the conjugation chemistry, experiments were performed to compare capture by (1) a polymer film lacking GO alone; (2) a polymer film lacking GO with the addition of anti-EpCAM; and (3) the polymer-GO film with full conjugation chemistry. The two control films showed significantly lower levels of capture with the polymer film and the polymer film with antibody capturing at 6.4% and 11.0% the level of the full chemistry, respectively (**Figure 5-8a**), with the increase in capture of the polymer with antibody condition a likely a result of physically adsorbed anti-EpCAM. This also suggests that very little of the capture antibody on the fully functional device is non-specifically bound.

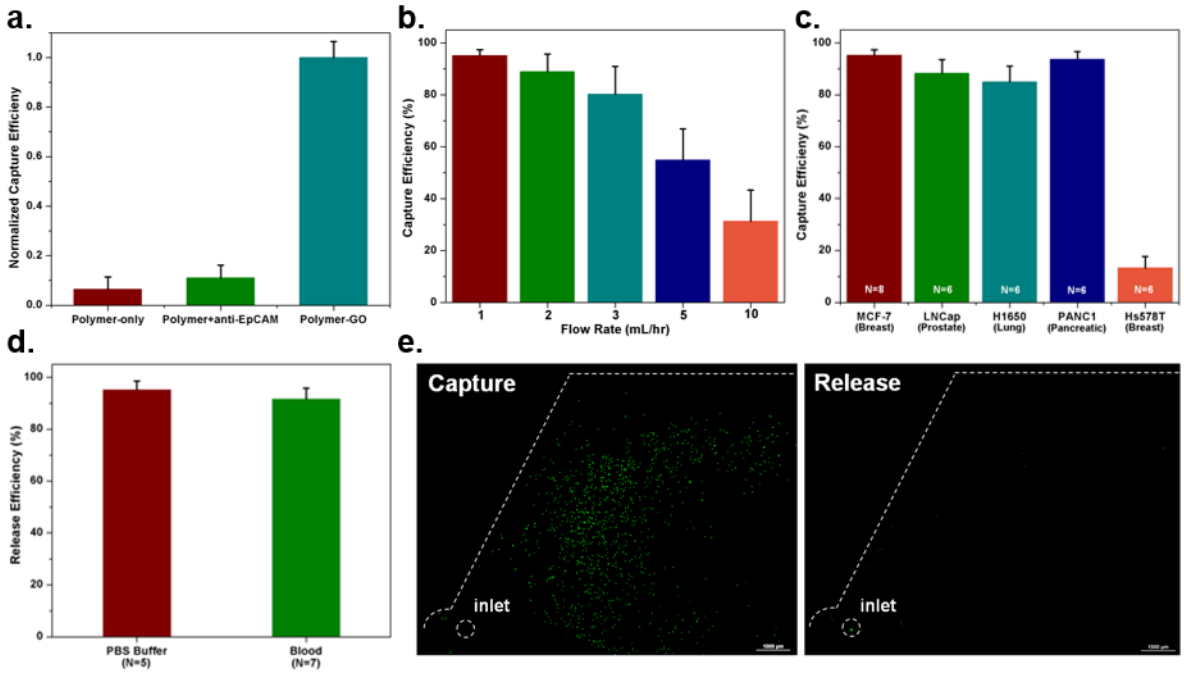

Figure 5-8 Device performance characterization. a) Capture efficiency of microfluidic devices featuring only the thermo-sensitive polymer, the thermo-sensitive polymer and non-specifically bound anti-EpCAM, and the polymer-GO film with specific conjugation chemistry as normalized by this last condition. b) Cell capture efficiency of the microfluidic polymer-GO device at various flow rates evaluated using a breast cancer cell line (MCF-7). Error bars show standard deviations (n=6). c) Capture efficiency of cell lines of varying origin and EpCAM expression levels. MCF-7 (n=8), PANC1, H1650, LNCaP, Hs578T (n=6). d) Release efficiency of the microfluidic polymer-GO device (MCF-7 cells were spiked into 1 mL of buffer or blood). e) Fluorescence microscope images of devices after capture and release of fluorescently-labeled MCF-7 cells (3).

To test the performance of the GO-polymer device for CTC capture, fluorescence labeled human breast cancer cell line MCF-7 cells (1,000 cells/mL) were spiked into buffer and flowed

through the GO-polymer device at different flow rates (1-10 mL/hr). The captured cells in the device and the non-captured cells collected in the waste were then counted. As expected, the capture efficiency decreased with flow rate. The capture efficiency rapidly decreased at flow rates greater than 5 mL/hr. In the 1–3 mL/hr range, the average capture efficiency was over 88.2% (n = 6 at each flow rate) with the highest capture of 95.21% at 1mL/hr (**Figure 5-8b**). To further investigate the effect of tumor type and EpCAM expression on capture efficiency, three high EpCAM expressing cell lines for various cancer types (MCF-7 breast cancer cells, LNCaP prostate cancer cells, and H1650 lung cancer cells), one low EpCAM expressing cancer-cell line (Panc-1 pancreatic cancer cells), and one EpCAM negative cancer cell line (Hs578T breast cancer cells) were selected for capture experiments at the flow rate of 1 mL/hr. The cells were fluorescently labeled and spiked into buffer at a concentration of 1000 cells/ml. The results indicate that the anti-EpCAM-coated GO-polymer device achieved high capture efficiency (84.93-95.21%) for EpCAM-positive cancer cells (**Figure 5-8c**). In contrast, a relatively low number of EpCAM-negative cells (Hs578T) were captured. Furthermore, the device is comparably effective in capturing different tumor cells, indicating the robust sensitivity of the device. After capturing cells on the devices, cell release experiments were carried out by flowing 1 mL cold PBS through devices cooled in ice at 100 μL/min (**Figure 5-8e**). Quantification of the cells in the devices before and after release showed an average cell release of 95.21% and 91.56% in buffer and blood experiments, respectively (**Figure 5-8d**). Furthermore, we tested the viability of the released cells by live dead assay. 91.68% of cells remained viable after release (**Table 5-3**).

Table 5-3 Experimental results from Live/Dead assay (MCF-7 cell line) (3).

Device	Live cells after release	Dead cells after release	Live/Dead (%)
D1	264	22	92.31
D2	353	7	98.06
D3	174	10	94.57
D4	270	35	88.52
D5	152	27	84.92
		Average	91.68

5.4.2.4 Clinical sample processing

To demonstrate the potential for CTC capture and release in clincial samples using the tunable polymer-GO composite film based device, blood samples obtained from 10 metastatic breast cancer patients and three pancreatic cancer patients were processed. Whole blood samples collected into EDTA tubes were processed at a flow rate of 1 mL/hr. Following a washing step, cells were released from the chip and deposited/spun onto glass slides by a cytospin centrifuge. CTCs in these samples were identified as DAPI-positive (shown in blue) nucleated cells staining positive for tumor markers (cytokeratin 7/8, shown in red) and negative for leukocyte markers (CD45, shown in green) (**Figure 5-9a**). CTCs were successfully recovered from 8 breast cancer patient samples and 2 pancreatic cancer patients (ranging from 2 to 20 CTCs/mL) (**Figure 5-9b**). The average number of CTCs recovered from breast samples was 5.6 CTCs/mL and from pancreatic samples was 8.3 CTCs/mL.

Released CTCs were viable and structurally intact, and hence could be readily investigated via standard clinical cytopathological and genetic testing. Here the feasibility of detecting HER2 amplification by fluorescence *in situ* hybridization (FISH) was examined, revealing HER2 amplification in one breast cancer patient (**Figure 5-9c**). One green signal indicates the presence of one copy of HER2, while one red signals indicates one copy of centromere 17 probe; the multiple green signals in the figure implied HER2 amplification.

5.5 Discussion

Initial attempts to fabricate a transparent CTC capture/release device centered around the technique of LbL. However, the inability to maintain high capture without retaining a high number of nonspecifically bound cells led to the pursuit of other avenues before entering the release phase of the project.

In the follow-up work, a microfluidic device bottom substrate was coated with a composite film of functionalized GO dispersed in a matrix of thermoresponsive polymer with a lower critical solution temperature (LCST) of 13°C. Surface available functionalized GO provided anchors for attaching the CTC capture antibody while the polymer matrix provided temperature dependent modulation of capture or release functionality. The microfluidic assembly facilitated the processing of patient blood samples within a simple planar device. Drop-casting the polymer-GO

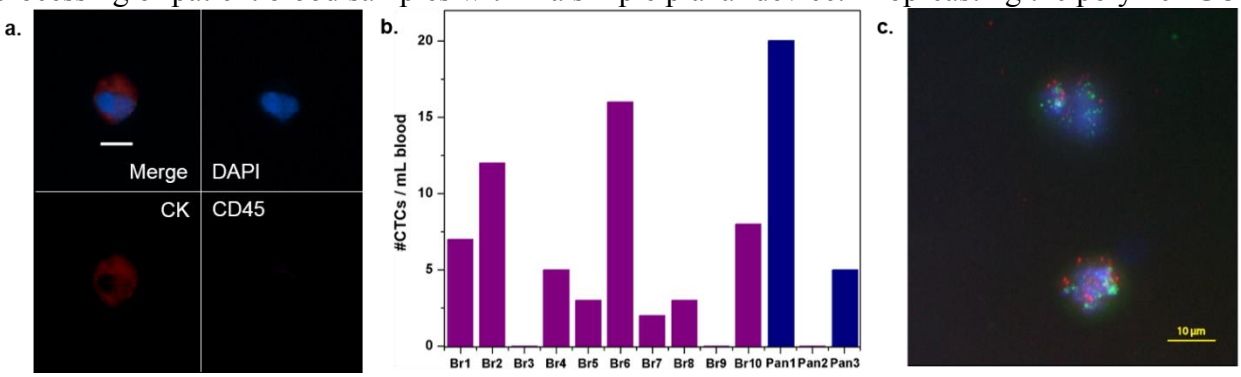

Figure 5-9 Patient sample processing with the thermosensitive polymer-GO release device. a) Fluorescence images of CTCs from breast cancer patient sample. Nucleated cells (blue) staining positive for cytokeratin 7/8 (red) and negative for the white blood cell marker CD45 (green) were enumerated as CTCs. Scale bar = 10 µm. b) CTC enumeration results from 10 breast cancer patients and 3 pancreatic cancer patients. c) Fluorescence in situ hybridization (FISH) image of CTCs of breast cancer patient sample Br10. HER2(green)/centromere 17 probe(red) (3).

blend on a patterned and surface modified substrate made such a device cheap and easy to fabricate. Moreover, the LCST of around 13°C for the polymer matrix made it possible to use the device at room temperature as opposed to higher temperatures (120), such that there were no concerns about inadvertently releasing the cells during the capture step. Additionally, cell release occurred under gentle conditions, maximizing the viability of released cells. The consolidation of the advantageous properties of GO-based capture with superior release functionality of the chosen polymer yielded a device that enables the study of these clinically interesting cells without many of the shortcomings of past technologies, while simultaneously presenting an easy, scalable fabrication method.

The downstream analysis facilitated by the efficient release of captured cells highlights the potential for this device's use in basic and clinical cancer investigation. As evidenced by data obtained from physiologic solutions containing spiked labeled cancer cells from multiple cancers and the processing of primary breast and pancreatic cancer patient blood samples, isolation of these rare cells with this device is highly feasible, completing the first step to unlocking the research opportunities presented by CTCs.

Compared with other CTC isolation strategies, immunoaffinity based technologies harvest CTCs with high sensitivity and purity (267), but have the drawback of tethering cells within the device. Overcoming this limitation, the thermosensitive polymer-GO device collected viable and intact CTCs in suspension after immunocapture, making it ideal for various downstream analyses that require the high integrity and purity of the targeted cell population, such as genotyping and single cell profiling. This advanced analysis of CTCs could become a "real-time" indicator to develop personalized therapy, as well as to bring valuable insights into the mechanism underlying cancer metastasis. Due to the low cost and ease of fabrication, this technology has the potential to

be scalable for commercialization. As the earlier GO based CTC isolation device, the GO Chip, featured high capture, low nonspecific binding, and reliable performance, upgrades to the device such that the new technology retains those characteristics while simultaneously enables high quality imaging and downstream analysis will continue to be the benchmark to which technology development aspires.

Chapter 6 Conclusion

6.1 Research summary

CTCs present the opportunity to further investigate the most devastating part of cancer – metastasis as propagated through those cells capable of traveling in the blood stream. To this end, the impetus for all research contained herein is motivated by the overarching aim of being able to better inform the patient. Through the study of both the biology of metastasis and the relation of these informative biomarkers to the trajectory of a specific patient's disease, CTCs have the potential to inform the choices made in disease management.

There remain unmet needs in the study and monitoring of genitourinary cancers, specifically those of the bladder and prostate. To address the need for an informative biomarker that provides more information than the PSA test, I present the alternative in circulating tumor cells, which, when isolated with the highly sensitive GO Chip technology, provided the options of investigating CTC counts, metrics related to CTC clusters, and RNA expression levels. In the second chapter of this thesis, I presented a pilot investigation into what prognostic information may be gleaned from mCRPC samples assayed in the form of whole blood processed across parallel GO Chips, one for enumeration and one for RNA extraction and analysis. CTCs were detected in all 41 samples processed for enumeration, with clusters presenting in 26/41 samples. This represents the highest percentage of prostate cancer patients in which CTC clusters have been detected. The parallel device was used to collect the cell lysate for RT-qPCR analysis. Gene expression levels were normalized to housekeeping genes and, with healthy control expression

levels subtracted, could be used to examine relative expression levels. With this information in hand, I could complete the bed to bench to bed cycle through the analysis of these enumeration metrics and RNA expression levels with respect to overall survival as well as clinical, PSA, and radiographic progression. Using the R programming language, I screened for genes that could be used to stratify patients into distinct prognostic categories to which I could ascribe a numeric score. By evaluating these scores in their different combinations, starting with those genes initially selected by their abilities to yield distinct groups as determined by a log rank p value calculated based on Kaplan-Meier analysis, I determined the combination of genes most prognostic as evaluated based on the area under the curve (AUC) from the resulting receiver operator characteristic curve (ROC) as well as the hazard ratio. The ultimate set of genes suggested the importance of a dedifferentiated phenotype in the prognosis of prostate cancer.

In the third chapter of this dissertation, we investigated protein-level expression of specific molecular markers in prostate cancer. Overexpression of HER2 is a hallmark of breast cancer and is assessed based on gene amplification as determined through fluorescence *in situ* hybridization (FISH). However, HER2 gene amplification is not observed in prostate cancer. Our investigation into the *protein* level overexpression of HER2 in prostate cancer revealed overexpression in primary prostate cancer tissue microarrays relative to the healthy prostate; additionally, investigation of HER2 expression in bone metastases revealed overexpression relative to the primary tissue. Subsequent knockdowns of HER2 in the prostate cancer cell line C4-2B inhibited growth of these cells when injected into mouse tibia as assayed through expression of the proliferative marker Ki67. Investigation of tumor initiating capacity based on either the expression of HER2 or its fellow epidermal growth factor receptor family member EGFR showed that high HER2 expressing cells as determined by flow sorting did not have increased spheroid forming

capacity relative to low HER2 expressing cells; in contrast, high EGFR expressing cells has statistically significantly higher spheroid forming capacity for both primary and secondary prostaspheres. This led to questions about the role of EGFR in cell survival in circulation in addition to tumor initiating capacity. I probed this question by analyzing a small cohort of mCRPC patients to determine the presence of EGFR-expressing CTCs. I detected CTCs in all 10 patients with EGFR+ CTCs evident in 9/10 patients. Intrapatient heterogeneity was also apparent through the varied percentage of EGFR+ CTCs amongst patients (median: 35.5%). Given the potential complimentary roles of HER2 in tumor cell proliferation and EGFR in tumor initiation and survival in the blood stream, we investigated the administration of dual inhibitors and cocktails of monoclonal antibodies to treat prostate cancer in mouse models. In these animal models, tumors had significantly lower numbers of viable cells compared with those animals treated with therapies specifically targeted against HER2/EGFR.

The ability to apply epidermal growth factor receptor family targeting drugs as well as therapies directed against additional targets was the impetus into our study of bladder cancer. In chapter four of this dissertation, I sought to apply the highly sensitive GO Chip to CTC isolation in bladder cancer, where previous investigations of CTCs were hampered by methodology, in this case the exclusive use of the CellSearch technology. Through the sensitive detection of bladder cancer CTCs through microfluidics and nanotechnology, I would have improved chances of investigating molecular markers of interest, specifically HER2 and EGFR as well as ADAM15 and CD31. These two pairs of markers have implications as far as available treatments and the mechanisms of metastasis. Because of the limited investigation into bladder cancer CTCs, I spent increased energy on developing the combination of antibodies for capture, as assayed through cell spike experiments, and primary and secondary antibodies used in detection. Two combinations of

antibodies were ultimately used to stain five metastatic bladder cancer patient samples. CTCs were detected in all five patients (range: 5-499 CTCs/mL), with detection above a threshold as determined using a healthy control occurring on 9/10 devices processed. Additionally, we were able to visualize the results on-chip, in contrast to PCR based methods sometimes used for bladder cancer CTCs, such that we were able to observe cell clusters ranging from 2-39 CTCs/cluster. Using an optimized combination of antibodies, I detected EGFR and CD31 on some of the CTCs, providing insight into how these cells spread.

While the GO Chip technology enabled the study of the presence of CTCs and CTC clusters; specific protein expression by those cells; and relative RNA expression levels by the bulk population captured on-chip, the full potential of CTCs may be better realized through further genetic characterization and other characterization at the single cell level. This will be best facilitated by the release of captured cells from the chip for subsequent analysis. To improve the current technology to enable this capability, I investigated two strategies for cell release. My initial studies involved the formation of a polymer substrate through Layer-by-Layer (LbL) deposition; this film could then be degraded by applying specific enzymes to degrade the film. Efforts included several polymer combinations with both ionic and van der Waals forces contributing to film formation. Films were ultimately enclosed in a polydimethylsiloxane (PDMS) chamber through irreversible corona discharge bonding. However, cell spikes in blood revealed difficulty in achieving a balance of two important CTC capture technology metrics: capture efficiency and purity. While the GO-PEG/PDDA device enabled high capture efficiency, too many white blood cells nonspecifically bound for the chip to be useful. Conversely, on the GO-TBA-PEG/NaHyaluronate devices, nonspecific binding of white blood cells was negligible. Unfortunately, so was the capture efficiency.

Fruitless troubleshooting efforts yielded a shift to an alternative release strategy. While the use of thermosensitive polymers for CTC release had been previously established, hindrances such as inconvenient processing temperatures or involved chemical processes has impeded convenient use in the clinical setting. Our strategy made use of a tunable copolymer, whose lower critical solution temperature (LCST) could be modulated by varying the ratio of its component parts, DEA and AP. As verified through cell spikes, the microfluidic device fabricated by enclosing a dropcast GO-TBA-PEG/polymer composite could serve as the basis for the same functionalization chemistry as the GO Chip, enabling highly efficient capture (greater than 84% across EpCAM-expressing cell lines). By cooling the device to approximately 4° C by placing it on ice and flowing chilled PBS, greater than 90% release was achieved in both buffer and whole blood. To verify clinical utility, we processed 10 breast and 3 pancreatic patient samples, detecting CTCs following the release step in 8/10 breast cancer patients and 2/3 pancreatic patient patients. We demonstrated proof-of-principle downstream analysis by performing HER2 FISH on CTCs captured from one breast cancer patient, revealing amplification.

6.2 Limitations and future directions

While the projects described above show great promise with regards to applying the aforementioned technologies to CTC isolation from patient samples, to more broadly apply such technologies and to generate data that would create true clinical impact, some limitations will need to be addressed.

In examining RNA expression levels, I determined an eight-gene signature associated with shorter overall survival. However, this result was based solely on a small training cohort, and will need to be validated with an adequately powered testing cohort. Additionally, the GO Chip based CTC analysis had thus far has been conducted in a metastatic cohort, but some of the greatest

opportunities in affecting change to patient treatment are in early stage and high risk patients. CTCs could be investigated as a prognostic biomarker for these patients with the goal of averting unnecessary surgery or therapeutics accompanied by harmful side effects. The current gene score could be tested in this cohort using the same techniques. Alternatively, a similar study to that in Chapter 2 could be conducted to identify markers that are more significant in earlier stage patients. Given the mounting evidence of the importance of stemlike cells in disease progression, detecting these markers in CTCs could provide clinicians and patients with the information they need to decide how aggressively to pursue treatment.

To draw significant clinical conclusions, future studies will need to move past the exploratory phase to asking specific questions and selecting the specific cohort to answer those questions. Cohorts considered in this work were selected mainly based on availability, and while all patients had metastatic disease, treatment regimens and clinical characteristics were diverse, though not in a distribution that enabled meaningful comparison. Future work should involve cohort selection for specific characteristics based on the research question and of a size large enough to generate more robust conclusions.

To facilitate the generation of larger cohorts, bottlenecks in sample processing need to be addressed. All microfluidic devices are currently fabricated in-house. Subsequent large scale studies would benefit from readily available devices produced more consistently than by our current small batch protocol. The biggest hurdle to the commercial production of this chip, as discovered through our limited collaboration with the Coulter Translational Research Partnership Program, is the chamber. Because the silicon substrate is produced using conventional microchip fabrication techniques, generating that component at scale would likely be feasible. However, there are many requirements of the PDMS chamber that prove difficult to fulfill. PDMS is more suited

to prototyping rather than large scale production (268), but whatever material we would use for large scale production would have to retain the optical transparency of PDMS (and possibly improve upon its tendency to autofluoresce) even once machined or molded with the 50 μm-height channel. While injection molding would solve the problems associated with machining, an injection mold is expensive, leading to apprehension in using them for prototypes, without which a design cannot be finalized. However, as it is now possible to 3D print injection molds (269), the price has dropped precipitously. This would allow for the large-scale production of chambers fabricated from an optically transparent material that can be corona discharge bonded to the silicon substrate, including various thermoplastic polymers (46).

Other limitations to large-scale sample processing are related to the time lag associated with sample throughput and the staining/imaging/analysis workflow. A device redesign incorporating radial flow would improve throughput, as has been previously described (270), while ideally retaining the high sensitivity and purity of the original GO Chip. This is an investigation currently in progress in the lab. Imaging and analysis roadblocks may be eased by upgrading our current microscope system and making use of automated image analysis, training software to conduct a preliminary pass on collected image using our wealth of CTC images, to find the location of these cells on-chip, and to take higher magnification images.

Beyond the current patient sample processing paradigm, limitations to downstream analysis result in part from the fact that the captured cells remain tethered to the chip. While we have developed a thermosensitive polymer-GO release chip (Chapter 5, (3)), subsequent work with that device suffered from issues of reliability, so future directions in downstream analysis may need to be preceded by the development of new release strategies. To minimize changes to an already relatively successful technology, one strategy would be to shift the focus of the release

mechanism from the point at which the capture conjugation chemistry is tethered to the chip to the point where the antibody is tethered to the avidin. In chromatography, a conceptually similar technique involves exploiting the affinity of avidin with its binding partners (271). Desthiobiotin (DBS) was developed as a moiety that binds with avidin with lower affinity than biotin such that it may be ultimately displaced by a biotin solution. This approach has been used recently to release captured exosomes (272) and could be adapted to the release of captured CTCs. To do so, a DSB-conjugated antibody, such as anti-EpCAM, would be introduced to the chip at the point where we currently use a biotinylated antibody. Following cell capture, cells could be eluted from the chip using a biotin solution.

Even upon the advent of a mass produced high-throughput GO Chip with release enable, an additional challenge is that CTCs provide a limited amount of biological material to study and yet have the potential to provide a great deal of information should we be able to best use it. One way to maximize our ability to collect data from CTCs would be to expand day 0 CTCs in culture. Culture of CTCs has been previously attempted, but has previously been limited to cell line cell spike experiments (88) and CTCs isolated from animal models (273) or has featured issues with repeatability (274) and proliferation beyond the maintenance of the initial cell number (75). Some limited success occurred in the case of colon cancer where CTCs isolated using RosetteSep from two patients were cultured successfully for two months (275). However, both samples were taken from patients with greater than 300 CTCs/7.5 mL blood, and one of the cultures died off after the two-month period. There are multiple examples of CTC culture from breast cancer patient samples. CTCs isolated using fluorescence activated cell sorting (FACS) for “brain metastasis selected markers” were successfully cultured in three out of eight samples, allowing further examination in mouse xenograft models (276). The CTC-iChip has been used to culture breast cancer CTCs with

a success rate of 6/36. A subsequent study also using the iChip studied HER2+ and HER2- populations in CTCs cultured from three breast cancer patients. In prostate cancer, CTC culture has been conducted with CTCs isolated by the filtration device MetaCell; however, while 64.3% of cultures were successful from patients with detectable CTCs, CTCs were only detected in 52% of prostate cancer patients assayed (277). Three dimensional organoid culture techniques (278) have been used to culture biopsies taken from metastases from advanced prostate cancer patients, including blood samples yielding greater than 100 CTCs per 10 mL blood (279), however culture was only demonstrated successfully for one blood sample. A promising method for CTC expansion has been demonstrated by our group using a coculture model with early stage lung cancer circulating tumor cells both isolated with and proliferated on a microfluidic platform (122).

To enable CTC culture, a higher amount of "starting material," i.e. day 0 CTCs, would be desirable, and may be enabled by high throughput processing of greater sample volumes. For each of the above culture strategies, optimization of several factors was necessary to achieve even modest success, with the composition of the cell culture media, presence of coculture cells, hypoxic conditions, adherent or nonadherent surfaces, and application of extracellular matrix proteins all serving as variable parameters. This suggests that attempts of genitourinary cancer CTC culture will require multiple informed choices of conditions. However, given that Matrigel is a near constant in the prior establishment of prostate cell lines suggests that it is a requirement, while the complications introduced by the use of coculture cells suggest that they should be avoided.

Both high sensitivity capture of CTCs and their subsequent culture of captured CTCs could enable additional downstream genetic analysis for both personalized medicine and biological study. Prostate CTCs have already been examined for the androgen receptor splice variant 7 (AR-

V7), which has been associated with resistance to enzalutamide and abiraterone (155). A follow up study found that men with the splice variant had a better response to taxanes than AR targeted therapies (280), showing the promise of CTCs in assisting clinical decisions. Future work on prostate cancer genetics may look at the different genetic directions the cancer may take through sampling and analyzing early stage patients. Mutations in SPOP have been found to be mutually exclusive with ETS gene fusions (281), with other exclusive mutations suggesting different disease mechanisms. Knowledge of different genetic aberrations could inform treatment selection, such as the use of PARP inhibitors in the case of ETS fusion positive patient or PI3K inhibitors in the case of amplification along that pathway (282). Sampling from the blood selects those cancer cells that have already completed the first steps of metastasis, and may therefore feature the genetic characteristic representative of the advancing disease. Similarly, the study of capture and/or cultured bladder cells may in the short term prevent the understaging of the disease and in the long term elucidate potential therapeutic targets.

Metastasis is at the root of over 90% of cancer death, but through the collaboration of biologists, clinicians, and engineers, we possess the skills to optimize and improve current technology to conduct the studies necessary to study the weaknesses of this disease. Through the analysis of those cells responsible for disease spread, we have shown our ability to learn about the molecular markers involved and the trajectory of the disease, and further study will contribute to illuminating a molecular picture.

References

1. Kozminsky M, Nagrath S. Circulating Tumor Cells, Cancer Stem Cells, and Emerging Microfluidic Detection Technologies With Clinical Applications. In: Liu H, Lathia JD, editors. Cancer Stem Cells: Targeting the Roots of Cancer, Seeds of Metastasis, and Sources of Therapy Resistance. New York: Elsevier Science; 2016. p. 473-97.

2. Gupta GP, Massagué J. Cancer metastasis: building a framework. Cell. 2006 Nov 17;127(4):679-95.

3. Yoon HJ, Shanker A, Wang Y, Kozminsky M, Jin Q, Palanisamy N, et al. Tunable Thermal-Sensitive Polymer–Graphene Oxide Composite for Efficient Capture and Release of Viable Circulating Tumor Cells. Advanced materials. 2016;28(24):4891-7.

4. Day KC, Hiles GL, Kozminsky M, Dawsey SJ, Paul A, Broses LJ, et al. HER2 and EGFR overexpression support metastatic progression of prostate cancer to bone. Cancer research. 2017;77(1):74-85.

5. Weigelt B, Peterse JL, van't Veer LJ. Breast cancer metastasis: markers and models. Nature reviews cancer. 2005;5(8):591-602.

6. Chambers AF, Groom AC, MacDonald IC. Dissemination and growth of cancer cells in metastatic sites. Nature Reviews Cancer. 2002;2(8):563-72.

7. Fidler IJ. The pathogenesis of cancer metastasis: the 'seed and soil'hypothesis revisited. Nat Rev Cancer. 2003;3(6):453-8.

8. Thiery JP. Epithelial-mesenchymal transitions in tumour progression. Nature Reviews Cancer. 2002;2(6):442-54.

9. Yamaguchi H, Wyckoff J, Condeelis J. Cell migration in tumors. Current opinion in cell biology. 2005;17(5):559-64.

10. Christiansen JJ, Rajasekaran AK. Reassessing epithelial to mesenchymal transition as a prerequisite for carcinoma invasion and metastasis. Cancer research. 2006;66(17):8319-26.

11. van Denderen BJW, Thompson EW. Cancer: The to and fro of tumour spread. Nature. 2013;493(7433):487-8.

12. Tsai JH, Donaher JL, Murphy DA, Chau S, Yang J. Spatiotemporal regulation of epithelial-mesenchymal transition is essential for squamous cell carcinoma metastasis. Cancer cell. 2012.

13. Ocaña OH, Córcoles R, Fabra Á, Moreno-Bueno G, Acloque H, Vega S, et al. Metastatic colonization requires the repression of the epithelial-mesenchymal transition inducer Prrx1. Cancer cell. 2012.

14. Klein CA. Parallel progression of primary tumours and metastases. Nature Reviews Cancer. 2009;9(4):302-12.

15. Paterlini-Brechot P, Benali NL. Circulating tumor cells (CTC) detection: Clinical impact and future directions. Cancer Letters. 2007 8/18/;253(2):180-204.

16. Yoon HJ, Kozminsky M, Nagrath S. Emerging Role of Nanomaterials in Circulating Tumor Cell Isolation and Analysis. ACS Nano. 2014 Mar 25;8(3):1995-2017.

17. Kozminsky M, Wang Y, Nagrath S. The incorporation of microfluidics into circulating tumor cell isolation for clinical applications. Current Opinion in Chemical Engineering. 2016;11:59-66.

18. Cristofanilli M, Hayes DF, Budd GT, Ellis MJ, Stopeck A, Reuben JM, et al. Circulating tumor cells: a novel prognostic factor for newly diagnosed metastatic breast cancer. J Clin Oncol. 2005 Mar 1;23(7):1420-30.

19. Budd GT, Cristofanilli M, Ellis MJ, Stopeck A, Borden E, Miller MC, et al. Circulating tumor cells versus imaging—predicting overall survival in metastatic breast cancer. Clinical Cancer Research. 2006;12(21):6403-9.

20. Hayes DF, Cristofanilli M, Budd GT, Ellis MJ, Stopeck A, Miller MC, et al. Circulating tumor cells at each follow-up time point during therapy of metastatic breast cancer patients predict progression-free and overall survival. Clinical Cancer Research. 2006 Jul 15;12(14):4218-24.

21. Sastre J, Maestro ML, Puente J, Veganzones S, Alfonso R, Rafael S, et al. Circulating tumor cells in colorectal cancer: correlation with clinical and pathological variables. Ann Oncol. 2008 May;19(5):935-8.

22. Cohen SJ, Punt CJ, Iannotti N, Saidman BH, Sabbath KD, Gabrail NY, et al. Prognostic significance of circulating tumor cells in patients with metastatic colorectal cancer. Ann Oncol. 2009 Jul;20(7):1223-9.

23. Cohen SJ, Punt CJA, Iannotti N, Saidman BH, Sabbath KD, Gabrail NY, et al. Relationship of circulating tumor cells to tumor response, progression-free survival, and overall survival in patients with metastatic colorectal cancer. Journal of Clinical Oncology. 2008 Jul 1;26(19):3213-21.

24. de Bono JS, Scher HI, Montgomery RB, Parker C, Miller MC, Tissing H, et al. Circulating tumor cells predict survival benefit from treatment in metastatic castration-resistant prostate cancer. Clinical Cancer Research. 2008 Oct 1;14(19):6302-9.

25. Mocellin S, Hoon D, Ambrosi A, Nitti D, Rossi CR. The prognostic value of circulating tumor cells in patients with melanoma: a systematic review and meta-analysis. Clinical cancer research. 2006;12(15):4605-13.

26. Pantel K, Brakenhoff RH, Brandt B. Detection, clinical relevance and specific biological properties of disseminating tumour cells. Nature Reviews Cancer. 2008 May;8(5):329-40.

27. Danila DC, Fleisher M, Scher HI. Circulating tumor cells as biomarkers in prostate cancer. Clinical Cancer Research. 2011;17(12):3903-12.

28. Jonathan D. Rapid translation of circulating tumor cell biomarkers into clinical practice: technology development, clinical needs and regulatory requirements. Lab on a Chip. 2014;14(1):24-31.

29. Aceto N, Bardia A, Miyamoto DT, Donaldson MC, Wittner BS, Spencer JA, et al. Circulating tumor cell clusters are oligoclonal precursors of breast cancer metastasis. Cell. 2014;158(5):1110-22.

30. Cristofanilli M, Budd GT, Ellis MJ, Stopeck A, Matera J, Miller MC, et al. Circulating tumor cells, disease progression, and survival in metastatic breast cancer. New England Journal of Medicine. 2004;351(8):781-91.

31. Olmos D, Arkenau HT, Ang JE, Ledaki I, Attard G, Carden CP, et al. Circulating tumour cell (CTC) counts as intermediate end points in castration-resistant prostate cancer (CRPC): a single-centre experience. Annals of oncology. 2009;20(1):27-33.

32. Allard WJ, Matera J, Miller MC, Repollet M, Connelly MC, Rao C, et al. Tumor cells circulate in the peripheral blood of all major carcinomas but not in healthy subjects or patients with nonmalignant diseases. Clinical Cancer Research. 2004 Oct 15;10(20):6897-904.

33. Shaffer DR, Leversha MA, Danila DC, Lin O, Gonzalez-Espinoza R, Gu B, et al. Circulating tumor cell analysis in patients with progressive castration-resistant prostate cancer. Clinical Cancer Research. 2007;13(7):2023-9.

34. Danila DC, Heller G, Gignac GA, Gonzalez-Espinoza R, Anand A, Tanaka E, et al. Circulating tumor cell number and prognosis in progressive castration-resistant prostate cancer. Clinical Cancer Research. 2007 Dec 1;13(23):7053-8.

35. Leversha MA, Han J, Asgari Z, Danila DC, Lin O, Gonzalez-Espinoza R, et al. Fluorescence in situ hybridization analysis of circulating tumor cells in metastatic prostate cancer. Clinical cancer research : an official journal of the American Association for Cancer Research. 2009;15(6):2091-7.

36. Attard G, Swennenhuis JF, Olmos D, Reid AH, Vickers E, A'Hern R, et al. Characterization of ERG, AR and PTEN gene status in circulating tumor cells from patients with castration-resistant prostate cancer. Cancer Res. 2009 Apr 1;69(7):2912-8.

37. Scher HI, Heller G, Molina A, Attard G, Danila DC, Jia X, et al. Circulating tumor cell biomarker panel as an individual-level surrogate for survival in metastatic castration-resistant prostate cancer. Journal of clinical oncology. 2015;33(12):1348-55.

38. Lorente D, Olmos D, Mateo J, Bianchini D, Seed G, Fleisher M, et al. Decline in Circulating Tumor Cell Count and Treatment Outcome in Advanced Prostate Cancer. European Urology. 2016.

39. Seal SH. A sieve for the isolation of cancer cells and other large cells from the blood. Cancer. 1964 May;17(5):637-42.

40. Vona G, Sabile A, Louha M, Sitruk V, Romana S, Schutze K, et al. Isolation by size of epithelial tumor cells - A new method for the immunomorphological and molecular characterization of circulating tumor cells. Am J Pathol. 2000 Jan;156(1):57-63.

41. Vona G, Estepa L, Béroud C, Damotte D, Capron F, Nalpas B, et al. Impact of cytomorphological detection of circulating tumor cells in patients with liver cancer. Hepatology. 2004;39(3):792-7.

42. Werner SL, Graf RP, Landers M, Valenta DT, Schroeder M, Greene SB, et al. Analytical validation and capabilities of the epic CTC platform: enrichment-free circulating tumour cell detection and characterization. Journal of Circulating Biomarkers. 2015;4:3.

43. Scher HI, Lu D, Schreiber NA, Louw J, Graf RP, Vargas HA, et al. Association of AR-V7 on circulating tumor cells as a treatment-specific biomarker with outcomes and survival in castration-resistant prostate cancer. JAMA oncology. 2016;2(11):1441-9.

44. McDaniel AS, Ferraldeschi R, Krupa R, Landers M, Graf R, Louw J, et al. Phenotypic diversity of circulating tumour cells in patients with metastatic castration-resistant prostate cancer. Bju international. 2016.

45. Whitesides GM. The origins and the future of microfluidics. Nature. 2006 Jul 27;442(7101):368-73.

46. Becker H, Locascio LE. Polymer microfluidic devices. Talanta. 2002;56(2):267-87.

47. Haeberle S, Zengerle R. Microfluidic platforms for lab-on-a-chip applications. Lab on a Chip. 2007;7(9):1094-110.

48. McDonald JC, Whitesides GM. Poly (dimethylsiloxane) as a material for fabricating microfluidic devices. Accounts of Chemical Research. 2002 Jul;35(7):491-9.

49. Khandurina J, McKnight TE, Jacobson SC, Waters LC, Foote RS, Ramsey JM. Integrated system for rapid PCR-based DNA analysis in microfluidic devices. Analytical Chemistry. 2000;72(13):2995-3000.

50. Erickson D, Li D. Integrated microfluidic devices. Analytica Chimica Acta. 2004;507(1):11-26.

51. Hofman VJ, Ilie MI, Bonnetaud C, Selva E, Long E, Molina T, et al. Cytopathologic detection of circulating tumor cells using the isolation by size of epithelial tumor cell method: promises and pitfalls. Am J Clin Pathol. 2011 Jan;135(1):146-56.

52. Pinzani P, Salvadori B, Simi L, Bianchi S, Distante V, Cataliotti L, et al. Isolation by size of epithelial tumor cells in peripheral blood of patients with breast cancer: correlation with real-time reverse transcriptase–polymerase chain reaction results and feasibility of molecular analysis by laser microdissection. Human Pathology. 2006 6//;37(6):711-8.

53. Zhou M-D, Hao S, Williams AJ, Harouaka RA, Schrand B, Rawal S, et al. Separable Bilayer Microfiltration Device for Viable Label-free Enrichment of Circulating Tumour Cells. Scientific Reports. 2014 12/09/online;4:7392.

54. Harouaka RA, Zhou M-D, Yeh Y-T, Khan WJ, Das A, Liu X, et al. Flexible Micro Spring Array Device for High-Throughput Enrichment of Viable Circulating Tumor Cells. Clinical Chemistry. 2014;60(2):323-33.

55. Huang LR, Cox EC, Austin RH, Sturm JC. Continuous Particle Separation Through Deterministic Lateral Displacement. Science. 2004;304(5673):987-90.

56. Ozkumur E, Shah AM, Ciciliano JC, Emmink BL, Miyamoto DT, Brachtel E, et al. Inertial focusing for tumor antigen-dependent and -independent sorting of rare circulating tumor cells. Sci Transl Med. 2013 Apr 3;5(179):179ra47.

57. Sollier E, Go DE, Che J, Gossett DR, O'Byrne S, Weaver WM, et al. Size-selective collection of circulating tumor cells using Vortex technology. Lab on a Chip. 2014;14(1):63-77.

58. Hou HW, Warkiani ME, Khoo BL, Li ZR, Soo RA, Tan DS-W, et al. Isolation and retrieval of circulating tumor cells using centrifugal forces. Sci Rep. 2013 02/12/online;3.

59. Kim TH, Yoon HJ, Stella P, Nagrath S. Cascaded spiral microfluidic device for deterministic and high purity continuous separation of circulating tumor cells. Biomicrofluidics. 2014 Nov;8(6):064117.

60. Sun J, Li M, Liu C, Zhang Y, Liu D, Liu W, et al. Double spiral microchannel for label-free tumor cell separation and enrichment. Lab on a chip. 2012 Oct 21;12(20):3952-60.

61. Warkiani ME, Guan G, Luan KB, Lee WC, Bhagat AAS, Kant Chaudhuri P, et al. Slanted spiral microfluidics for the ultra-fast, label-free isolation of circulating tumor cells. Lab on a Chip. 2014;14(1):128-37.

62. Khoo BL, Warkiani ME, Tan DS-W, Bhagat AAS, Irwin D, Lau DP, et al. Clinical Validation of an Ultra High-Throughput Spiral Microfluidics for the Detection and Enrichment of Viable Circulating Tumor Cells. PLoS ONE. 2014;9(7):e99409.

63. Gupta V, Jafferji I, Garza M, Melnikova VO, Hasegawa DK, Pethig R, et al. ApoStream™, a new dielectrophoretic device for antibody independent isolation and recovery of viable cancer cells from blood. Biomicrofluidics. 2012;6(2):024133.

64. Ding X, Peng Z, Lin S-CS, Geri M, Li S, Li P, et al. Cell separation using tilted-angle standing surface acoustic waves. Proceedings of the National Academy of Sciences. 2014 Sep 9;111(36):12992-7.

65. Li P, Mao Z, Peng Z, Zhou L, Chen Y, Huang P-H, et al. Acoustic separation of circulating tumor cells. Proceedings of the National Academy of Sciences. 2015;112(16):4970-5.

66. Nagrath S, Sequist LV, Maheswaran S, Bell DW, Irimia D, Ulkus L, et al. Isolation of rare circulating tumour cells in cancer patients by microchip technology. Nature. 2007 Dec 20;450(7173):1235-9.

67. Riethdorf S, Wikman H, Pantel K. Review: Biological relevance of disseminated tumor cells in cancer patients. International journal of cancer. 2008;123(9):1991-2006.

68. Maheswaran S, Sequist LV, Nagrath S, Ulkus L, Brannigan B, Collura CV, et al. Detection of mutations in EGFR in circulating lung-cancer cells. New England Journal of Medicine. 2008 Jul 24;359(4):366-77.

69. Gleghorn JP, Pratt ED, Denning D, Liu H, Bander NH, Tagawa ST, et al. Capture of circulating tumor cells from whole blood of prostate cancer patients using geometrically enhanced differential immunocapture (GEDI) and a prostate-specific antibody. Lab on a chip. 2010 Jan 7;10(1):27-9.

70. Kirby BJ, Jodari M, Loftus MS, Gakhar G, Pratt ED, Chanel-Vos C, et al. Functional characterization of circulating tumor cells with a prostate-cancer-specific microfluidic device. PloS one. 2012;7(4):e35976.

71. Galletti G, Sung MS, Vahdat LT, Shah MA, Santana SM, Altavilla G, et al. Isolation of breast cancer and gastric cancer circulating tumor cells by use of an anti HER2-based microfluidic device. Lab on a Chip. 2014;14(1):147-56.

72. Lee HJ, Cho H-Y, Oh JH, Namkoong K, Lee JG, Park J-M, et al. Simultaneous capture and< i> in situ</i> analysis of circulating tumor cells using multiple hybrid nanoparticles. Biosensors and Bioelectronics. 2013.

73. Stott SL, Hsu C, Tsukrov DI, Yu M, Miyamoto DT, Waltman BA, et al. Isolation of circulating tumor cells using a microvortex-generating herringbone-chip. PNAS. 2010;107(43):18392-7.

74. Yu M, Bardia A, Wittner BS, Stott SL, Smas ME, Ting DT, et al. Circulating breast tumor cells exhibit dynamic changes in epithelial and mesenchymal composition. Science. 2013 Feb 1;339(6119):580-4.

75. Sheng W, Ogunwobi OO, Chen T, Zhang J, George TJ, Liu C, et al. Capture, release and culture of circulating tumor cells from pancreatic cancer patients using an enhanced mixing chip. Lab on a Chip. 2014;14(1):89-98.

76. Casavant BP, Strotman LN, Tokar JJ, Thiede SM, Traynor AM, Ferguson JS, et al. Paired diagnostic and pharmacodynamic analysis of rare non-small cell lung cancer cells enabled by the VerIFAST platform. Lab Chip. 2014 Jan 7;14(1):99-105.

77. Sperger JM, Strotman LN, Welsh A, Casavant BP, Chalmers Z, Horn S, et al. Integrated analysis of multiple biomarkers from circulating tumor cells enabled by exclusion-based analyte isolation. Clinical Cancer Research. 2016.

78. McCarley RL, Vaidya B, Wei S, Smith AF, Patel AB, Feng J, et al. Resist-free patterning of surface architectures in polymer-based microanalytical devices. Journal of the American Chemical Society. 2005;127(3):842-3.

79. Adams AA, Okagbare PI, Feng J, Hupert ML, Patterson D, Gottert J, et al. Highly efficient circulating tumor cell isolation from whole blood and label-free enumeration using polymer-based microfluidics with an integrated conductivity sensor. J Am Chem Soc. 2008 Jul 9;130(27):8633-41.

80. Dharmasiri U, Balamurugan S, Adams AA, Okagbare PI, Obubuafo A, Soper SA. Highly efficient capture and enumeration of low abundance prostate cancer cells using prostate-specific membrane antigen aptamers immobilized to a polymeric microfluidic device. Electrophoresis. 2009;30(18):3289-300.

81. Jackson JM, Witek MA, Hupert ML, Brady C, Pullagurla S, Kamande J, et al. UV activation of polymeric high aspect ratio microstructures: ramifications in antibody surface loading for circulating tumor cell selection. Lab on a Chip. 2014;14(1):106-17.

82. Kamande JW, Hupert ML, Witek MA, Wang H, Torphy RJ, Dharmasiri U, et al. Modular microsystem for the isolation, enumeration, and phenotyping of circulating tumor cells in patients with pancreatic cancer. Anal Chem. 2013 Oct 1;85(19):9092-100.

83. Hoshino K, Huang Y-Y, Lane N, Huebschman M, Uhr JW, Frenkel EP, et al. Microchip-based immunomagnetic detection of circulating tumor cells. Lab on a Chip. 2011;11(20):3449-57.

84. Huang Y-y, Hoshino K, Chen P, Wu C-h, Lane N, Huebschman M, et al. Immunomagnetic nanoscreening of circulating tumor cells with a motion controlled microfluidic system. Biomedical Microdevices. 2012:1-9.

85. Issadore D, Chung J, Shao H, Liong M, Ghazani AA, Castro CM, et al. Ultrasensitive clinical enumeration of rare cells ex vivo using a micro-hall detector. Science translational medicine. 2012;4(141):141ra92.

86. Castro CM, Ghazani AA, Chung J, Shao H, Issadore D, Yoon T-J, et al. Miniaturized nuclear magnetic resonance platform for detection and profiling of circulating tumor cells. Lab on a Chip. 2014;14(1):14-23.

87. Kim S, Han S-I, Park M-J, Jeon C-W, Joo Y-D, Choi I-H, et al. Circulating Tumor Cell Microseparator Based on Lateral Magnetophoresis and Immunomagnetic Nanobeads. Analytical Chemistry. 2013;85(5):2779-86.

88. Wen C-Y, Wu L-L, Zhang Z-L, Liu Y-L, Wei S-Z, Hu J, et al. Quick-Response Magnetic Nanospheres for Rapid, Efficient Capture and Sensitive Detection of Circulating Tumor Cells. ACS nano. 2013.

89. Earhart CM, Hughes CE, Gaster RS, Ooi CC, Wilson RJ, Zhou LY, et al. Isolation and mutational analysis of circulating tumor cells from lung cancer patients with magnetic sifters and biochips. Lab on a Chip. 2014;14(1):78-88.

90. Maeda Y, Yoshino T, Matsunaga T. Novel nanocomposites consisting of in vivo-biotinylated bacterial magnetic particles and quantum dots for magnetic separation and fluorescent labeling of cancer cells. Journal of Materials Chemistry. 2009;19(35):6361-6.

91. Wang L, Asghar W, Demirci U, Wan Y. Nanostructured substrates for isolation of circulating tumor cells. Nano Today. 2013;8(4):374-87.

92. Wang S, Wang H, Jiao J, Chen KJ, Owens GE, Kamei Ki, et al. Three-Dimensional Nanostructured Substrates toward Efficient Capture of Circulating Tumor Cells. Angewandte Chemie. 2009;121(47):9132-5.

93. Wang S, Liu K, Liu J, Yu ZTF, Xu X, Zhao L, et al. Highly efficient capture of circulating tumor cells by using nanostructured silicon substrates with integrated chaotic micromixers. Angewandte Chemie International Edition. 2011;50(13):3084-8.

94. Hou S, Zhao H, Zhao L, Shen Q, Wei KS, Suh DY, et al. Capture and Stimulated Release of Circulating Tumor Cells on Polymer-Grafted Silicon Nanostructures. Advanced Materials. 2012.

95. Chen L, Liu X, Su B, Li J, Jiang L, Han D, et al. Aptamer-Mediated Efficient Capture and Release of T Lymphocytes on Nanostructured Surfaces. Advanced Materials. 2011;23(38):4376-80.

96. Shen Q, Xu L, Zhao L, Wu D, Fan Y, Zhou Y, et al. Specific Capture and Release of Circulating Tumor Cells Using Aptamer-Modified Nanosubstrates. Advanced Materials. 2013.

97. Zhang N, Deng Y, Tai Q, Cheng B, Zhao L, Shen Q, et al. Electrospun TiO2 Nanofiber-Based Cell Capture Assay for Detecting Circulating Tumor Cells from Colorectal and Gastric Cancer Patients. Advanced Materials. 2012.

98. Hou S, Zhao L, Shen Q, Yu J, Ng C, Kong X, et al. Polymer Nanofiber-Embedded Microchips for Detection, Isolation, and Molecular Analysis of Single Circulating Melanoma Cells. Angewandte Chemie International Edition. 2012.

99. Chen W, Weng S, Zhang F, Allen S, Li X, Bao L, et al. Nanoroughened Surfaces for Efficient Capture of Circulating Tumor Cells without Using Capture Antibodies. ACS nano. 2012.

100. Ivanov I, Stojcic J, Stanimirovic A, Sargent E, Nam RK, Kelley SO. Chip-based nanostructured sensors enable accurate identification and classification of circulating tumor cells in prostate cancer patient blood samples. Analytical Chemistry. 2013;85(1):398.

101. Liu Z, Robinson JT, Sun X, Dai H. PEGylated nanographene oxide for delivery of water-insoluble cancer drugs. Journal of the American Chemical Society. 2008;130(33):10876-7.

102. Mohanty N, Berry V. Graphene-based single-bacterium resolution biodevice and DNA transistor: interfacing graphene derivatives with nanoscale and microscale biocomponents. Nano letters. 2008;8(12):4469-76.

103. Lu CH, Yang HH, Zhu CL, Chen X, Chen GN. A graphene platform for sensing biomolecules. Angewandte Chemie. 2009;121(26):4879-81.

104. Stoller MD, Park S, Zhu Y, An J, Ruoff RS. Graphene-based ultracapacitors. Nano letters. 2008;8(10):3498-502.

105. Xu J, Wang K, Zu S-Z, Han B-H, Wei Z. Hierarchical nanocomposites of polyaniline nanowire arrays on graphene oxide sheets with synergistic effect for energy storage. ACS nano. 2010;4(9):5019-26.

106. Dikin DA, Stankovich S, Zimney EJ, Piner RD, Dommett GHB, Evmenenko G, et al. Preparation and characterization of graphene oxide paper. Nature. 2007;448(7152):457-60.

107. Park S, Lee K-S, Bozoklu G, Cai W, Nguyen ST, Ruoff RS. Graphene oxide papers modified by divalent ions—enhancing mechanical properties via chemical cross-linking. ACS nano. 2008;2(3):572-8.

108. Stankovich S, Dikin DA, Dommett GH, Kohlhaas KM, Zimney EJ, Stach EA, et al. Graphene-based composite materials. nature. 2006;442(7100):282-6.

109. Ramanathan T, Abdala A, Stankovich S, Dikin D, Herrera-Alonso M, Piner R, et al. Functionalized graphene sheets for polymer nanocomposites. Nature nanotechnology. 2008;3(6):327-31.

110. Park S, Ruoff RS. Chemical methods for the production of graphenes. Nature nanotechnology. 2009;4(4):217-24.

111. Stankovich S, Dikin DA, Piner RD, Kohlhaas KA, Kleinhammes A, Jia Y, et al. Synthesis of graphene-based nanosheets via chemical reduction of exfoliated graphite oxide. carbon. 2007;45(7):1558-65.

112. Dreyer DR, Park S, Bielawski CW, Ruoff RS. The chemistry of graphene oxide. Chemical Society Reviews. 2010;39(1):228-40.

113. Sun X, Liu Z, Welsher K, Robinson JT, Goodwin A, Zaric S, et al. Nano-graphene oxide for cellular imaging and drug delivery. Nano research. 2008;1(3):203-12.

114. Loh KP, Bao Q, Eda G, Chhowalla M. Graphene oxide as a chemically tunable platform for optical applications. Nature chemistry. 2010;2(12):1015-24.

115. Yoon HJ, Kim TH, Zhang Z, Azizi E, Pham TM, Paoletti C, et al. Sensitive capture of circulating tumour cells by functionalized graphene oxide nanosheets. Nature nanotechnology. 2013 Oct;8(10):735-41.

116. Wei Z, Barlow DE, Sheehan PE. The assembly of single-layer graphene oxide and graphene using molecular templates. Nano letters. 2008;8(10):3141-5.

117. Wang H, Wang X, Li X, Dai H. Chemical self-assembly of graphene sheets. Nano Research. 2009;2(4):336-42.

118. Rhim AD, Thege FI, Santana SM, Lannin TB, Saha TN, Tsai S, et al. Detection of circulating pancreas epithelial cells in patients with pancreatic cystic lesions. Gastroenterology. 2014 Mar;146(3):647-51.

119. Torphy RJ, Tignanelli CJ, Kamande JW, Moffitt RA, Herrera Loeza SG, Soper SA, et al. Circulating tumor cells as a biomarker of response to treatment in patient-derived xenograft mouse models of pancreatic adenocarcinoma. PloS one. 2014 Feb 19;9(2):e89474.

120. Ke Z, Lin M, Chen JF, Choi JS, Zhang Y, Fong A, et al. Programming thermoresponsiveness of NanoVelcro substrates enables effective purification of circulating tumor cells in lung cancer patients. ACS Nano. 2015 Jan 27;9(1):62-70.

121. Ting DT, Wittner BS, Ligorio M, Vincent Jordan N, Shah AM, Miyamoto DT, et al. Single-cell RNA sequencing identifies extracellular matrix gene expression by pancreatic circulating tumor cells. Cell Rep. 2014 Sep 25;8(6):1905-18.

122. Zhang Z, Shiratsuchi H, Lin J, Chen GA, Reddy RM, Azizi E, et al. Expansion of CTCs from early stage lung cancer patients using a microfluidic co-culture model. Oncotarget. 2014 Dec 15;5(23):12383-97.

123. Yu M, Bardia A, Aceto N, Bersani F, Madden MW, Donaldson MC, et al. Cancer therapy. Ex vivo culture of circulating breast tumor cells for individualized testing of drug susceptibility. Science (New York, NY). 2014 Jul 11;345(6193):216-20.

124. What are the key statistics about prostate cancer? Atlanta, GA: American Cancer Society; 2014.

125. Lilja H, Ulmert D, Vickers AJ. Prostate-specific antigen and prostate cancer: prediction, detection and monitoring. Nature Reviews Cancer. 2008;8(4):268-78.

126. Wolf A, Wender RC, Etzioni RB, Thompson IM, D'Amico AV, Volk RJ, et al. American Cancer Society guideline for the early detection of prostate cancer: update 2010. CA: a cancer journal for clinicians. 2010;60(2):70-98.

127. Heinlein CA, Chang C. Androgen Receptor in Prostate Cancer. Endocr Rev. 2004;25(2):276-308.

128. Shen MM, Abate-Shen C. Molecular genetics of prostate cancer: new prospects for old challenges. Genes & development. 2010;24(18):1967-2000.

129. Israeli RS, Powell CT, Corr JG, Fair WR, Heston WDW. Expression of the prostate-specific membrane antigen. Cancer research. 1994;54(7):1807-11.

130. What are the key statistics about bladder cancer? Atlanta, GA: American Cancer Society; 2014.

131. Dinney CPN, McConkey DJ, Millikan RE, Wu X, Bar-Eli M, Adam L, et al. Focus on bladder cancer. Cancer cell. 2004;6(2):111-6.

132. Schulz WA. Understanding urothelial carcinoma through cancer pathways. International journal of cancer. 2006;119(7):1513-8.

133. Castillo-Martin M, Domingo-Domenech J, Karni-Schmidt O, Matos T, Cordon-Cardo C, editors. Molecular pathways of urothelial development and bladder tumorigenesis. Urologic Oncology: Seminars and Original Investigations; 2010: Elsevier.

134. McConkey DJ, Lee S, Choi W, Tran M, Majewski T, Lee S, et al., editors. Molecular genetics of bladder cancer: emerging mechanisms of tumor initiation and progression. Urologic Oncology: Seminars and Original Investigations; 2010: Elsevier.

135. Grivas PD, Day M, Hussain M. Urothelial carcinomas: a focus on human epidermal receptors signaling. American journal of translational research. 2011;3(4):362-73.

136. Svatek RS, Hollenbeck BK, Holmäng S, Lee R, Kim SP, Stenzl A, et al. The economics of bladder cancer: costs and considerations of caring for this disease. European urology. 2014;66(2):253-62.

137. Cheng L, Davison DD, Adams J, Lopez-Beltran A, Wang L, Montironi R, et al. Biomarkers in bladder cancer: Translational and clinical implications. Critical reviews in oncology/hematology. 2014;89(1):73-111.

138. Berthold DR, Pond GR, Soban F, de Wit R, Eisenberger M, Tannock IF. Docetaxel plus prednisone or mitoxantrone plus prednisone for advanced prostate cancer: updated survival in the TAX 327 study. Journal of Clinical Oncology. 2008;26(2):242-5.

139. Scher HI, Fizazi K, Saad F, Taplin M-E, Sternberg CN, Miller K, et al. Increased survival with enzalutamide in prostate cancer after chemotherapy. New England Journal of Medicine. 2012;367(13):1187-97.

140. Ryan CJ, Smith MR, De Bono JS, Molina A, Logothetis CJ, De Souza P, et al. Abiraterone in metastatic prostate cancer without previous chemotherapy. New England Journal of Medicine. 2013;368(2):138-48.

141. Mehra N, Zafeiriou Z, Lorente D, Terstappen LW, de Bono JS. CCR 20th Anniversary Commentary: Circulating Tumor Cells in Prostate Cancer. Clinical cancer research. 2015;21(22):4992-5.

142. Pantel K, Alix-Panabières C. Real-time liquid biopsy in cancer patients: fact or fiction? Cancer research. 2013;73(21):6384-8.

143. Maheswaran S, Haber DA. Circulating tumor cells: a window into cancer biology and metastasis. Current opinion in genetics & development. 2010 Feb;20(1):96-9.

144. Stott SL, Lee RJ, Nagrath S, Yu M, Miyamoto DT, Ulkus L, et al. Isolation and Characterization of Circulating Tumor Cells from Patients with Localized and Metastatic Prostate Cancer. Sci Transl Med. 2010;2(25):25ra3.

145. Stott SL, Hsu CH, Tsukrov DI, Yu M, Miyamoto DT, Waltman BA, et al. Isolation of circulating tumor cells using a microvortex-generating herringbone-chip. Proceedings of the National Academy of Sciences. 2010 Oct 26;107(43):18392-7.

146. Miyamoto DT, Zheng Y, Wittner BS, Lee RJ, Zhu H, Broderick KT, et al. RNA-Seq of single prostate CTCs implicates noncanonical Wnt signaling in antiandrogen resistance. Science. 2015;349(6254):1351-6.

147. Park S, Ang RR, Duffy SP, Bazov J, Chi KN, Black PC, et al. Morphological Differences between Circulating Tumor Cells from Prostate Cancer Patients and Cultured Prostate Cancer Cells. PloS one. 2014;9(1):e85264.

148. Chen JF, Ho H, Lichterman J, Lu YT, Zhang Y, Garcia MA, et al. Subclassification of prostate cancer circulating tumor cells by nuclear size reveals very small nuclear circulating tumor cells in patients with visceral metastases. Cancer. 2015;121(18):3240-51.

149. Scher HI, Morris MJ, Stadler WM, Higano C, Basch E, Fizazi K, et al. Trial design and objectives for castration-resistant prostate cancer: updated recommendations from the Prostate Cancer Clinical Trials Working Group 3. Journal of Clinical Oncology. 2016;34(12):1402-18.

150. RCoreTeam. R: A Language and Environment for Statistical Computing. Vienna, Austria: R Foundation for Statistical Computing; 2014; Available from: http://www.R-project.org/.

151. Therneau T, Atkinson B, Ripley B. rpart: Recursive Partitioning and Regression Trees. 2015; R package version 4.1-9:[Available from: http://CRAN.R-project.org/package=rpart.

152. Therneau TM. A Package for Survival Analysis in S. 2015; version 2.38:[Available from: http://CRAN.R-project.org/package=survival.

153. Heagerty PJ, Saha-Chaudhuri P. survivalROC: Time-dependent ROC curve estimation from censored survival data. 2013; R package version 1.0.3:[Available from: http://CRAN.R-project.org/package=survivalROC.

154. Therneau TM, Grambsch P. Extending the Cox model. Edited by P Bickel, P Diggle, S Fienberg, K Krickeberg. 2000:51.

155. Antonarakis ES, Lu C, Wang H, Luber B, Nakazawa M, Roeser JC, et al. AR-V7 and resistance to enzalutamide and abiraterone in prostate cancer. New England Journal of Medicine. 2014;371(11):1028-38.

156. Miyamoto DT, Lee RJ, Stott SL, Ting DT, Wittner BS, Ulman M, et al. Androgen Receptor Signaling in Circulating Tumor Cells as a Marker of Hormonally Responsive Prostate Cancer. Cancer Discovery. 2012 Nov;2(11):995-1003.

157. Meyer CP, Pantel K, Tennstedt P, Stroelin P, Schlomm T, Heinzer H, et al., editors. Limited prognostic value of preoperative circulating tumor cells for early biochemical recurrence in patients with localized prostate cancer. Urologic Oncology: Seminars and Original Investigations; 2016: Elsevier.

158. Collins AT, Berry PA, Hyde C, Stower MJ, Maitland NJ. Prospective identification of tumorigenic prostate cancer stem cells. Cancer research. 2005 Dec 1;65(23):10946-51.

159. Schroeder A, Herrmann A, Cherryholmes G, Kowolik C, Buettner R, Pal S, et al. Loss of androgen receptor expression promotes a stem-like cell phenotype in prostate cancer through STAT3 signaling. Cancer research. 2014;74(4):1227-37.

160. Qin J, Liu X, Laffin B, Chen X, Choy G, Jeter CR, et al. The PSA−/lo prostate cancer cell population harbors self-renewing long-term tumor-propagating cells that resist castration. Cell stem cell. 2012;10(5):556-69.

161. Zeng Y, Abdallah A, Lu J-P, Wang T, Chen Y-H, Terrian DM, et al. δ-Catenin promotes prostate cancer cell growth and progression by altering cell cycle and survival gene profiles. Molecular cancer. 2009;8(1):19.

162. Han B, Bhowmick N, Qu Y, Chung S, Giuliano A, Cui X. FOXC1: an emerging marker and therapeutic target for cancer. Oncogene. 2017;36(28):3957-63.

163. DeHaan AM, Wolters NM, Keller ET, Ignatoski KMW. EGFR ligand switch in late stage prostate cancer contributes to changes in cell signaling and bone remodeling. The Prostate. 2009;69(5):528-37.

164. Traish A, Morgentaler A. Epidermal growth factor receptor expression escapes androgen regulation in prostate cancer: a potential molecular switch for tumour growth. British journal of cancer. 2009;101(12):1949-56.

165. Shah RB, Ghosh D, Elder JT. Epidermal growth factor receptor (ErbB1) expression in prostate cancer progression: correlation with androgen independence. The Prostate. 2006;66(13):1437-44.

166. Craft N, Shostak Y, Carey M, Sawyers CL. A mechanism for hormone-independent prostate cancer through modulation of androgen receptor signaling by the HER-2/neu tyrosine kinase. Nature medicine. 1999;5(3):280-5.

167. Piccart-Gebhart MJ, Procter M, Leyland-Jones B, Goldhirsch A, Untch M, Smith I, et al. Trastuzumab after adjuvant chemotherapy in HER2-positive breast cancer. New England Journal of Medicine. 2005;353(16):1659-72.

168. Barthelemy P, Leblanc J, Goldbarg V, Wendling F, Kurtz J-E. Pertuzumab: development beyond breast cancer. Anticancer research. 2014;34(4):1483-91.

169. Minner S, Jessen B, Stiedenroth L, Burandt E, Köllermann J, Mirlacher M, et al. Low level HER2 overexpression is associated with rapid tumor cell proliferation and poor prognosis in prostate cancer. Clinical Cancer Research. 2010;16(5):1553-60.

170. Riethdorf S, Muller V, Zhang L, Rau T, Loibl S, Komor M, et al. Detection and HER2 expression of circulating tumor cells: prospective monitoring in breast cancer patients treated in the neoadjuvant GeparQuattro trial. Clin Cancer Res. 2010 May 1;16(9):2634-45.

171. Pestrin M, Bessi S, Puglisi F, Minisini AM, Masci G, Battelli N, et al. Final results of a multicenter phase II clinical trial evaluating the activity of single-agent lapatinib in patients with HER2-negative metastatic breast cancer and HER2-positive circulating tumor cells. A proof-of-concept study. Breast cancer research and treatment. 2012;134(1):283.

172. Paoletti C, Muniz MC, Thomas DG, Griffith KA, Kidwell KM, Tokudome N, et al. Development of circulating tumor cell-endocrine therapy index in patients with hormone receptor-positive breast cancer. Clin Cancer Res. 2015 Jun 1;21(11):2487-98.

173. Aktas B, Kasimir-Bauer S, Müller V, Janni W, Fehm T, Wallwiener D, et al. Comparison of the HER2, estrogen and progesterone receptor expression profile of primary tumor, metastases and circulating tumor cells in metastatic breast cancer patients. BMC cancer. 2016;16(1):522.

174. Fehm T, Müller V, Aktas B, Janni W, Schneeweiss A, Stickeler E, et al. HER2 status of circulating tumor cells in patients with metastatic breast cancer: a prospective, multicenter trial. Breast cancer research and treatment. 2010;124(2):403-12.

175. Jordan NV, Bardia A, Wittner BS, Benes C, Ligorio M, Zheng Y, et al. HER2 expression identifies dynamic functional states within circulating breast cancer cells. Nature. 2016.

176. Khoo BL, Warkiani ME, Tan DS, Bhagat AA, Irwin D, Lau DP, et al. Clinical validation of an ultra high-throughput spiral microfluidics for the detection and enrichment of viable circulating tumor cells. PLoS One. 2014;9(7):e99409.

177. Payne RE, Yagüe E, Slade MJ, Apostolopoulos C, Jiao LR, Ward B, et al. Measurements of EGFR expression on circulating tumor cells are reproducible over time in metastatic breast cancer patients. 2009.

178. Punnoose EA, Atwal S, Liu W, Raja R, Fine BM, Hughes BG, et al. Evaluation of circulating tumor cells and circulating tumor DNA in non–small cell lung cancer: Association with clinical endpoints in a phase II clinical trial of pertuzumab and erlotinib. Clinical Cancer Research. 2012;18(8):2391-401.

179. Molina JR, Kaufmann SH, Reid JM, Rubin SD, Gálvez-Peralta M, Friedman R, et al. Evaluation of lapatinib and topotecan combination therapy: tissue culture, murine xenograft, and phase I clinical trial data. Clinical Cancer Research. 2008;14(23):7900-8.

180. Strecker TE, Shen Q, Zhang Y, Hill JL, Li Y, Wang C, et al. Effect of lapatinib on the development of estrogen receptor–negative mammary tumors in mice. Journal of the National Cancer Institute. 2009;101(2):107-13.

181. Gril B, Palmieri D, Bronder JL, Herring JM, Vega-Valle E, Feigenbaum L, et al. Effect of lapatinib on the outgrowth of metastatic breast cancer cells to the brain. Journal of the National Cancer Institute. 2008;100(15):1092-103.

182. Friess T, Scheuer W, Hasmann M. Combination treatment with erlotinib and pertuzumab against human tumor xenografts is superior to monotherapy. Clinical Cancer Research. 2005;11(14):5300-9.

183. Rubin MA, Dunn R, Strawderman M, Pienta KJ. Tissue microarray sampling strategy for prostate cancer biomarker analysis. The American journal of surgical pathology. 2002;26(3):312-9.

184. Kuefer R, Day KC, Kleer CG, Sabel MS, Hofert MD, Varambally S, et al. ADAM15 disintegrin is associated with aggressive prostate and breast cancer disease. Neoplasia. 2006;8(4):319-29.

185. Rubin MA, Putzi M, Mucci N, Smith DC, Wojno K, Korenchuk S, et al. Rapid ("warm") autopsy study for procurement of metastatic prostate cancer. Clinical cancer research. 2000;6(3):1038-45.

186. Gleason DF. Classification of prostatic carcinomas. Cancer chemotherapy reports. 1966;50(3):125-8.

187. Najy AJ, Day KC, Day ML. The ectodomain shedding of E-cadherin by ADAM15 supports ErbB receptor activation. Journal of Biological Chemistry. 2008;283(26):18393-401.

188. Ithimakin S, Day KC, Malik F, Zen Q, Dawsey SJ, Bersano-Begey TF, et al. HER2 drives luminal breast cancer stem cells in the absence of HER2 amplification: implications for efficacy of adjuvant trastuzumab. Cancer research. 2013;73(5):1635-46.

189. Garraway IP, Sun W, Tran CP, Perner S, Zhang B, Goldstein AS, et al. Human prostate sphere-forming cells represent a subset of basal epithelial cells capable of glandular regeneration in vivo. The Prostate. 2010;70(5):491-501.

190. Portillo-Lara R, Alvarez MM. Enrichment of the Cancer Stem Phenotype in Sphere Cultures of Prostate Cancer Cell Lines Occurs through Activation of Developmental Pathways Mediated by the Transcriptional Regulator ΔNp63α. PloS one. 2015;10(6):e0130118.

191. Rajasekhar VK, Studer L, Gerald W, Socci ND, Scher HI. Tumour-initiating stem-like cells in human prostate cancer exhibit increased NF-κB signalling. Nature communications. 2011;2:162.

192. Rybak AP, He L, Kapoor A, Cutz J-C, Tang D. Characterization of sphere-propagating cells with stem-like properties from DU145 prostate cancer cells. Biochimica et Biophysica Acta (BBA)-Molecular Cell Research. 2011;1813(5):683-94.

193. Scher HI, Sarkis A, Reuter V, Cohen D, Netto G, Petrylak D, et al. Changing pattern of expression of the epidermal growth factor receptor and transforming growth factor alpha in the progression of prostatic neoplasms. Clinical Cancer Research. 1995;1(5):545-50.

194. Jorda M, Morales A, Ghorab Z, Fernandez G, Nadji M, Block N. Her2 expression in prostatic cancer: a comparison with mammary carcinoma. The Journal of urology. 2002;168(4):1412-4.

195. Chow N-H, Chan S-H, Tzai T-S, Ho C-L, Liu H-S. Expression profiles of ErbB family receptors and prognosis in primary transitional cell carcinoma of the urinary bladder. Clinical cancer research. 2001;7(7):1957-62.

196. Jimenez RE, Hussain M, Bianco FJ, Vaishampayan U, Tabazcka P, Sakr WA, et al. Her-2/neu overexpression in muscle-invasive urothelial carcinoma of the bladder. Clinical Cancer Research. 2001;7(8):2440-7.

197. Weihua Z, Tsan R, Huang W-C, Wu Q, Chiu C-H, Fidler IJ, et al. Survival of cancer cells is maintained by EGFR independent of its kinase activity. Cancer cell. 2008;13(5):385-93.

198. Mueller KL, Yang Z-Q, Haddad R, Ethier SP, Boerner JL. EGFR/Met association regulates EGFR TKI resistance in breast cancer. Journal of molecular signaling. 2010;5(1):8.

199. Miettinen PJ, Berger JE, Meneses J, Phung Y, Pedersen RA, Werb Z, et al. Epithelial immaturity and multiorgan failure in mice lacking epidermal growth factor receptor. Nature. 1995;376(6538):337-41.

200. Litvinov IV, Vander Griend DJ, Xu Y, Antony L, Dalrymple SL, Isaacs JT. Low-calcium serum-free defined medium selects for growth of normal prostatic epithelial stem cells. Cancer research. 2006;66(17):8598-607.

201. Rybak AP, Ingram AJ, Tang D. Propagation of human prostate cancer stem-like cells occurs through EGFR-mediated ERK activation. PloS one. 2013;8(4):e61716.

202. Azizi E, Nagrath S, Kozminsky M, Wicha MS. Cancer Stem Cells and Circulating Tumor Cells: Molecular Markers, Isolation Techniques, and Clinical Implications. Circulating Tumor Cells: Springer; 2016. p. 75-97.

203. Dittrich A, Gautrey H, Browell D, Tyson-Capper A. The HER2 Signaling Network in Breast Cancer—Like a Spider in its Web. Journal of mammary gland biology and neoplasia. 2014;19(3-4):253-70.

204. Yeo SK, Wen J, Chen S, Guan J-L. Autophagy differentially regulates distinct breast cancer stem-like cells in murine models via EGFR/Stat3 and Tgfβ/Smad signaling. Cancer research. 2016;76(11):3397-410.

205. Cathomas R, Rothermundt C, Klingbiel D, Bubendorf L, Jaggi R, Betticher DC, et al. Efficacy of cetuximab in metastatic castration-resistant prostate cancer might depend on EGFR and PTEN expression: results from a phase II trial (SAKK 08/07). Clinical cancer research. 2012;18(21):6049-57.

206. Nabhan C, Lestingi TM, Galvez A, Tolzien K, Kelby SK, Tsarwhas D, et al. Erlotinib has moderate single-agent activity in chemotherapy-naive castration-resistant prostate cancer: final results of a phase II trial. Urology. 2009;74(3):665-71.

207. Liu G, Chen Y-H, Kolesar J, Huang W, DiPaola R, Pins M, et al., editors. Eastern Cooperative Oncology Group Phase II Trial of lapatinib in men with biochemically relapsed, androgen dependent prostate cancer. Urologic Oncology: Seminars and Original Investigations; 2013: Elsevier.

208. Key Statistics for Bladder Cancer. Atlanta, GA: American Cancer Society; 2017 [cited 2017 July 13, 2017].

209. D'Costa JJ, Goldsmith JC, Wilson JS, Bryan RT, Ward DG. A systematic review of the diagnostic and prognostic value of urinary protein biomarkers in urothelial bladder cancer. Bladder cancer. 2016;2(3):301-17.

210. Gorin MA, Verdone JE, van der Toom E, Bivalacqua TJ, Allaf ME, Pienta KJ. Circulating tumour cells as biomarkers of prostate, bladder, and kidney cancer. Nature Reviews Urology. 2016.

211. Skacel M, Fahmy M, Brainard JA, Pettay JD, Biscotti CV, Liou LS, et al. Multitarget fluorescence in situ hybridization assay detects transitional cell carcinoma in the majority of patients with bladder cancer and atypical or negative urine cytology. The Journal of urology. 2003;169(6):2101-5.

212. Bladder cancer: diagnosis and management. National Institute for Health and Care Excellence; 2017 [cited 2017 July 13, 2017]; Available from: https://www.nice.org.uk/guidance/ng2/chapter/1-recommendations#diagnosing-and-staging-bladder-cancer-2.

213. Naoe M, Ogawa Y, Morita J, Omori K, Takeshita K, Shichijyo T, et al. Detection of circulating urothelial cancer cells in the blood using the CellSearch System. Cancer. 2007;109(7):1439-45.

214. Rink M, Chun FKH, Minner S, Friedrich M, Mauermann O, Heinzer H, et al. Detection of circulating tumour cells in peripheral blood of patients with advanced non-metastatic bladder cancer. BJU international. 2011;107(10):1668-75.

215. Flaig TW, Wilson S, van Bokhoven A, Varella-Garcia M, Wolfe P, Maroni P, et al. Detection of circulating tumor cells in metastatic and clinically localized urothelial carcinoma. Urology. 2011;78(4):863-7.

216. Gazzaniga P, Gradilone A, De Berardinis E, Busetto GM, Raimondi C, Gandini O, et al. Prognostic value of circulating tumor cells in nonmuscle invasive bladder cancer: a CellSearch analysis. Annals of oncology. 2012;23(9):2352-6.

217. Guzzo TJ, McNeil BK, Bivalacqua TJ, Elliott DJ, Sokoll LJ, Schoenberg MP, editors. The presence of circulating tumor cells does not predict extravesical disease in bladder cancer patients prior to radical cystectomy. Urologic Oncology: Seminars and Original Investigations; 2012: Elsevier.

218. Rink M, Chun FK, Dahlem R, Soave A, Minner S, Hansen J, et al. Prognostic role and HER2 expression of circulating tumor cells in peripheral blood of patients prior to radical cystectomy: a prospective study. European urology. 2012;61(4):810-7.

219. Busetto GM, Ferro M, Del Giudice F, Antonini G, Chung BI, Sperduti I, et al. The Prognostic Role of Circulating Tumor Cells (CTC) in High-risk Non–muscle-invasive Bladder Cancer. Clinical Genitourinary Cancer. 2017.

220. Grivas PD, Day KC, Karatsinides A, Paul A, Shakir N, Owainati I, et al. Evaluation of the antitumor activity of dacomitinib in models of human bladder cancer. Molecular medicine (Cambridge, Mass). 2013;19:367-76.

221. Hiles GL, Bucheit A, Rubin JR, Hayward A, Cates AL, Day KC, et al. ADAM15 is functionally associated with the metastatic progression of human bladder cancer. PloS one. 2016;11(3):e0150138.

222. Lucas N, Najy AJ, Day ML. The therapeutic potential of ADAM15. Current pharmaceutical design. 2009;15(20):2311-8.

223. Lertkiatmongkol P, Liao D, Mei H, Hu Y, Newman PJ. Endothelial functions of platelet/endothelial cell adhesion molecule-1 (CD31). Current opinion in hematology. 2016;23(3):253-9.

224. Brunner A, Prelog M, Verdorfer I, Tzankov A, Mikuz G, Ensinger C. EpCAM is predominantly expressed in high grade and advanced stage urothelial carcinoma of the bladder. Journal of clinical pathology. 2008;61(3):307-10.

225. Cima I, Kong SL, Sengupta D, Tan IB, Phyo WM, Lee D, et al. Tumor-derived circulating endothelial cell clusters in colorectal cancer. Science translational medicine. 2016;8(345):345ra89-ra89.

226. Alix-Panabieres C, Pantel K. Challenges in circulating tumour cell research. Nat Rev Cancer. 2014 Sep;14(9):623-31.

227. Yoon HJ, Kim TH, Zhang Z, Azizi E, Pham TM, Paoletti C, et al. Sensitive capture of circulating tumour cells by functionalized graphene oxide nanosheets. Nature nanotechnology. 2013 Oct;8(10):735-41.

228. Hatch A, Hansmann G, Murthy SK. Engineered alginate hydrogels for effective microfluidic capture and release of endothelial progenitor cells from whole blood. Langmuir : the ACS journal of surfaces and colloids. 2011 Apr 5;27(7):4257-64.

229. Shah AM, Yu M, Nakamura Z, Ciciliano J, Ulman M, Kotz K, et al. Biopolymer system for cell recovery from microfluidic cell capture devices. Analytical chemistry. 2012 Apr 17;84(8):3682-8.

230. Reategui E, Aceto N, Lim EJ, Sullivan JP, Jensen AE, Zeinali M, et al. Tunable nanostructured coating for the capture and selective release of viable circulating tumor cells. Adv Mater. 2015 Mar 4;27(9):1593-9.

231. Hou S, Zhao H, Zhao L, Shen Q, Wei KS, Suh DY, et al. Capture and stimulated release of circulating tumor cells on polymer-grafted silicon nanostructures. Adv Mater. 2013 Mar 20;25(11):1547-51.

232. Liu H, Liu X, Meng J, Zhang P, Yang G, Su B, et al. Hydrophobic interaction-mediated capture and release of cancer cells on thermoresponsive nanostructured surfaces. Adv Mater. 2013 Feb 13;25(6):922-7.

233. Shah AM, Yu M, Nakamura Z, Ciciliano J, Ulman M, Kotz K, et al. Biopolymer system for cell recovery from microfluidic cell capture devices. Analytical chemistry. 2012;84(8):3682-8.

234. Hatch A, Hansmann G, Murthy SK. Engineered alginate hydrogels for effective microfluidic capture and release of endothelial progenitor cells from whole blood. Langmuir. 2011;27(7):4257-64.

235. Liu H, Liu X, Meng J, Zhang P, Yang G, Su B, et al. Hydrophobic Interaction-Mediated Capture and Release of Cancer Cells on Thermoresponsive Nanostructured Surfaces. Advanced Materials. 2013;25(6):922-7.

236. Kotov NA. Layer-by-layer self-assembly: The contribution of hydrophobic interactions. Nanostructured Materials. 1999;12(5):789-96.

237. Ostrander JW, Mamedov AA, Kotov NA. Two modes of linear layer-by-layer growth of nanoparticle-polylectrolyte multilayers and different interactions in the layer-by-layer deposition. Journal of the American Chemical Society. 2001;123(6):1101-10.

238. Shim BS, Zhu J, Jan E, Critchley K, Kotov NA. Transparent conductors from layer-by-layer assembled SWNT films: importance of mechanical properties and a new figure of merit. ACS nano. 2010;4(7):3725-34.

239. Jiang B, Barnett JB, Li B. Advances in polyelectrolyte multilayer nanofilms as tunable drug delivery systems. Nanotechnology, Science and Applications. 2009;2:21-7.

240. Zhang X, Chen H, Zhang H. Layer-by-layer assembly: from conventional to unconventional methods. Chemical Communications. 2007 (14):1395-405.

241. Kotov NA, Dékány I, Fendler JH. Ultrathin graphite oxide–polyelectrolyte composites prepared by self-assembly: Transition between conductive and non-conductive states. Advanced Materials. 1996;8(8):637-41.

242. Xu Y, Hong W, Bai H, Li C, Shi G. Strong and ductile poly (vinyl alcohol)/graphene oxide composite films with a layered structure. Carbon. 2009;47(15):3538-43.

243. Hirata M, Gotou T, Ohba M. Thin-film particles of graphite oxide. 2: Preliminary studies for internal micro fabrication of single particle and carbonaceous electronic circuits. Carbon. 2005;43(3):503-10.

244. Han Y, Lu Y. Characterization and electrical properties of conductive polymer/colloidal graphite oxide nanocomposites. Composites Science and Technology. 2009;69(7):1231-7.

245. Tymosiak-Zielińska A, Borkowska Z. Interfacial properties of polycrystalline gold electrodes in tetraalkylammonium electrolytes. Electrochimica Acta. 2001;46(20):3073-82.

246. Nakamura K, Maitani Y, Lowman AM, Takayama K, Peppas NA, Nagai T. Uptake and release of budesonide from mucoadhesive, pH-sensitive copolymers and their application to nasal delivery. Journal of Controlled Release. 1999 9/20/;61(3):329-35.

247. Nitschke M, Gramm S, Götze T, Valtink M, Drichel J, Voit B, et al. Thermo-responsive poly(NiPAAm-co-DEGMA) substrates for gentle harvest of human corneal endothelial cell sheets. Journal of Biomedical Materials Research Part A. 2007;80A(4):1003-10.

248. Stile RA, Healy KE. Thermo-Responsive Peptide-Modified Hydrogels for Tissue Regeneration. Biomacromolecules. 2001 2001/03/01;2(1):185-94.

249. Cunliffe D, Smart CA, Tsibouklis J, Young S, Alexander C, Vulfson EN. Bacterial adsorption to thermoresponsive polymer surfaces. Biotechnology Letters. 2000 2000/01/01;22(2):141-5.

250. Huber DL, Manginell RP, Samara MA, Kim B-I, Bunker BC. Programmed Adsorption and Release of Proteins in a Microfluidic Device. Science. 2003 July 18, 2003;301(5631):352-4.

251. Das TK, Prusty S. Graphene-Based Polymer Composites and Their Applications. Polymer-Plastics Technology and Engineering. 2013 2013/03/16;52(4):319-31.

252. Wu Q, Xu Y, Yao Z, Liu A, Shi G. Supercapacitors based on flexible graphene/polyaniline nanofiber composite films. ACS nano. 2010 Apr 27;4(4):1963-70.

253. Zhuang XD, Chen Y, Liu G, Li PP, Zhu CX, Kang ET, et al. Conjugated-polymer-functionalized graphene oxide: synthesis and nonvolatile rewritable memory effect. Adv Mater. 2010 Apr 18;22(15):1731-5.

254. Li GL, Liu G, Li M, Wan D, Neoh KG, Kang ET. Organo- and Water-Dispersible Graphene Oxide−Polymer Nanosheets for Organic Electronic Memory and Gold Nanocomposites. The Journal of Physical Chemistry C. 2010 2010/07/29;114(29):12742-8.

255. Sahoo NG, Bao H, Pan Y, Pal M, Kakran M, Cheng HKF, et al. Functionalized carbon nanomaterials as nanocarriers for loading and delivery of a poorly water-soluble anticancer drug: a comparative study. Chemical Communications. 2011;47(18):5235-7.

256. Kim H, Namgung R, Singha K, Oh I-K, Kim WJ. Graphene Oxide–Polyethylenimine Nanoconstruct as a Gene Delivery Vector and Bioimaging Tool. Bioconjugate Chemistry. 2011 2011/12/21;22(12):2558-67.

257. Hu S-H, Chen Y-W, Hung W-T, Chen IW, Chen S-Y. Quantum-Dot-Tagged Reduced Graphene Oxide Nanocomposites for Bright Fluorescence Bioimaging and Photothermal Therapy Monitored In Situ. Advanced Materials. 2012;24(13):1748-54.

258. Kumar S, Raj S, Kolanthai E, Sood AK, Sampath S, Chatterjee K. Chemical functionalization of graphene to augment stem cell osteogenesis and inhibit biofilm formation on polymer composites for orthopedic applications. ACS applied materials & interfaces. 2015;7(5):3237-52.

259. Chaudhuri B, Bhadra D, Moroni L, Pramanik K. Myoblast differentiation of human mesenchymal stem cells on graphene oxide and electrospun graphene oxide–polymer composite fibrous meshes: importance of graphene oxide conductivity and dielectric constant on their biocompatibility. Biofabrication. 2015;7(1):015009.

260. Thampi S, Muthuvijayan V, Parameswaran R. Mechanical characterization of high-performance graphene oxide incorporated aligned fibroporous poly (carbonate urethane) membrane for potential biomedical applications. Journal of Applied Polymer Science. 2015;132(16).

261. Pant HR, Pokharel P, Joshi MK, Adhikari S, Kim HJ, Park CH, et al. Processing and characterization of electrospun graphene oxide/polyurethane composite nanofibers for stent coating. Chemical Engineering Journal. 2015;270:336-42.

262. Jo YS, Van Der Vlies AJ, Gantz J, Antonijevic S, Demurtas D, Velluto D, et al. RAFT homo-and copolymerization of N-acryloyl-morpholine, piperidine, and azocane and their self-assembled structures. Macromolecules. 2008;41(4):1140-50.

263. Cecchet F, De Meersman B, Demoustier-Champagne S, Nysten B, Jonas AM. One Step Growth of Protein Antifouling Surfaces: Monolayers of Poly(ethylene oxide) (PEO) Derivatives

on Oxidized and Hydrogen-Passivated Silicon Surfaces. Langmuir : the ACS journal of surfaces and colloids. 2006 2006/01/01;22(3):1173-81.

264. Ithimakin S, Day KC, Malik F, Zen Q, Dawsey SJ, Bersano-Begey TF, et al. HER2 Drives Luminal Breast Cancer Stem Cells in the Absence of HER2 Amplification: Implications for Efficacy of Adjuvant Trastuzumab. Cancer research. 2013 March 1, 2013;73(5):1635-46.

265. Picart C. Polyelectrolyte multilayer films: from physico-chemical properties to the control of cellular processes. Current medicinal chemistry. 2008;15(7):685-97.

266. Hoshino K, Taniguchi M, Kitao T, Morohashi S, Sasakura T. Preparation of a new thermo-responsive adsorbent with maltose as a ligand and its application to affinity precipitation. Biotechnol Bioeng. 1998 Dec 5;60(5):568-79.

267. Arya SK, Lim B, Rahman ARA. Enrichment, detection and clinical significance of circulating tumor cells. Lab on a Chip. 2013;13(11):1995-2027.

268. Bhattacharjee N, Urrios A, Kang S, Folch A. The upcoming 3D-printing revolution in microfluidics. Lab on a Chip. 2016;16(10):1720-42.

269. Babaei V, Ramos J, Lu Y, Webster G, Matusik W. FabSquare: Fabricating Photopolymer Objects by Mold 3D Printing and UV Curing. IEEE Computer Graphics and Applications. 2017;38(3):34-42.

270. Murlidhar V, Zeinali M, Grabauskiene S, Ghannad-Rezaie M, Wicha MS, Simeone DM, et al. A Radial Flow Microfluidic Device for Ultra-High-Throughput Affinity-Based Isolation of Circulating Tumor Cells. Small. 2014 Dec 10;10(23):4895-904.

271. Hirsch JD, Eslamizar L, Filanoski BJ, Malekzadeh N, Haugland RP, Beechem JM, et al. Easily reversible desthiobiotin binding to streptavidin, avidin, and other biotin-binding proteins: uses for protein labeling, detection, and isolation. Analytical biochemistry. 2002;308(2):343-57.

272. Wan Y, Cheng G, Liu X, Hao S-J, Nisic M, Zhu C-D, et al. Rapid magnetic isolation of extracellular vesicles via lipid-based nanoprobes. Nature Biomedical Engineering. 2017;1:0058.

273. Kang JH, Krause S, Tobin H, Mammoto A, Kanapathipillai M, Ingber DE. A combined micromagnetic-microfluidic device for rapid capture and culture of rare circulating tumor cells. Lab on a Chip. 2012;12(12):2175-81.

274. Rye PD, Høifødt HK, Overli GE, Fodstad O. Immunobead filtration: a novel approach for the isolation and propagation of tumor cells. The American journal of pathology. 1997;150(1):99.

275. Cayrefourcq L, Mazard T, Joosse S, Solassol J, Ramos J, Assenat E, et al. Establishment and characterization of a cell line from human circulating colon cancer cells. Cancer Res. 2015 Mar 1;75(5):892-901.

276. Zhang L, Ridgway LD, Wetzel MD, Ngo J, Yin W, Kumar D, et al. The identification and characterization of breast cancer CTCs competent for brain metastasis. Sci Transl Med. 2013 Apr 10;5(180):180ra48.

277. Kolostova K, Broul M, Schraml J, Cegan M, Matkowski R, Fiutowski M, et al. Circulating tumor cells in localized prostate cancer: isolation, cultivation in vitro and relationship to T-stage and Gleason score. Anticancer Research. 2014;34(7):3641-6.

278. Karthaus WR, Iaquinta PJ, Drost J, Gracanin A, van Boxtel R, Wongvipat J, et al. Identification of Multipotent Luminal Progenitor Cells in Human Prostate Organoid Cultures. Cell. 2014.

279. Gao D, Vela I, Sboner A, Iaquinta PJ, Karthaus WR, Gopalan A, et al. Organoid Cultures Derived from Patients with Advanced Prostate Cancer. Cell. 2014.

280. Antonarakis ES, Lu C, Luber B, Wang H, Chen Y, Nakazawa M, et al. Androgen receptor splice variant 7 and efficacy of taxane chemotherapy in patients with metastatic castration-resistant prostate cancer. JAMA oncology. 2015;1(5):582-91.

281. Barbieri CE, Tomlins SA, editors. The prostate cancer genome: perspectives and potential. Urologic Oncology: Seminars and Original Investigations; 2014: Elsevier.

282. Roychowdhury S, Chinnaiyan AM. Advancing precision medicine for prostate cancer through genomics. Journal of Clinical Oncology. 2013;31(15):1866-73.